Engineering the Plasmon Resonance of Gold Nanoshells for Biological Applications

Department of Engineering

Nesrine Nagui Taha

February 2010

Dissertation submitted February 2010 by the author for the degree of Master of Philosophy to the University of Cambridge, Wolfson College

Research funding was provided by the Nanoscience Research Laboratory of the University of Cambridge Engineering Department. Degree was sponsored by Cambridge Overseas Trust.
Research supervisor: Prof. Mark Welland

Abstract

Within this research I have investigated the effect of pH and the ratio of gold to silica colloids on the formation of nanoshell precursor seed particles thereby leading to the optimization of the process by which gold nanoshells are formed. With a focus on nanoshells for the thermal ablation of cancer cells, 104.5 nm core shell particles having a peak resonance at 940 nm were formed. The study also presents two new methods by which 'textured' nanoshells may be formed for use in applications such as substrates for Surface Enhanced Raman Spectroscopy. The thesis has also investigated the effect of temperature on the surface morphology of the gold nanoshells. Investigations in this respect have led to the finding that the formation of nanoshells at an elevated temperature allows for the generation of nanoshells having a smooth surface morphology, irrespective of the shell thickness.

Dedication

To my mom, dad and Dana, Malak & Mazin for their unconditional love and support and to my husband for loving me and helping me realize my dreams, no matter how far they take us.

Table of Contents

Chapter I: Introduction & Background

I .a. Introduction

A hundred and fifty years ago, when Michael Faraday published his detailed account of the preparation and properties of colloidal gold, little was anticipated regarding the exploitation of the optical properties of gold colloids in the many ways they are used today. Far before the time of Faraday, colloids had been used for many years in the colouration of stained glass and in the preparation of what was known to the Ancient Romans as the 'elixir of life'. It was only in the beginning of the 20th century that several discoveries and inventions made possible the in-depth study of colloids and in particular gold. Examples of these milestones are Svedberg's development of the ultracentrifuge (Svedberg, 1923), followed by Zsigmondy's invention of the ultramicroscope (Zsigmondy, 1926) and also Gustuv Mie's description of the optical properties of colloidal gold through his solution of Maxwell's equations (Mie, 1908). Additionally, with the development of the electron microscope in the mid 1900s, the use of colloidal gold in biological applications such as immunogold labelling (Hayat, 1989) was an addition to the list of significant properties and applications of colloidal gold.

Over the past decade, developments in the emerging field of nanoscience have garnered the many properties of colloidal gold, now more commonly known as gold nanoparticles, for various applications including biological ones. Examples of these applications are biosensing and imaging in addition to nanoparticle-assisted therapeutic techniques such as drug delivery and thermal ablation of tumours. Thereby, developments in the fields of Physics, Chemistry and Colloid Science, over the past century, have paved the way for what we have today in Nanoscale science: The ability to control properties of material at the nanoscale.

I .b. Thesis Purpose and Outline

The aim of this research has been to develop improved gold nanoshells with the purpose of the future use in biological applications. Nanoshells were favoured over other types of nanoparticles due to the possibility of using a single particle for both sensing and therapeutic applications in addition to the biocompatibility of gold and silica.

Due to the limitations on availability of clear, detailed literature regarding the optimization of the chemicals used in the formation of gold nanoshells, (Park et al, Pham et al, Averitt et al and Westcott et al) it was also necessary to investigate the various steps of nanoshell formation and determine the optimum conditions which would lead to the formation of nanoshells of the desired quality.

Nanoshells made, in accordance with the protocol developed in this study, would have a plasmon resonance in the near infra red region of the spectrum, such that they would be suited for use in biological applications. Attempts would be made to produce gold nanoshells that have the greatest possible shift into the 'biological water window' (600-1200 nm) thus minimizing the absorption of the radiation by tissues (Wang et al, 2007).

This thesis presents an account of gold nanoshells and details of their formation. Chapter II, Background, presents a description of the nanoshell and the details the steps of how this composite nanoparticle is made. Also presented in the background chapter are the optical properties of these particles and how these optical properties may be harnessed for the use in various applications with an emphasis on biological applications such as drug delivery and malignant tumour thermal ablation. Chapter III reports on the results of the experiments conducted within this study. The results include a detailed analysis of the many factors affecting the formation, growth and optical properties of gold nanoshells. The results of the experimental work are discussed at each stage. Chapter IV provides a summary and conclusion to the work done with in this thesis. Finally, Chapter V portrays the proposed future work, within the nano-oncology arena, through the presentation of a brief account of preliminary experimental work carried out within this scope of research. Details of the stepwise formation of the gold nanoshells, the materials, including quantities, used in addition to the equipment and techniques used in characterization are presented in Appendix A, Materials and Methodology. Similarly, details of biological experiments conducted with Glioblastoma multiforme cancer cells are presented in Appendix B, Biological Experiments. Appendix C contains the optical constants (Johnson et al, 1972) used to determine the dielectric constants of gold at various wavelengths.

Chapter II: Background

II .a. Introduction

The beauty of metal nanoshells stems from the ability to tune their optical properties by modification of their geometry, in addition to the capability of designing them so as to confine and enhance electromagnetic fields in their proximity. Metal nanoshells, comprising a dielectric core and a thin metal shell, possess optical properties that may be exploited at different spectral wavelengths. Examples include wave-guiding at radio frequencies and medical applications at visible and near infrared wavelengths. In this chapter, the foundations of understanding and designing metal nanoshells are laid down. The next section presents an overview of the various types of cancer treatments including nanoscale drug delivery and radiation therapeutic techniques. A comparison between the different nanoscale therapeutic techniques is provided. Section II. c. provides a description of the metal nanoshell and its optical significance. This is then followed by several consecutive sections that investigate the science behind the formation of the nanoshells. The chapter ends in a detailed description of the multi-step process used, in this study, to generate metal nanoshells as well as a summary of the factors affecting the quality of the nanoshells and their optical properties.

II. b. The choice of nanoparticles

Research in the field of nanoscience has provided numerous types of nanoparticles to be utilized in biological applications. The motivation behind the use of nanoparticles in biological applications is a result of the early disease detection and localized treatment ability provided through the use of these particles (Halas, 2005). Although there are various biological applications, this discussion will focus on the applications of nanoparticles in oncology. Figure 1 below illustrates the different types of cancer therapies. Traditional cancer treatments consist of radiation therapy, chemotherapy or a combination of both (www.cancer.gov). In chemotherapy, cytotoxic drugs are injected into the body in order to kill cancerous cells (www.cancer.gov). The problem with this type of therapy is that it affects all proliferating cells within the body equally (www.cancer.gov). As for radiation therapy, it utilizes high energy radiation in the form of x-rays, gamma rays or radioactive sources in order to kill cancer cells. This type of therapy also has numerous side effects the most significant of which is the destruction of healthy tissues alone with cancerous ones in addition to the re-growth of the tumour (www.cancer.gov).

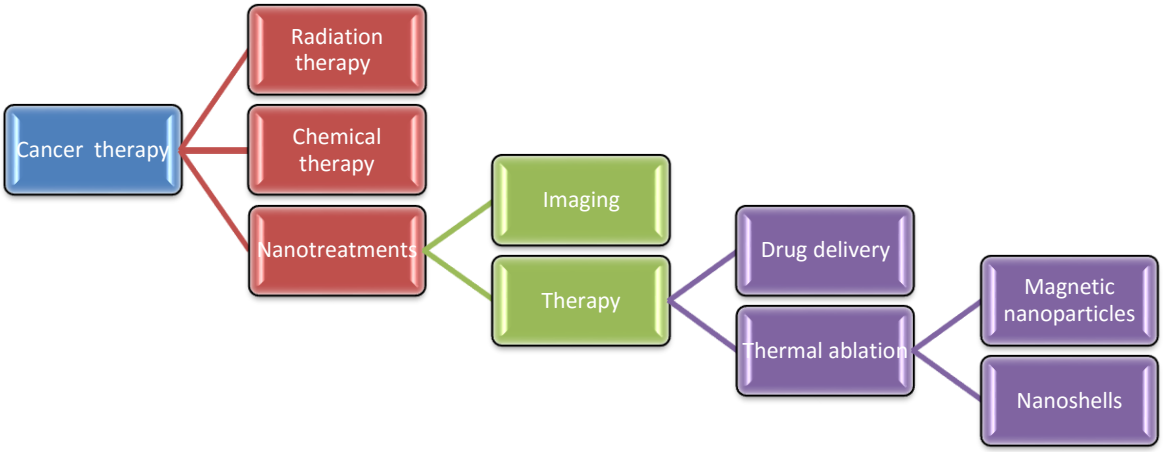

Figure 1 Cancer therapy

Treatments using nanotechnology provide an alternative route to the traditional therapeutic techniques, but most significantly, nanotechnology provides directional, targeted treatments that are localized to the locations within the human body where tumours or cancer cells exist.

There are currently numerous types of nanoparticles or nanostructures that are used in the field of oncology. These nanostructures include: liposomes, dendrimers, quantum dots, magnetic nanoparticles, gold nanoparticles and the gold nanoshells, described in this thesis. Table 1 provides a comparison between the main types of nanoparticles used in medicinal applications. The criteria for comparison are the imaging, drug delivery and radiation therapy that the particles provide.

Liposomes are phospholipid nanovehicles having a bilayer membrane and are used to transport cytotoxic drugs to tumour locations (Lukyanov et al, 2004 and Park, 2001). Dendrimers are spherical nanoparticles made of uniformly ordered branches of polymers that are used in diagnostic and drug delivery applications owing to their structure which allows for the conjunction of various functional groups to their surface (Majoros I, Baker JR, Jr. 2008, Scavicens et al 2008). The use of dendrimers in drug delivery applications has been

demonstrated to reduce the systematic toxicity which is presented by traditional chemotherapy (Majoros I, Baker JR, Jr. 2008).

Quantum dots are nanoparticles made from semiconducting materials such as CdSe, CdTe, CdS, PbSe, ZnS, ZnSe, GaAs, GaN, InP or InAs (Scavicens et al 2008). Quantum dots are designed to absorb light at certain wavelengths, a function of their size, and then re-emit light which is then used to image and indicate the location of a tumour (West et al 2000 and Scavicens et al 2008). The photostability of these fluorophore nanoparticles and their 'tuneable emission spectra' in addition to their resistance to chemical degradation make them favourable contrast agents for imaging applications (Scavicens et al 2008, Lowery, 2007, www.nano.gov).

As for thermal ablation of tumours, this has been achieved using energy resulting from radiofrequency (RF) waves, ultrasounds, magnetic nanoparticles in combination with an oscillating magnetic field, gold nanoparticles and gold nanoshells in conjunction with visible and near-infrared radiation. In RF ablation, an electrode and a ground pad, placed in the vicinity of the tumour, are used to induce its ablation (Gazelle et al and 2000, Lowery, 2007). The RF waves travel from the electrode to the ground pad heating up the tumour and causing its 'retardation' (Gazelle et al, 2000 and Lowery, 2007). This procedure does not result in the complete regression of the tumour; additionally it does not differentiate between healthy and cancerous tissues (Solbiati et al, 1997). The tumour cells outside the area affected by the heat remain active and usually result in the re-growth of the tumour (Gazelle et al, 2000). Similarly, the use of ultrasound in the ablation of tumours is achieved through using ultrasound probes placed in the proximity of the tumour causing cell death by the induction of heat to the healthy and cancerous cells in the proximity of the probes (Hazle et al, 2002 and Lowery, 2007). In this type of therapy, as is the case of RF induced ablation, cancerous cells further away from the probes remain unaffected and result in the re-growth of the tumour (Hazle et al, 2002).

Magnetic nanoparticles, which are made of iron oxides, are also used for imaging and thermal ablation. Research by Ito (Ito et al, 2003) has indicated that this means of thermal ablation does not provide enough heat to the peripheries of the tumour where the particles do not accumulate in large enough numbers(this is because research conducted using magnetic nanoparticles relies on particles directly injected into a specific location within the tumour (Jordon, 2008)) . This results in the persistence of the peripheral

cancerous cells leading to tumour re-growth. Additionally, the use of iron oxide particles necessitates the use a volume of particles equal to approximately 10% the size of the tumour (Hilger et al, 2002 and Lowery, 2007) and it has not yet been demonstrated that there is a means of removing these toxic nanoparticles from the body post-treatment.

In the case of gold nanoparticles and nanoshells, these particles have been determined to be biocompatible by the United States Food and Drug Administration (U.S.F.D.A.). Hence, although research is yet to provide means of 'flushing' these particles out of the body post-ablation, the presence of these particles in the body does not pose the same toxicity posed by iron oxide particles or quantum dots.

As for gold nanoparticles and nanoshells, the main difference between these two types of particles, as shall be discussed in detail at a later stage, is the wider optical tunability displayed by the nanoshells in comparison to gold nanoparticles. Gold nanoparticles present an absorption peak at approximately 520 nm; a peak which overlaps with the absorption by haemoglobin (Hilger et al, 2002 and Weissleder, 2001).

In conclusion, unlike all the nanoparticles and therapeutic techniques discussed in this section, nanoshells provide the capability to detect the presence of cancerous cells at an early stage, deliver cytotoxic drug to tumour locations and to thermally ablate tumours with no re-growth (Halas, 2001). Additionally, nanoshells are biocompatible (U.S.F.D.A.) and have been proven to be cytotoxic only upon irradiation (Lowery et al, 2007). Thermal ablation is a favourable means of eliminating tumours because tumours are more susceptible to damage by heating compared to healthy tissues (Dewhirst et al, 1982 and Crochet et al, 2006). Additionally, gold nanoshells are optically tunable in the visible and near infrared regions of the spectrum where absorption by tissues and cells are minimal.

In the following section the science of nanoshells and the theory behind their formation and success in optical tunability in presented.

Nanoparticle / *Functionality*	Liposomes	Dendrimers	Quantum dots	Magnetic nanoparticles	Gold nanoparticles	Gold nanoshells	References
Imaging	N/A	√	√	√	√	√	Demirovic, 2005 Michaelis, 2006 Schiffelers, 2003 Reynolds,2003
Localized drug delivery	√	√			√	√	
Thermal ablation	N/A	N/A	N/A	√	√	√ $55^{O}C+$	Lowery, 2007
Range of operation/tunability	N/A	N/A	Size dependant		500-600 nm	600-1200 nm	Halas, 2002 Halas, 2005
Toxicity			Highly toxic	Toxic	biocompatible	biocompatible	Aguire, 2003 Halas, 2002
Disadvantages			Toxicity	- Maximum temperatures achieved $43^{O}C$ -Longer treatment required in order to achieve hypothermal temperature requirement in comparison to Nanoshells -Total particle volume needed is approximately 10% the size of the tumour - Peripheral cells remain un affected thus resulting in tumour re-growth -Toxic	- Narrow therapeutic range -Peak absorption overlaps with absorption by haemoglobin -Location of peak absorption is controlled via controlling the amount of particles that accumulate at the tumour site		Ito, 2003 Hilger, 2002 Weissleder, 2001
Advantages	-Can deliver both hydrophobic and hydrophilic drugs to tumour locations -Have been shown to increase drug delivery/concentration to up to 700 times traditional methods					-Wide therapeutic window compared to solid gold particles -Single particle imaging and therapy -Biocompatibility -Cytotoxic only upon irradiation -Surface easily functionalized	Lowery,2005,2007 O'Neal 2004 Loo,2004 Hirsch, 2003,2004 Park, 2001 Noble, 2004

Table 1 Summary of nanoparticles used in cancer treatment

II. c. The science of nanoshells

Due to the small size of nanoparticles, their properties are very different from the properties of their bulk counterpart (Kreibig et al, 1995). The optical and physical properties of nanoparticles within this size regime are what make nanoparticles of interest in various applications were the bulk materials would not be able to function similarly (Kreibig et al, 1995). Additionally, nanoshell dispersions are in essence colloidal dispersions. Thereby, nanoshells are affected by all the factors that affect colloidal solutions. In the following sections, the properties that nanoshells bring to their applications in terms of the effect of their size on their physical properties are portrayed. Additionally, the factors that affect these colloidal dispersions, and in turn our ability to exploit these colloidal properties in the formation of gold nanoshells, are presented.

1. Structure of metal nanoshells

Metal nanoshells, a term coined by Halas in 1998, are nanoscale core shell particles that comprise a dielectric core and a thin metal shell of the order of a few nanometers as illustrated in Figure 2. In Figure 2, the core has a radius of r_1 and dielectric constant $\boldsymbol{\varepsilon}_1$, the surrounding shell has a radius of r_2 and a dielectric constant $\boldsymbol{\varepsilon}_2$ and the embedding medium has a dielectric constant $\boldsymbol{\varepsilon}_3$.

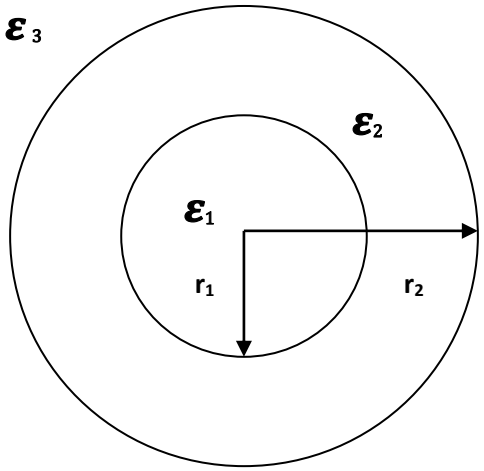

Figure 2 Nanoshell geometry

Nanoshells are unique in that they may be designed so as to allow for the enhancement of electromagnetic radiation in the proximity of the particles through the collective oscillation of the conduction electrons, at resonance conditions. This effect is depicted in Figure 3

(Bohren et al, 1995, Maier et al, 2005) whereby the figure illustrates the extinction cross-section of the particle in comparison to its actual size. Moreover, by controlling the dimensions of the nanoshell, in particular the ratio of the radii of the core/shell the optical properties of the nanoshells may be tuned over the visible and near-infrared regions of the spectrum. The size of the dielectric core determines the wavelength at which the resonance occurs and the thickness of the shell determines the scattering and absorption cross-section of the nanoshell. Figure 4 and Figure 5 below illustrate the effect of varying the geometry of the nanoshell on the position of the resonance and the extinction or total cross-section 'σ_{ext}' (absorption and scattering) of the nanoshells.

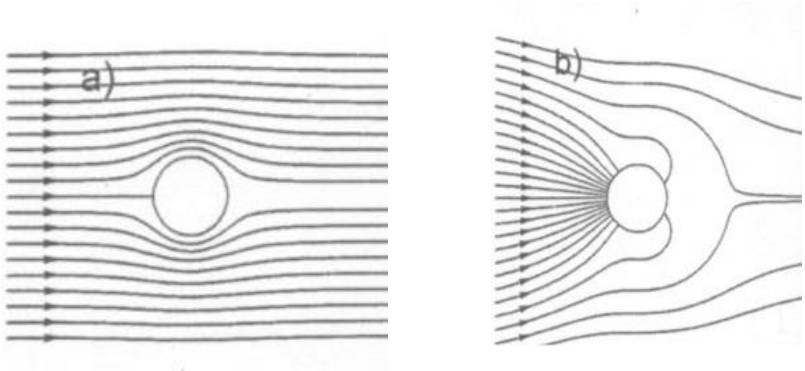

Figure 3 Schematic illustrating electromagnetic field surrounding particle (a) away from resonance condition and (b) at resonance frequency

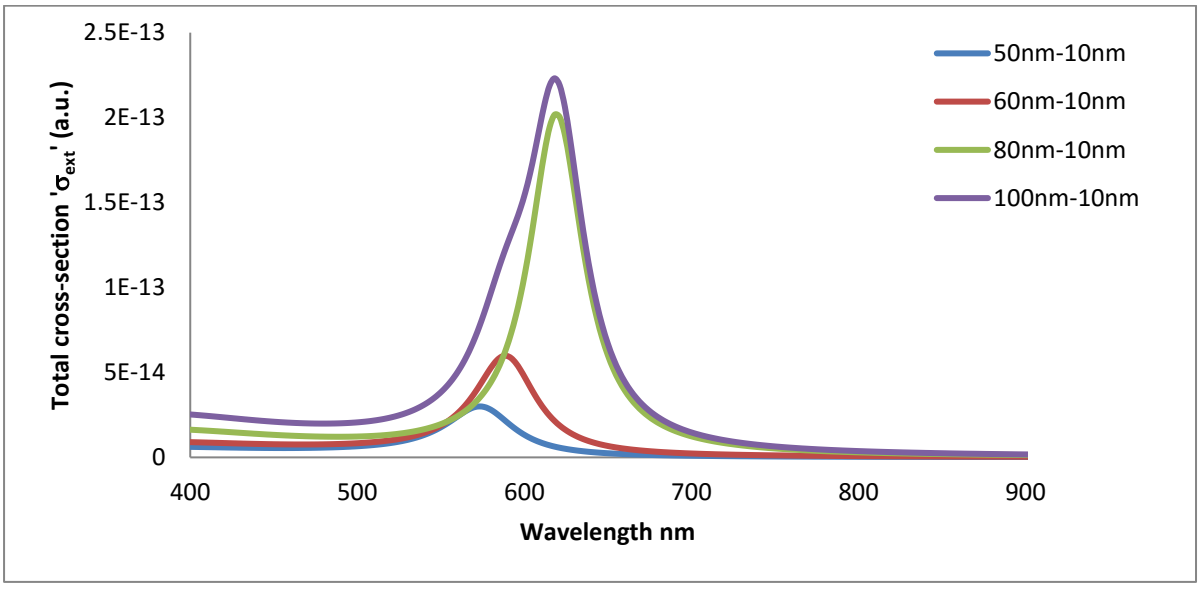

Figure 4 Effect of varying the core diameter of a 10 nm shell

In essence, the smaller the dielectric core the more the resonance is shifter to shorter wavelengths and the thinner the gold shell, more the resonance is shifted to longer wavelengths. Additionally, when the thickness of the shell approaches the diameter of the silica core, the curve resembles that of a solid gold cluster.

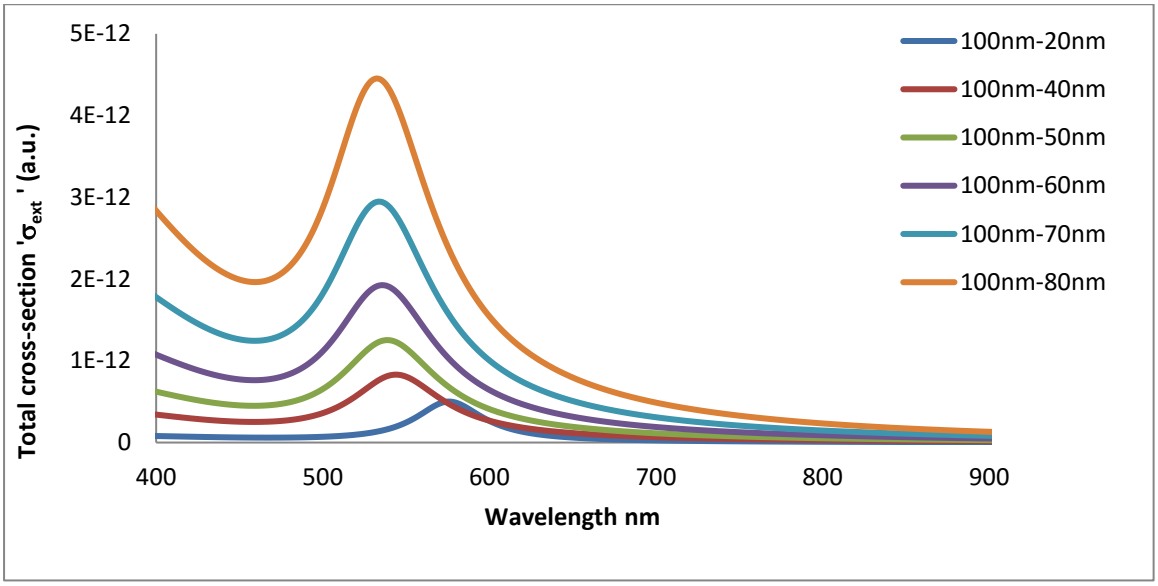

Figure 5 Effect of varying the thickness of a gold shell on a 100 nm silica core

The following section provides detailed accounts of the plasmon resonance and the way in which the optical properties of the nanoshells may be tuned compared to those of the metal nanoparticle of the same size.

2. Plasmons

The plasmon resonance is the collective resonance of the conduction electrons in a metal (Maier, 2007 and Kreibig et al, 1995). At certain frequencies, a function of the metal under consideration, the electromagnetic radiation causes a polarization of the electrons with respect to the positive cores, Figure 6. The coupling of this incident radiation with the polarized electrons results in the oscillation of the electrons with respect to the positive core. This collective oscillation of the conduction electrons is termed plasmon oscillation or resonance and the coupling of the plasmons with the radiation is termed plasmon resonance polariton. It occurs at frequencies that are termed plasmon frequencies. For most metals the plasmon frequencies normally occur at frequencies near UV (Kreibig et al, 1995) and this is the main reason behind the shiny metallic appearance of aluminium, for example.

For noble metals, such as gold, this occurs at visible frequencies thus making gold one of the plasmon material of choice for applications within the visible region of the spectrum.

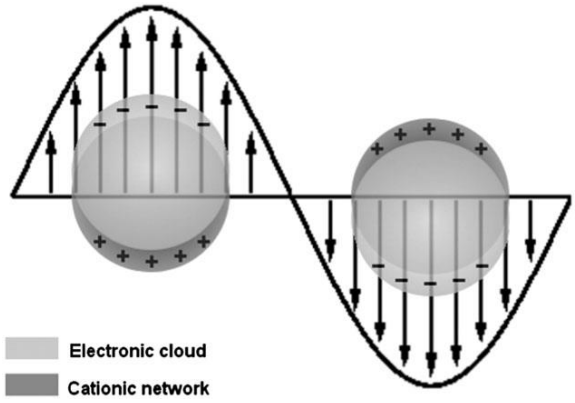

Figure 6 Polarization of nanoparticles with respect to positive core (Moores, 2006)

Gold nanoshells are better than gold nanoparticles in plasmonic applications due to their construction. This is because of the nanoscale shell as rather than the solid particle. This difference may be understood by the plasmon hybridization concept described below.

3. Plasmon hybridization

The plasmon resonance of the metal nanoshells as opposed to the solid metal nanoparticles may be understood by means of the plasmon hybridization model (Norlander et al, 2004, Steele et al, 2007 and Prodan et al, 2003).

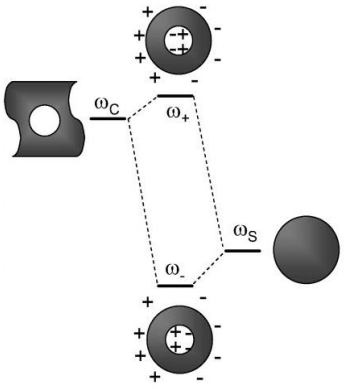

Figure 7 Plasmon Hybridization model (Prodan, 2003)

As previously noted, the incident electromagnetic radiation causes the resonance of the electrons, of the particle, with respect to the positive cores. In the case of the nanoshell, this resonance occurs at both the outer and inner surfaces of the metal shell. Both these resonances cannot exist separately (Prodan et al, 2003); they interact and result in a hybrid

resonance. This hybrid resonance is a result of the bonding or anti bonding of the inner and outer surface plasmons as depicted by Figure 7. This is very similar to the idea of the bonding and anti-bonding molecular orbits (Norlander et al, 2004). The interaction of both the resonances results in a strong plasmon resonance at a lower energy, while the anti-bonding of the resonances results in a higher energy, weaker resonance, Figure 8.

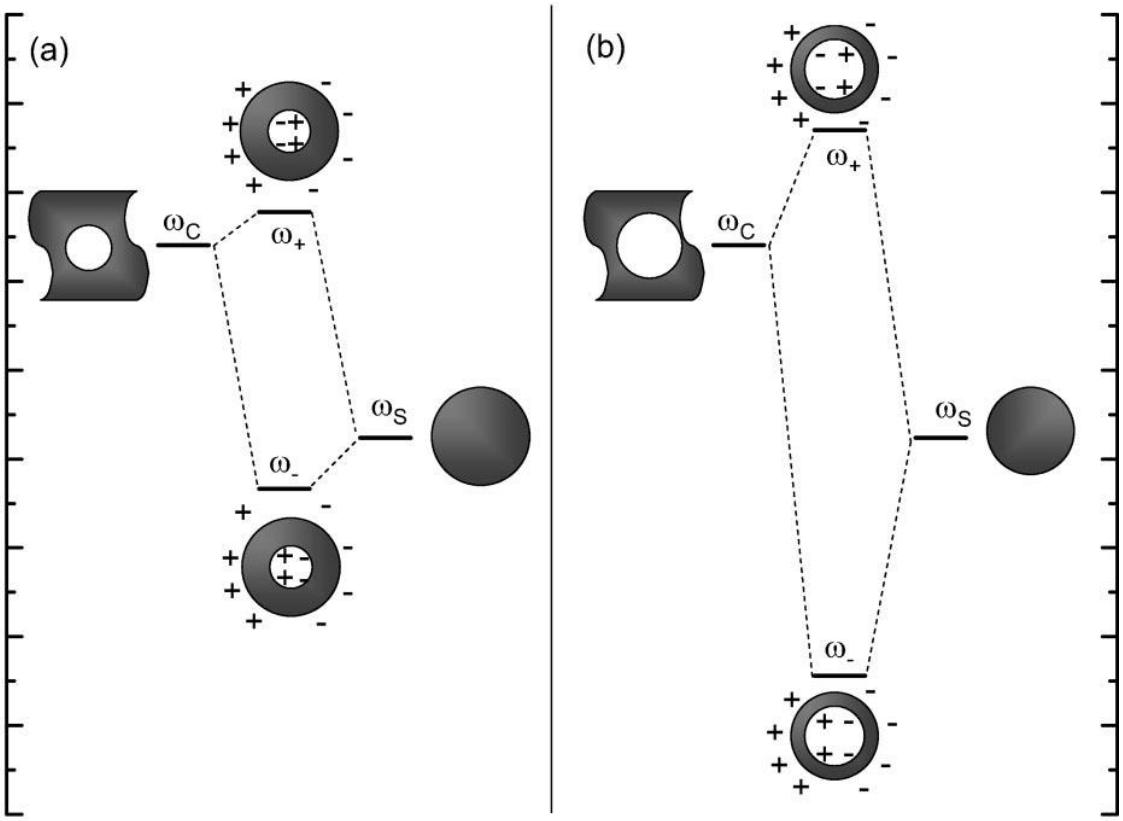

Figure 8 Energy diagram illustrating the plasmon hybridization in a metallic nanoshell for (a) thick and (b) thin shells. ω_c is the resonance of the nanocavity and $\omega_s$is the resonance of the nanosphere (Nordlander et al, 2004).

The pre-eminence of the nanoshell in comparison to the solid metal nanoparticle ensues from this plasmon hybridization theory, which permits the control the resonance of the nanoshell at wavelengths ranging from the visible to the far infrared region of the spectrum (Halas et al, 2003, Prodan et al, 2003 and Nordlander et al, 2004). By controlling the location of the resonance, one is also able to control the wavelength at which the particles absorb or scatter through the control of the particles' dimensions, as is illustrated in Figure 9 and Figure 10. The figures illustrate two different cases. In the first, the nanoshell has a core diameter of 100 nm and a shell thickness of 20 nm. In the second case, the core is 100 nm while the shell is 4 nm. In the case of the thicker shell, the extinction cross-section is dominated by scattering, while in the case of the thinner shell, the extinction cross-section

is dominated by absorption. It is also important to note that in the case of the thinner shell, the magnitude of the extinction cross-section is smaller due to the presence of fewer atoms in the shell in comparison to the thicker shell.

In order to tailor nanoshells with specific resonance conditions, one must be able to predict how the geometry of the gold nanoshell will affect its optical properties and the location and amplitude of the resonance.

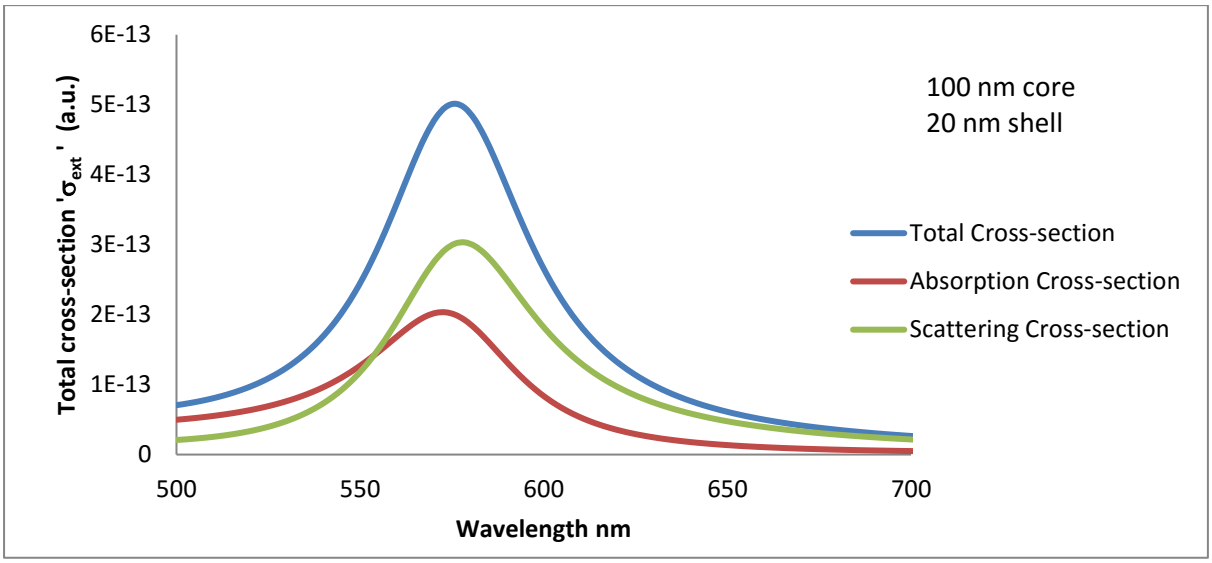

Figure 9 Theoretical Mie Spectrum of a 100 nm core-20 nm shell, predicted using quasi-static approximation (peak at 578 nm)

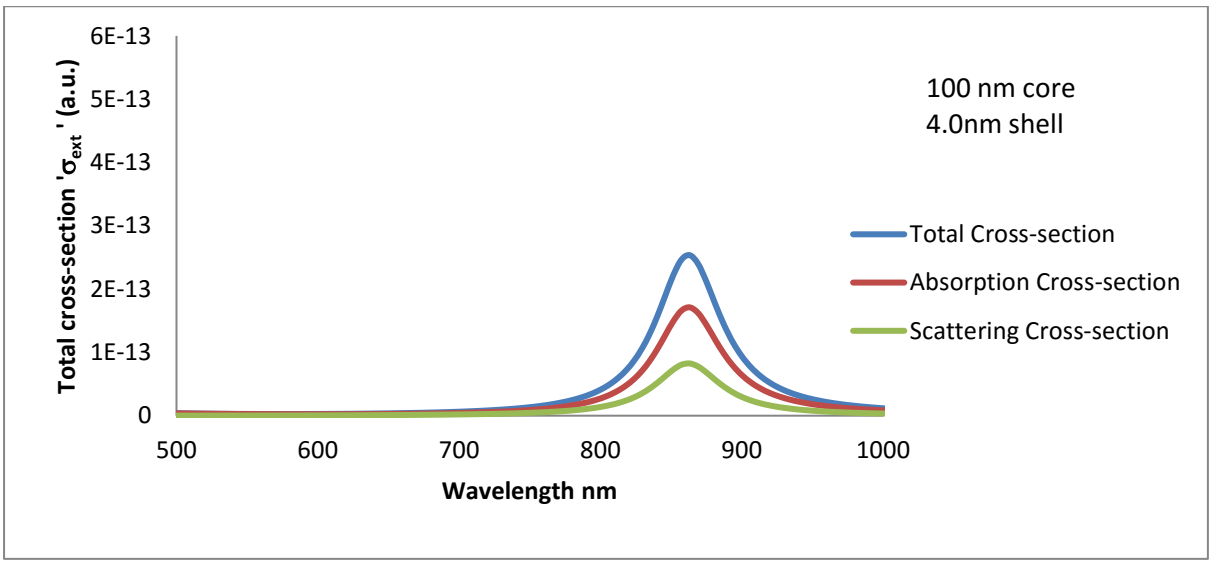

Figure 10 Theoretical Mie Spectrum of a 100 nm core-4 nm shell, predicted using quasi-static approximation (peak at 865 nm)

In other words, it is important to be able to make theoretical predictions of the response of the nanoshells to the incident electromagnetic field. In the section below, on Mie theory and the Quasistatic approximation, an account of the theoretical tools one can use to predict the optical response of metal nanoshells, are provided.

4. Mie Theory and Quasistatic approximation

In 1908, Gustav Mie (Mie, 1908) illustrated the optical properties of spherical nanoparticles with his solution of Maxwell's equations for an isotropic sphere that is embedded in a homogeneous medium. This was followed, several years later, by further solutions by Aden and Kerker (Aden et al, 1951). Aden and Kerkers' solution of Maxwell's equations followed along Mie's solution, but was for the boundary conditions of two concentric spheres, the nanoshell. The idea behind the solution is to match the boundary conditions for the electric and magnetic fields at both the outer surface of the sphere and the outer surface of the shell and to solve Maxwell's equations for those conditions. The solution to the equations yields the absorption and scattering coefficients. Using these coefficients, it is possible to predict the response of the particles to the incident electromagnetic radiation.

The solution enables one to determine the polarization and the scattering and absorption cross-sections for a particle, of a given geometry and dielectric constant, in addition to the intensities of the local fields both inside and surrounding the particle (Kreibig et al, 1995). The relation between the scattering and absorption cross-sections and the loss of the intensity of incident light due to absorption and/or scattering is understood using Equation 1 Equation 2.

$$\Delta I_{\text{abs}} = I_{\text{o}}(1 - e^{-\text{N}\sigma_{\text{abs}}})$$

Equation 1 Loss of incident beam intensity due to absorption

$$\Delta I_{\text{sca}} = I_{\text{o}}(1 - e^{-\text{N}\sigma_{\text{sca}}})$$

Equation 2 Loss of incident beam intensity due to scattering

Equation 1 and Equation 2 present the loss of intensity due to purely absorbing and purely scattering particles using the Lambert-Beer law. N is the number of particles and σ_{abs} and σ_{sca} are the absorption and scattering cross-sections, respectively. In these solutions of, Maxwell's equations, only the dielectric constants of the materials (both core and shell) and the dielectric constant of the embedding medium need to be specified. No other property of

the material is required (Kreibig et al, 1995, Bohren et al, 1998). Both the core and the embedding medium are non-absorbing and the material of the nanoshell is assumed to be non-magnetic (Maier, 2007, Kreibig et al, 1995, Born et al, 1999). The term "extinction cross-section" refers to how the field is dissipated within the volume of the nanoparticle (Hulst, 1981).

- ***Generalized Maxwell's solution***

The solutions to Maxwell's equations were first provided by Mie, but due to the complexity of the solution several approximations have been provided by many scholars. The time-dependent local density approximation (TDLDA) (Prodan et al, 2003) and the vector basis solution (Sarkar et al, 1997) are examples of these solutions. In this study, the quasistatic approximation is adopted as it provides an approximation of the response of the nanoshells that is appropriate for the size regime used in this research. For larger particles it would not be acceptable due to the retardation effects that come into play when the size of the particle becomes comparable to the size of the incident radiation (Keribig et al, 1995). In this study, the term 'retardation effects' is used to refer to the spatial variation of the incident field within the volume of the particle.

- ***Quasistatic approximation***

The quasistatic approximation is a solution of Maxwell's equations in which the spatial variation of the electromagnetic field is neglected while taking into account the temporal dependence of the field (Keribig et al, 1995). Although this approximation results in a significantly simplified calculation, it provides an accurate approximation of the position of the resonance.

Other assumptions made within this approximation are that the nanoshells are perfectly spherical and that dipole-dipole (particle-particle) interactions are negligible. For the geometry of the nanoshell in Figure 2, the quasistatic approximation yields the following equation for the polarizability, α, (Averitt et al, 1999), of the nanoshells

$$\alpha = 4\,\pi\,\varepsilon_{\mathrm{o}} r_2^{\,3}\,\left\{\frac{\varepsilon_2\varepsilon_{\mathrm{a}} - \varepsilon_3\varepsilon_{\mathrm{b}}}{\varepsilon_2\varepsilon_{\mathrm{a}} + 2\varepsilon_3\varepsilon_{\mathrm{b}}}\right\}$$

Equation 3 Polarization, quasistatic approximation

where, $\boldsymbol{\varepsilon}_o$ is the permittivity of free space

$$\varepsilon_a = \varepsilon_1(\mathbf{3} - \mathbf{2}\boldsymbol{P}) + \mathbf{2}\varepsilon_2 P$$

$$\varepsilon_b = \varepsilon_1 P + \varepsilon_2(\mathbf{3} - \boldsymbol{P})$$

$$P = 1 - (\frac{r_1}{r_2})^3$$

Resonance occurs as the denominator in Equation 3 approaches zero, when $\boldsymbol{\varepsilon_2\varepsilon_a = 2\varepsilon_3\varepsilon_b}$. Thus resonance occurs at the point of maximum polarization.

The scattering cross-section is given by (Averitt et al, 1999)

$$\sigma_{\text{abs}} = \frac{128\,\pi^5}{3\lambda^4}\,\varepsilon_3{}^2 r_2{}^6 \left|\frac{\varepsilon_2\varepsilon_{\text{a}} - \varepsilon_3\varepsilon_{\text{b}}}{\varepsilon_2\varepsilon_{\text{a}} + 2\varepsilon_3\varepsilon_{\text{b}}}\right|$$

Equation 4 Scattering cross-section, quasistatic approximation

and the absorption cross-section is given by (Averitt et al, 1999)

$$\sigma_{\text{abs}} = \frac{8\,\pi^2\sqrt{\varepsilon_3}}{\lambda} r_2{}^3\,\text{Im}\left(\frac{\varepsilon_2\varepsilon_{\text{a}} - \varepsilon_3\varepsilon_{\text{b}}}{\varepsilon_2\varepsilon_{\text{a}} + 2\varepsilon_3\varepsilon_{\text{b}}}\right)$$

Equation 5 Absorption cross-section, quasistatic approximation

In this study, the above equations have been adopted in order to estimation of the location of the resonance. The absorption spectra depicted within this thesis are the extinction spectra σ which is the summation of σ_{sca} and σ_{abs}. Values of dielectric contants of gold, both real and imaginary, where calculated using the values of the optical constants of gold 'n' and 'k' obtained experimentally by Johnson (Johnson et al, 1972). The table containing these values is presented in Appendix C. In this study, the dielectric constant of silica, $\boldsymbol{\varepsilon}_1$, is considered to be 1.5 and that of embedding medium, $\boldsymbol{\varepsilon}_3$, is considered to be 1.3.

5. The stability of colloids

The following section details the factors affecting the stability of colloidal systems and in turn nanoshells dispersions. The surface charge on colloidal particles and its effect on the stability of these colloids as well as the electric double layer and the influence of ions on the Debye length are discussed.

Due to their high ratio of surface area to volume, colloidal dispersions are at a higher state of free energy, when compared to their bulk counterparts. As a result, colloidal dispersions are continuously striving to attain the least free state of energy by eliminating the 'colloidal state' (Everett, 1988). In doing so, colloids tend to aggregate and form larger particles that are of a lower free energy. In order to promote colloidal stability, an energy barrier must be created so as to prevent the dispersion from aggregating. There are two basic means of attaining the stability of a colloidal dispersion. Steric stabilization and charge stabilization (Everett, 1988). The stability of the colloidal dispersions, in this study, is attained through charge stabilization by using the charge on the surface of the colloids as a means of preventing the colloids from coagulating. The principles of charge stabilization are discussed below.

- ***The surface charge and the electric double layer:***

The functional groups on the surfaces of the particles, the silica core and the gold seeds, play an important role in both the stability of the particles and their attachment to other particles. Surface groups of particles in which the surfaces contain basic groups ionize in solution forming a positive charge on their surface. The dissociation of surfaces containing an acidic group, on the other hand, results in a negative surface charge. These effects are depicted in Figure 11 and Figure 12, respectively.

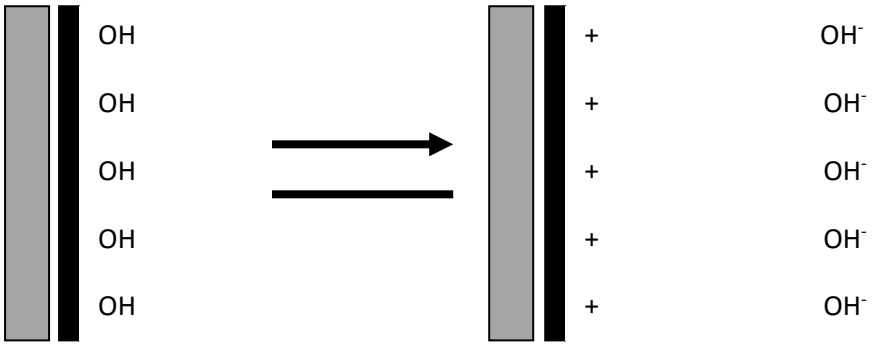

Figure 11 A positively charged surface resulting from the ionisation of a basic group (Hunter, 1993)

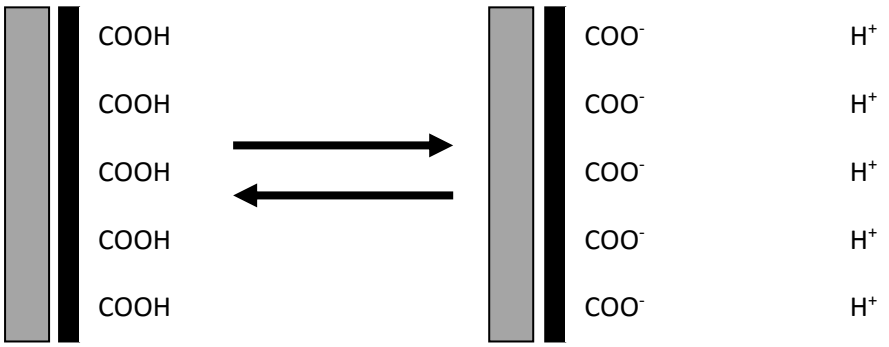

Figure 12 A negatively charged surface resulting from the ionisation of an acidic group (Hunter, 1993)

The magnitude of the surface charge varies as a function of the strength of the acidic or basic surface functional group. It is possible to vary this strength as a function of pH. As a consequence, acidic pHs reduce or suppress the charge of acidic functional groups, while basic pHs reduce the strength of the surface charge of basic functional groups (Everett, 1988); conversely, acids protonate basic surface groups.

Low pH values: $NH_2 + H^+ \rightarrow NH_3^+$ (Hunter, 1993)

High pH values: $COOH + OH^- \rightarrow COO^- + H_2O$ (Hunter, 1993)

- ***Derjaguin, Landau, Verwey and Overbeek theory (DLVO theory)***

  Within a colloidal solution, the colloids are subjected to repulsive and attractive forces, the sum of which, together with the potential of the solution, defines the potential of the colloidal solution.

$$\boldsymbol{V_T = V_A + V_R + V_S}$$

Where,

V_T is the total energy, V_A is the contribution due to attractive forces, V_R is the contribution due to repulsive forces and V_S is the potential energy of the solution. V_S is negligible in comparison to the repulsive and attractive potentials. The attractive and repulsive potentials are defined as follows

$$\boldsymbol{V_A = -A(12\pi D^2)}$$

Equation 6 Attractive potential between colloidal particles in a dispersion (Malvern Instruments Ltd)

$$V_R = 2\pi\varepsilon a\xi^2 e^{-\kappa D}$$

Equation 7 Repulsive potential between colloidal particles in a dispersion (Malvern Instruments Ltd)

In Equation 6 and Equation 7, 'A' is Hanmaker constant, 'a' is the radius of the particle, 'π' is the permeability of the solvent, 'ξ' is the zeta potential and 'D' in the inter-particle distance.

Figure 13 illustrates the relation between the charge on the surface of a particle and the zeta potential. In turn, the figure also illustrates the electric double layer which surrounds colloidal particles in solution. The electric double layer surrounding a colloidal particle is a result of the ionization of the surface group whilst the particle is in solution. As the term implies, the electric double layer consists of two layers: the stern layer, which is closely bound to the surface, and the diffuse layer, which is less closely bound to the surface (Hunter, 1993).Figure 14 illustrates the relation between the attractive van der Waal forces (V_A) and the repulsive forces caused by the electric double layer (V_R) and resulting in a net energy barrier preventing the particles from coagulation. The height of this barrier, the energy required to overcome the interparticle forces resulting in their stability, may be reduced, as illustrated in Figure 15, by adding ions to the dispersion.

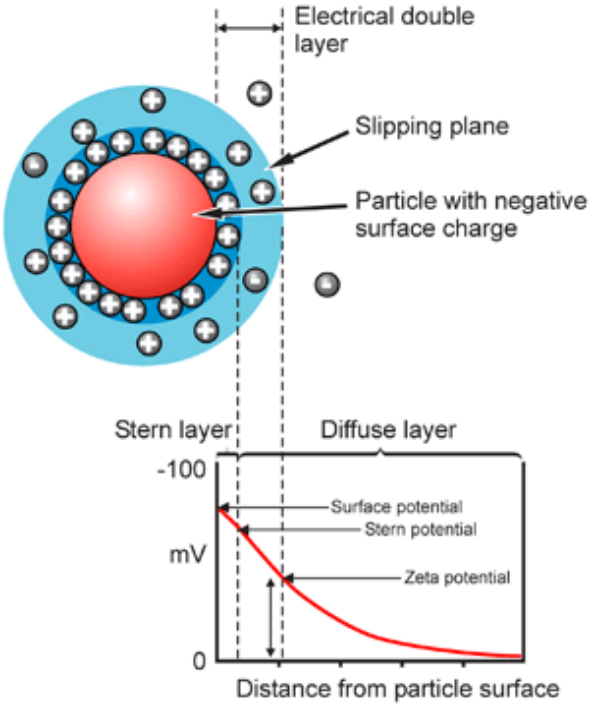

Figure 13 Schematic representation of zeta potential (Malvern Instruments Ltd)

As the number of ions in a colloidal solution is increased, the electric double layer is compressed and reduced, and vice versa. The compression of the double layer results in the reduction of the repulsive forces and the particles are able to come closer to one another.

In the presence of the secondary minimum, Figure 15, as a result of the compression of the electric double layer, the mere collision of particles with one another due to their motion may cause them to coagulate (Everett, 1988).

A measure of the thickness of the electric double layer is the Debye length.

$$\boldsymbol{\kappa^{-1} = \frac{10}{\sqrt{I(mM)}}}$$

Equation 8 Debye length ()

where

κ^{-1} debye length (nm)
I ionic strength (mM or mmol/L)

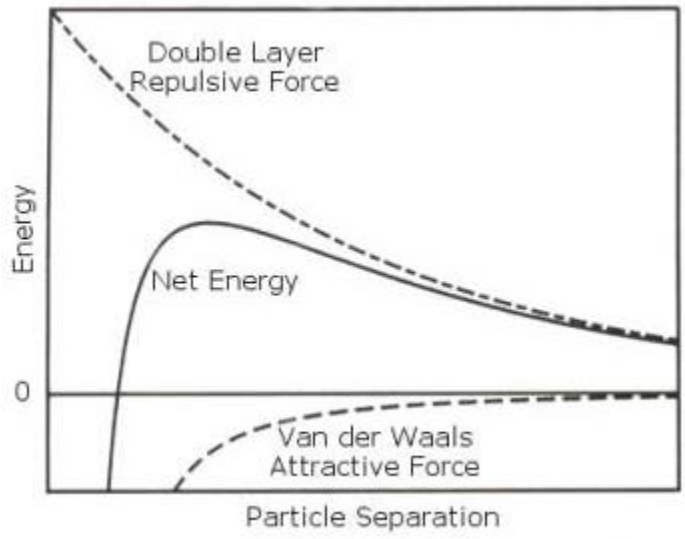

Figure 14 Potential energy of colloidal dispersion versus particle separation (Everett, 1988)

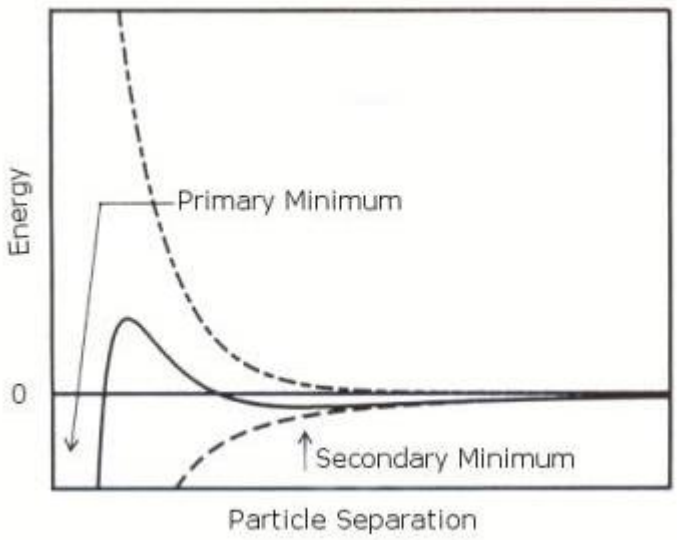

Figure 15 Formation of a secondary minimum due to the addition of ions to the dispersion (Everett, 1988)

6. Making gold nanoshells

The following sections describe the steps of making gold nanoshells, starting with the silica core and ending with the complete gold shell. The factors and parameters that influence the different stages of the nanoshell formation are also presented. Briefly, the process involves attaching of seed gold particles (2 nm gold colloids) to the surface of the silica and then using these 'seed particles' as nucleation sites for the growth of a continuous gold shell. Although the process seems straightforward, there are many factors that come into play and thereby affect the quality of the final product. Details of this process are outlined below. Details of the quantities and materials used to make nanoshells, in this study, are presented in Appendix A.

STEP I: Silica core

The first step of nanoshell formation is to make the dielectric core. The importance of having a dielectric core stems from the plasmon resonance perspective. The presence of a dielectric material in contact with the gold allows for the confinement of the resonance within the spherical geometry of the nanoshell. This construction gives rise to a restoring force which causes the sustained oscillation of the electrons in the nanoparticle (Maier, 2007).

The use of silica has been favoured over other dielectric material as the chemistry of making monodisperse, spherical silica nanoparticles is well known (Stober et al, 1967, Halas, 1999). Moreover, the surface functionalization of silica using organosilane is an equally established process (Badley et al, 1990). In the following sections, the importance of this property of silica will be discussed. Silica also has a low Hanmaker constant (Kandpal et al, 2007). This property of silica is very important as it imparts silica with its high resistance to coagulation (Kandpal et al, 2007). Another important property of silica is its chemical inertness, making it stable and unaffected by the oxidation or reduction reactions that may occur at its surface (Kandpal et al, 2006).

- ***The Stober method for silica growth***

Monodisperse silica colloids are grown in accordance with the Stober method (Stober et al, 1967). This involves the reduction of tetraethoxysilane, TEOS, ($Si(C_2H_5O)_4$) in the presence of alcohol and with the use of ammonia as a catalyst in the reaction (Stober et al, 1967 and Hirsch, 2003). This growth takes place in accordance with the reactions

indicated in Equation 9 below. This method affords monodisperse, amorphous silica particles the size of which is a function of the amounts of the reagents used (Hirsch et al, 2003).

$$Si(C_2H_5O)_4 + 4H_2O \rightarrow Si(OH)_4 + 4C_2H_5OH$$

$$Si(OH)_4 \rightarrow SiO_2 + 2H_2O$$

Equation 9 Formation of silica nanoparticles from TEOS (Kandpal et al, 2007)

Increasing the concentration of TEOS, in the alcohol, yields larger silica colloids; conversely its reduction leads to the formation of smaller silica colloids.

STEP II: Functionalization of silica

The Stober process, summarised above renders silica particles with a negative surface charge. In order to allow for the attachment of the seed gold particles, which also have a net negative charge on their surfaces, to the silica particles, the charges on the surfaces of the particles must be modified. Keeping in mind that in order to grow the continuous gold shell, the bond between the gold and the silica must be strong, is not sufficient for the attachment to be merely the result of electrostatic attraction. A strong attachment between the gold and the silica may be achieved by attaching a molecule on the surface of the silica that will form a covalent bond with the gold. This may be achieved by attaching a functional group on the surface of the silica colloids. It is preferable for the terminus of the functional group to have an electronegativity comparable to that of the gold. In this research, this has been achieved by functionalizing the surface of the silica colloids with 3-aminopropyl-trimethoxysilane (APTMS). This functionalization results in the attachment of an amine functional group on the surface of the silica colloids. Other functional groups such as aminopropylsilane, APS, and 3-mercaptopropyltriethoxysilane (MPTES) have been investigated by others (Oldenburg et al, 1999). However, the use of the MPTES has been avoided in this study because of the thiol bond that would result on the surface. This is because although the gold would attach, due to the affinity of the gold – sulphur bond, the sulphur would result in the contamination of the gold, as a result of that affinity (Duff et al, 1993).

Figure 16 and Figure 17 illustrate the APTMS molecule and the attachment of the APTMS to the surface of the silica.

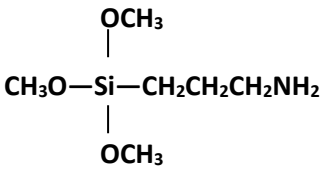

Figure 16 APTMS molecule

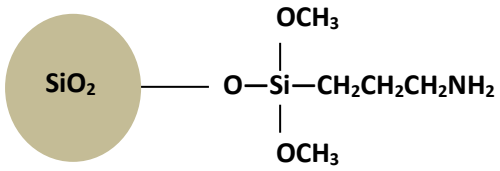

Figure 17 Silica nanoparticle functionalized with APTMS

STEP III: Ultrafine gold nanoparticles

The third step of the nanoshell formation process is the formation of the ultrafine gold sol. The seed gold colloids to be attached to the surface of the silica are of utmost importance to the nanoshell formation process. The final nanoshell size and morphology is significantly affected by the size of these seed particles, as will be shown later.

The seed particles are approximately 2 nm in size and are formed via the reduction of a gold salt, gold chloride, in solution (Duff et al, 1993). The gold chloride is formed by dissolving aurochloric acid in deionized water. The gold sol that is formed is largely dependent not only on the concentration of the reagents, but also on the reducing agent used in the sol formation. For example, using sodium citrate reduction affords citrate-capped gold sol and is performed at a temperature of $100^{O}C$ (Frens, 1973). This method of forming gold colloids yields particles having a negative surface charge. Similarly, Tetrakis hydroxyphosphonium chloride (THPC)-reduced gold colloids result in gold colloids that are THPC-capped and also have a negatively charged surface. The reasons for using THPC as a reducing agent, in this study, are several. Firstly, the purity of the gold shell has a significant effect on the plasmon resonance on the nanoshells (Kreibig et al, 1995). It is thus very important that the seed particles used in the formation of the shell are also pure gold sol. It is recommended that sulphur-containing reducing agents are not used, as the resulting gold particles are thought to be extensively contaminated with sulphur (Duff et al, 1993). For this reason, reducing agents such as sodium thiocyanate were avoided. Experiments by Baker and Usher (Baker et

al, 1940) indicate that the use of phosphine, and its compounds, as reducing agents for the formation of gold sol results in the formation of gold particles of much higher purity in comparison to the use of sulphur-containing reducing agents, which are known to form gold-sulphide particles (Duff et al, 1993). Secondly, THPC, in its partially hydrolyzed form, is known to act as a primary nucleating agent in the formation ultra fine gold particles of high concentration (Duff et al, 1993). The process takes place at room temperature, thus avoiding the high temperatures and the prolonged boiling that are necessary in the formation of sodium-citrate-reduced gold sol. Another reason for the selection of TPHC as a reducing agent is the suitability of phosphine capped gold nanoparticles in the treatment of cancer, as shown in current research (Berners-Price et al, 2006, and Fricker et al, 1996).

Tetrakis hydroxyphosphonium chloride gold:

The chemical formula of THPC is $P(CH_2OH)_4^+ Cl^-$. THPC is initially reacted with sodium hydroxide, NaOH, yielding an active reducing agent, formaldehyde, following the formula indicated in Equation 10.

$$P(CH_2OH)_4^+ + OH^- \longrightarrow P(CH_2OH)_4^+ + CH_2O + H_2O$$ (Duff et al, 1993)

Equation 10

$$P(CH_2OH)_3 + 2H_2O \longrightarrow O_2P(CH_2OH)_3 + 2H_2$$ (Duff et al, 1993)

Equation 11

The second step of the reaction is to reduce of the gold ions with formaldehyde. The newly formed gold colloids are protected by means of the capping agent produced through excessive hydrolysis, as shown in Equation 11.

$3HCHO + 9OH^- \rightarrow 3HCOO^- + 6H_2 + 6e^-$
$2Au^{+3} + 6e^- \rightarrow 2Au$

$2Au^{+3} + 3HCHO + 9OH^- \rightarrow 2Au + 3HCOO^- + 6H_2$

Equation 12

Although the mechanism by which gold is reduced in this reaction is not well understood (Duff et al, 1993), it is debated (Baiker et al, 1994), from the known chemistry of phosphine (Hoffman et al, 1930, Berners-Price et al, 2006 and Fluck et al, 2006), that the 2nm gold colloids that are formed may contain phosphorus. In this study, I have adopted the view that the phosphonium-gold bonding may only be an intermediate form which is eliminated when

the complete gold nanoparticles are formed and as the gold sol ages. The phosphonium becomes merely a protective, capping layer on the surface of the gold. In this research it is thought that the gold is reduced by the formaldehyde in accordance with Equation 12, thus leading to the formation of pure gold colloids.

STEP IV: *Decoration of the silica core with gold:*

'Gold decorated silica' (Halas) is a term that refers to the silica core particles with the 2nm gold nanoparticles attached to them. The purpose of the 2nm gold particles is to act as nucleation sites for the growth of the gold shell.

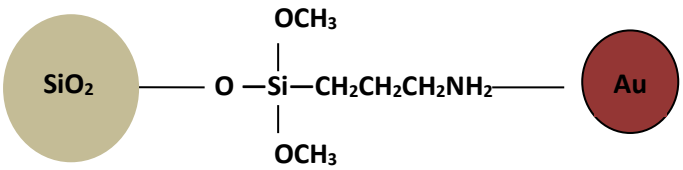

Figure 18 Attachment of the 2nm gold colloid to the surface of the silica via the APTMS molecule

The attachment of the 2 nm gold colloids to the silica core is initially an electrostatic attraction between the particles that results in the coordination of electrons between the functional groups, on the surface of the silica, and the terminal groups on the surface of the gold, as depicted in Figure 18. As previously mentioned, the chemical reaction by which the gold particles are made renders the surface of the particles negatively charged. The functionalization of the silica particles with the amine groups through the use of the 3-aminopropyltrimethoxysilane (APTMS) renders the surface of the silica positively charged. The mere presence of the positively and negatively charged colloids in solution results in an electrostatic attraction between the oppositely charged colloids. The efficiency of grafting of the gold seed particles onto the surface of the silica is controlled by two factors, the ratio of gold to silica particles in the solution and the strength of the surface charges on each of the colloids, the *zeta potential*.

STEP V: Gold shell growth

The final step of the nanoshell growth process is the formation of a continuous gold shell on the surface of the silica. This process involves further reduction of gold, from solution, onto the surface of the silica in order to form a continuous gold shell. This reduction involves the use of the gold particles, decorating the silica, as nucleation sites. Various reducing agents may be used for this process. In this study, formaldehyde was used as the reducing agent.

Other possible reducing agents could have been sodium borohydride and carbon monoxide (Halas, 2002). However, for this final step of the nanoshell formation process, it was important to choose a reducing agent that would enable the formation of a continuous shell. The rate of the further reduction of the gold onto the surface of the decorated silica particles is of importance; the slower the reduction of the gold onto the silica, the more complete and the more uniform the surface of the nanoshell (Brinston et al, 2008). Sodium borohydride was thus avoided because it is a very strong reducing agent that would not allow the formation of shells that were as smooth as those formed using formaldehyde (Hirsch et al, 2005).

Chapter Summary

Gold nanoshells are colloids whose formation through wet chemistry techniques renders particles that have a tuneable plasmon resonance. The formation of these shells is a multistep process whereby 2 nm gold colloids are attached to a silica core, the size of which dictates the location of the resonance. The attachment may be altered by controlling of the pH of the colloidal dispersion. The gold shell is grown by reducing gold salt in solution. The thickness of the shell is mainly a function of the amount of gold ions in solution.

Chapter III: Results and Discussion

Introduction:

This chapter describes the experiments that were carried out within the scope of this research. Detailed experimental procedures including the materials, methods, equipment utilized for the experiments, as well as a description of the characterization techniques are provided in Appendix A.

The aim of this study was to produce gold nanoshells that can be used for biological applications, with an emphasis on their use for the thermal ablation of cancer cells. The nanoshells must therefore have (1) plasmon resonance peaks in the near infrared region of the spectrum and (2) the thinnest shells possible so as to provide the greatest possible absorption (refer to the extinction spectrum in Figure 10).

In this study, these are the criteria used to define the quality of the nanoshells. This means that, in this study, nanoshells having a plasmon peak further into the near infrared region of the spectrum are considered of higher quality. For example, a dispersion of nanoshells having a plasmon peak at 780 nm is considered of higher quality compared to a dispersion having a peak at 690 nm. As for the seed particles, in this study, the quality was determined by the number of gold colloids decorating the surface of the silica because the more the gold on the surface of the silica the more uniform the shell and the fewer the gold colloids the more the resultant voids on the surface of the shell.

In reviewing the literature available on the formation of gold nanoshells, a summary of which has been provided in Table 2 , it has been found that, although the procedure for the growth of gold nanoshells has been well established, since 1951, by Aden and Kerker (Aden et al, 1951), the information available from various research groups is not sufficient to allow the particles to be formed. For instance, most research groups indicate formation of THPC, 2 nm gold colloids in accordance with Duff et al and silica in accordance with Stöber et al. Very little detail, however, is provided as to the ratio of gold to silica used in the formation of the seed particles. An exception is the recently published paper by Brinson et al, which indicates the use of 40 ml of THPC gold, formed in accordance with Duff et al, to 300 ul of (Stober) silica. Attempts to follow this protocol were not successful, as the extremely high ratio of gold to silica resulted in the coagulation of the seed particles possibly due to depletion interactions. Also, the amounts of gold presented by Kim et al

were found to be unnecessarily high, resulting in difficulty removing excess reagents. It was thus crucial to optimize (design) a protocol that would enable the formation of the required nanoshells.

Preliminary experiments led to the conclusion that within the five-step process of nanoshell formation described in Chapter II, several factors affect the final quality of the nanoshells, as depicted in Figure 19. Other experiments also indicated that the quality of the seed particles (gold-decorated silica particles) was the most significant factor affecting the final quality of the nanoshells.

A significant amount of the experimental work was thus dedicated to evaluating of the effect of seed particles on the nanoshell formation. The aim of this section of the investigation was to determine the optimum seed particle conditions that enabled the formation of good quality nanoshells. Equally, all other factors affecting the five-steps of the process were assessed and optimized.

Researcher	Core : Shell	Conditions		Optical spectrum	
		Effect of pH	Ratio of Au : SiO_2	Magnitude of absorption peak	Spectral width
Averitt et al	Gold sulphide	Not evaluated			
Westcott et al		Not evaluated			
Park et al	80: not mentioned	3.1,7,9.7,10.3,12.5	Not stated	Estimated to be 1.63(pH3.1), 1.4(9.7)	
Graf et al	120	Not evaluated			
Kim et al	100:10	Not mentioned	11-12 ml of Duff gold, no explicit mention of amount of silica	Estimated to be 1.66	247 nm
Brinson et al		Not mentioned	40 ml : 300ul	Not indicated	No units indicated on axes

Table 2 Summary of nanoshells in the literature

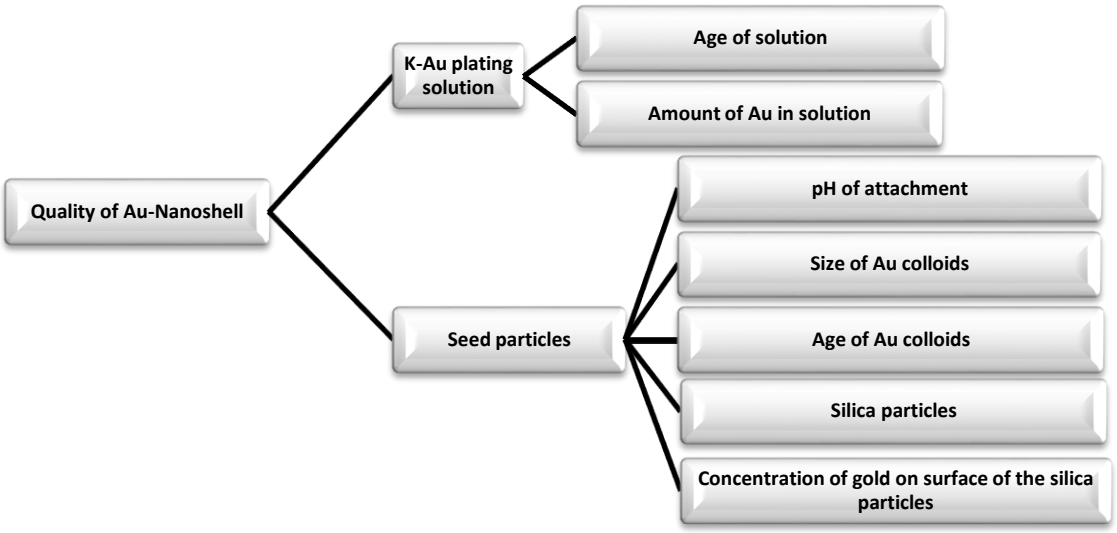

Figure 19 Hierarchy of parameters affecting the quality of gold nanoshells

The structure of this chapter is to provide a stepwise analysis of the nanoshell formation process and an outline of the factors affecting each step. Particular emphasis is provided on the formation of the seed particles. It was expected that the seed particles, being of a colloidal nature, would be affected by the pH at which the gold and silica colloids were attached to one another. It was also expected that the higher the ratio of the gold colloids to the silica, during seed particle formation, the greater the coverage of the gold on the surface of the silica.

This chapter is divided into four sections; the first section on 'seed particles', depicts the results obtained through experimental investigations of the effect of the seed particles on the quality of the nanoshells. The second section details the effect of the plating solution on the formation and completion of nanoshells. The third section summarizes the effect of various other conditions (size of silica, stirring and centrifuging) on the formation of monodisperse nanoshells. The final section provides a discussion of the UV-Vis spectra obtained for different nanoshells and outlines the reasons why the spectra deviate from theoretically obtained spectra. The chapter concludes with a summary of the findings from the experiments results, a set of proposed optimum conditions for nanoshell formation and a summary of the various factors found to positively / negatively affect the formation of high quality nanoshells.

III. a. Seed particles

This section presents a detailed review of the formation of the seed particles with the aim of optimizing their formation.

A review of the literature available on the heterocoagulation (Furusawa et al, 1991 and Li et al, 2002) of colloidal solutions leads to the conclusion that one of the factors affecting the quality of the seed particles is the pH value at which the attachment of the gold to the silica is carried out. Preliminary experiments indicated that the ratios of gold to silica, as used in the seed particle formation presented in the literature, caused several problems:

1. Excess gold had to be completely removed prior to proceeding with nanoshell formation. This was achieved through at least 5 wash cycles (Described in Appendix A).
2. The consecutive wash cycles resulted in the fusion of a percentage of seed particles to one another. This was an irreversible process resulting in the formation of large seed particles.
3. Failure to remove all excess gold caused the formation of gold clusters in the nanoshell dispersion and in several cases hindered the formation of complete nanoshells

As a result of the preliminary experimental work, undertaken in this study, it has been found necessary to investigate the effect of the pH of attachment on the formation of the seed particles. Additionally, it was found necessary to optimise the seed particle formation process by determining the optimum ratios of gold to silica that are required to form complete nanoshells without the need to resort to the use of the excessive amounts of gold that are used in the experiments described in literature.

Figure 20 presents a schematic of the nanoshell formation process followed in this study.

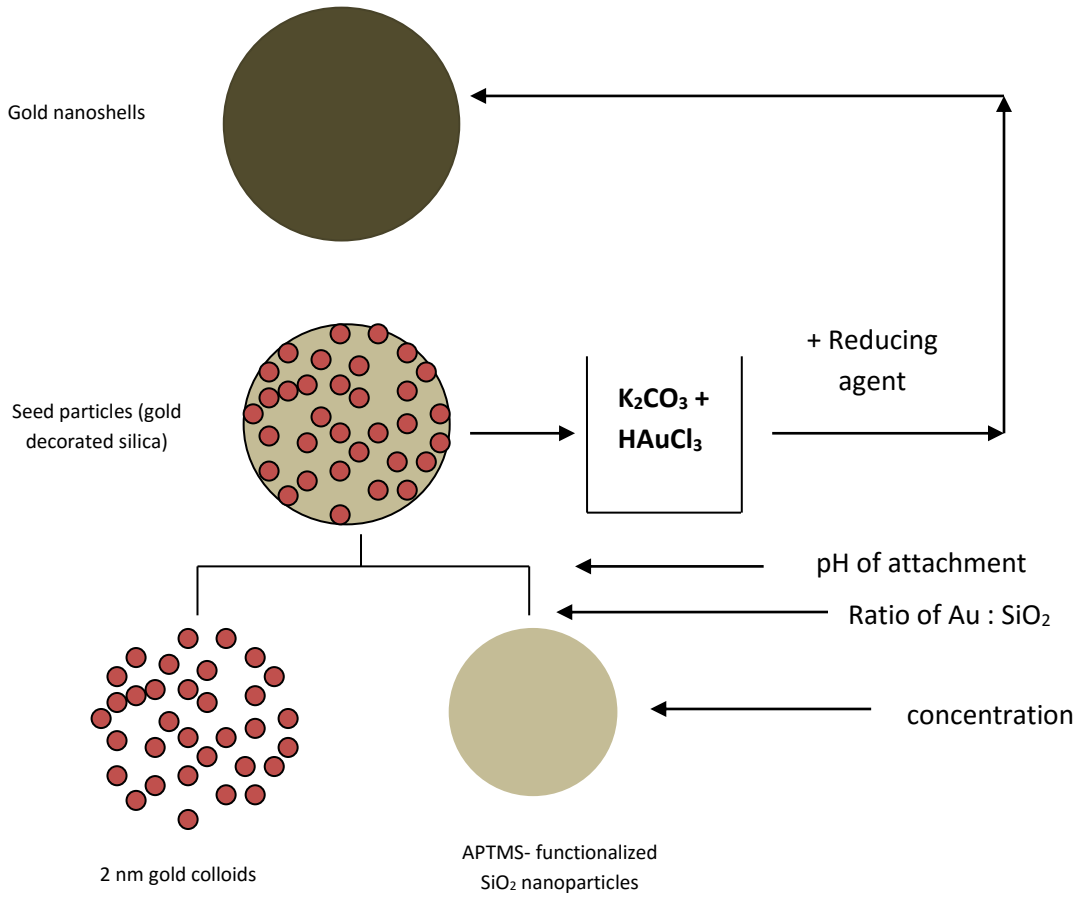

Figure 20 Schematic of the steps of nanoshell formation

The following sections provide a presentation and discussion of the factors that affect the formation of the seed particles, starting with the silica cores and ending with the gold decorated silica particles.

1. Silica nanoparticles

The first step of nanoshell formation is preparing the core particles. In this study the silica nanoparticles were purchased from Kisker. The 100 nm silica particles had a size distribution ranging between 66.5 and 185.1 nm as determined through dynamic light scattering and as presented in Figure 21. The size range of the silica particles was verified using SEM imaging so as to enable the determination of the shell thickness at a later stage. The size of the particles was determined according to the method explained in Appendix A.

This wide variation in size distribution was found to have a significant impact on the optical properties of the particles as will be discussed later in this Chapter.

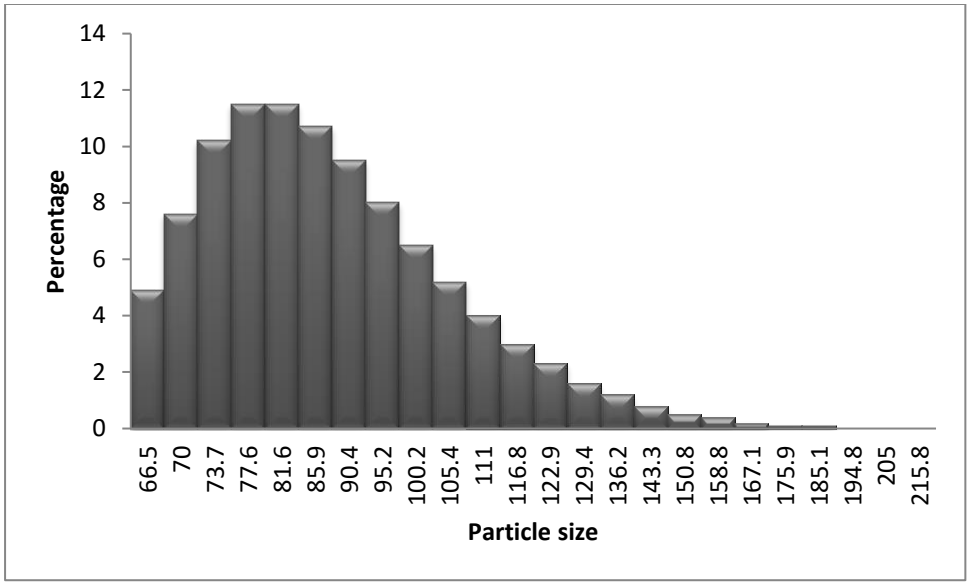

Figure 21 Size distribution of silica particles as determined though dynamic light scattering data provided by supplier

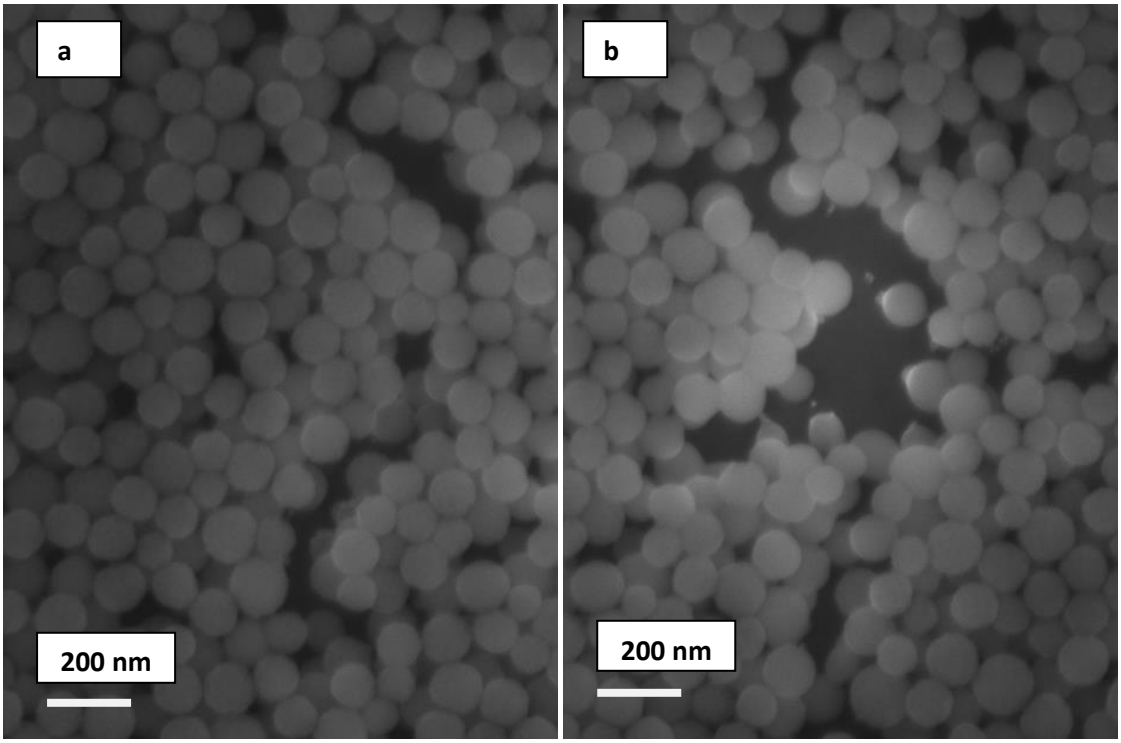

Figure 22 SEM images of (a) Bare 100 nm silica colloids (b) APTMS- functionalized 100 nm silica colloids (backscattered imaging mode)

As previously stated in Chapter II, the silica particles were subjected to a series of centrifuging and ultrasonication cycles (washing) as part of the nanoshell generation

process. Imaging at various stages has indicated that the silica particles do not fuse together as a result of this processing.

Additionally, no difference was observed between functionalized and un-functionalized silica in terms of size distribution, morphology or absorption at the visible wavelengths. Figure 22 presents images of pre- and post-functionalized silica showing no variation in morphology. The results indicate that at this initial step of nanoshell formation no significant parameters affected the formation of the nanoshells, other than the affect of the size distribution of the silica on the optical spectra of the nanoshells.

2. The THPC- Au nanoparticles

The formation of the 2 nm THPC-gold colloids which constitute nucleation sites on which the gold shells grow on the surface of the silica is a significant step of the seed particle formation. It was expected that the size and concentration of the gold on the surface of the silica would affect the final shell morphology. Figure 23 illustrates the absorption spectrum of the THPC-capped-gold colloids versus that of the functionalized silica. The spectra indicate that the silica displays no absorption at visible or near infrared wavelengths. The absorption of the gold colloids produced in this study was at approximately 507 nm. Due to the ultra small size of these particles, the spectrum does not show a sharp peak; this finding agrees with the data collected by Westcott (Westcott et al, 1998), Doremus (Doremus et al 1992), Preston (Preston et al, 2009) and Duff (Duff et al, 1993). The size of the particles was shown to range from 1.78 to 2.69 nm, using TEM. It was not possible to determine the size of these colloids using dynamic light scattering due to their small size.

It was possible to form larger sized particles by varying the ratio of $HAuCl_4$ to the ratio of THPC. The more the $HAuCl_4$ added the larger the final size of the gold particles and vice versa.

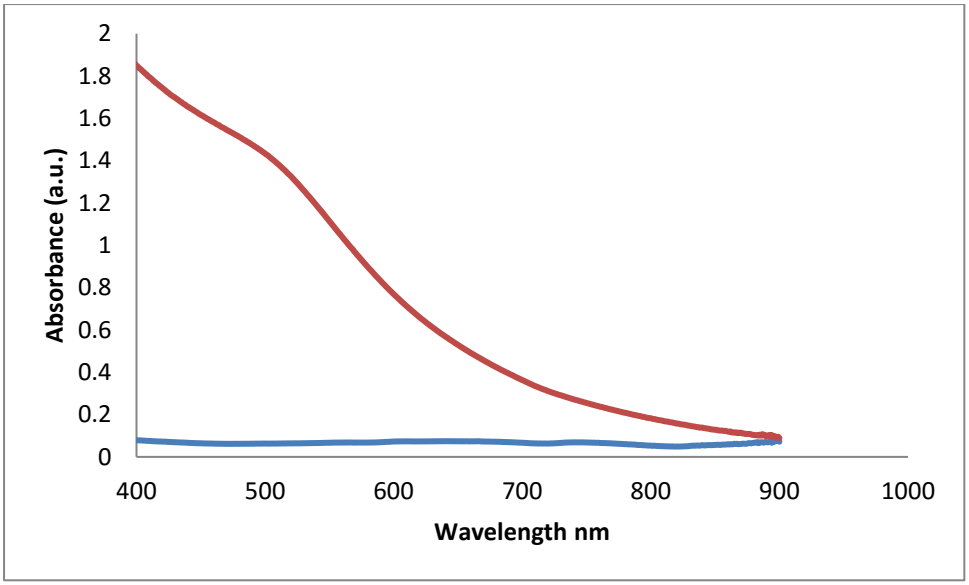

Figure 23 Absorption spectra of 100 nm functionalized silica colloids (blue curve) and 2 nm THPC-gold colloids (red curve). Silica has no absorption in the optical region of the spectrum and gold has an absorption at approximately 507 nm

No attempt was made to make smaller particles as it has been reported (Westcott et al, 1998) that, particles less than 2nm in diameter are 'very unstable' and have a high tendency to aggregate into larger particles over the course of several days (Averitt et al, 1999 and Duff et al 1993). Attempts to form nanoshells using larger gold seeds, 5 to 10 nm, resulted in the formation of thicker shells that were not smooth or homogenous as presented in Figure 24.

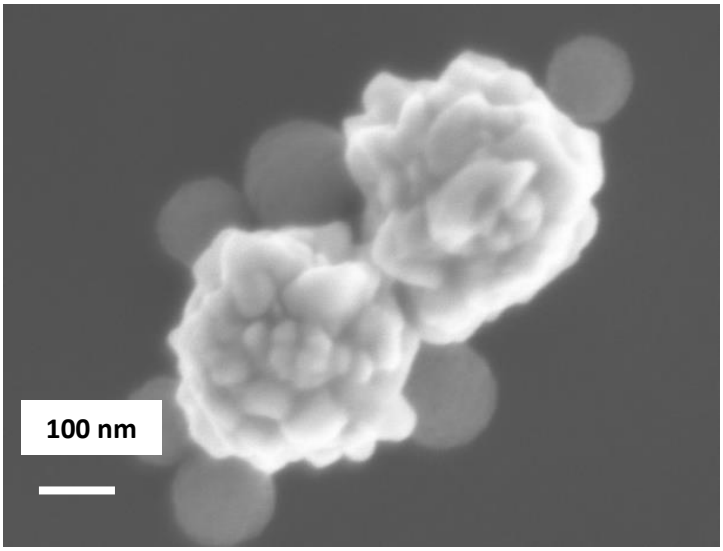

Figure 24 SEM image of nanoshells resulting from use of 10 nm seed gold colloids (backscattered imaging mode)

It was therefore concluded that the 2nm gold colloids would be the best size suited for use as nucleation sites.

3. Gold- decorated silica 'seed particles'

As mentioned previously, preliminary experimental findings have indicated the importance of the step in which the 2 nm gold particles are immobilized onto the surface of the silica particles resulting in the formation of the 'seed particles' (The terms seed particles and gold-decorated silica are adopted from the Halas research group). The gold particles on the surface of the silica are then used as nucleation sites for the growth of the gold shell as depicted in the schematic of Figure 25. With the aim of determining the conditions which render seed particles conducive to the formation of high quality nanoshells, and with the anticipation that the more nucleation sites on the surface of the silica cores the more uniform and continuous the gold shells, experiments were designed to assess the effect of the pH of attachment and the ratio of 2 nm gold particles, to that of the silica cores, on the amount of gold colloids covering the surface of the silica. This investigation would lead to the determination of the optimum conditions for seed particle formation. In turn, the effect of the formation conditions of the seed particles, on the quality of the gold shell and its morphology were also assessed. The results of these experiments are illustrated in the following sections.

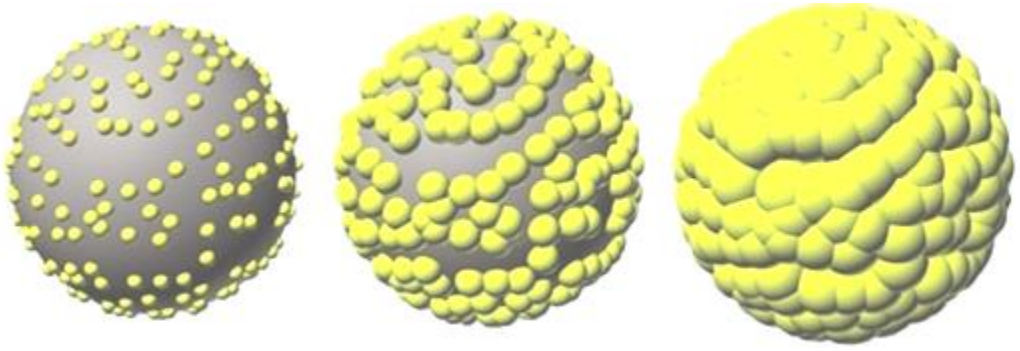

Figure 25 Schematic diagram illustrating growth of gold shell from decorated silica to complete shell (Halas, 2002)

1. Effect of pH

In this section, the results obtained from investigating the effect of the pH on the attachment of the 2 nm gold colloids to the surface of the silica are presented. The section is divided into two parts: the first dealing with the formation of the seed particles at various

pH conditions and the second examining the effect of these seed particles on the final quality and morphology of the nanoshells formed using these seed particles

- **Seed particles**

The first step in studying the effect of pH on the attachment of the gold to the silica was to determine the iso-electric points of both the silica and gold colloidal solutions. The iso-electric point is defined as the pH at which the charge on the surface of the particles amounts to zero. It was anticipated that performing the attachment at a pH value close to that at which the iso-electric point of the gold colloids occurs would provide the highest possible coverage on the surface of the silica. This is because at the point where the charge on the surface of the gold is the least, the electrostatic repulsion between the gold colloids would be minimized and it is then possible to attach more particles on the surface of the silica. The iso-electric points of the gold and the silica dispersions were determined by modifying the pH of each of the colloidal solutions, individually, using hydrochloric acid and sodium hydroxide. The respective zeta potential was measured at each value of pH. It was determined that the iso-electric point of the functionalized silica particles was at a pH of approximately 6. The iso-electric point of the gold, on the other hand was approximated as being at a pH below 3. No investigations at pH values below 3 were attempted in order to avoid denaturing the protective, stabilizing layer on the surface of the gold particles. Figure 26 illustrates the values of zeta potential obtained for the different values of pH.

The next step was to attempt the attachment of the gold to the silica at various values of pH in order to determine how the coverage and attachment at those values of pH differed from the attachment carried out at near iso-electric point conditions. The effect of pH on the formation of the seed particles was determined by analyzing the results obtained at pH values between 3 and 12.

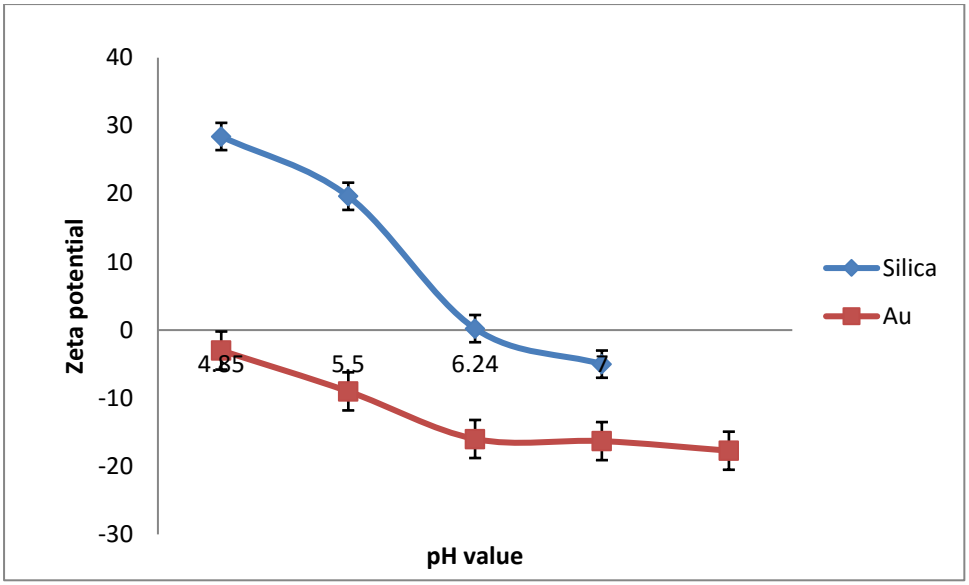

Figure 26 Iso-electric points of Silica and Gold –Plot of zeta potential versus pH

Results of the investigations of the effect of pH on the attachment of the gold to the silica are summarized in Figure 28. The figure depicts SEM images of the surface of the silica covered with THPC-gold colloids under four different pH conditions; the values of pH investigated are: 3.25, 4.63, 7.74 and 11.99. The results indicated that there was a large variation between the arrangements of the gold particles on the surface of the silica at high basic and or extremely acidic values of pH.

At low values of pH, 3.25, the attachment of the gold colloids onto the surface of the silica was in the form of small groups of five to seven, 2 nm particle clusters, as seen in Figure 28 (a). The size of each of the clusters ranged from 5-7 nm, indicating that each cluster was made of two to three, 2 nm gold colloids. Conversely, at high values of pH, 11.99, the attachment of the particles was in the form of very tiny (5-8 nm) individual clusters on the surface of the silica, Figure 28 (d). Figure 28 (b) and (c) illustrate the arrangement of the gold at pH values of 4.63 and 7.74 respectively. The attachment of the gold colloids in the former case was in the form of 2 nm gold colloids uniformly distributed on the surface of the silica. In the case of the pH- 7.74 seed particles, the distribution of the gold seeds on the surface of the silica was in the form of both 2 nm colloids as well as 5-7 nm colloids. The overall number of gold particles that attached to the surface of the silica was not found to vary significantly with the variation of pH, for a given ratio of gold to silica particles.

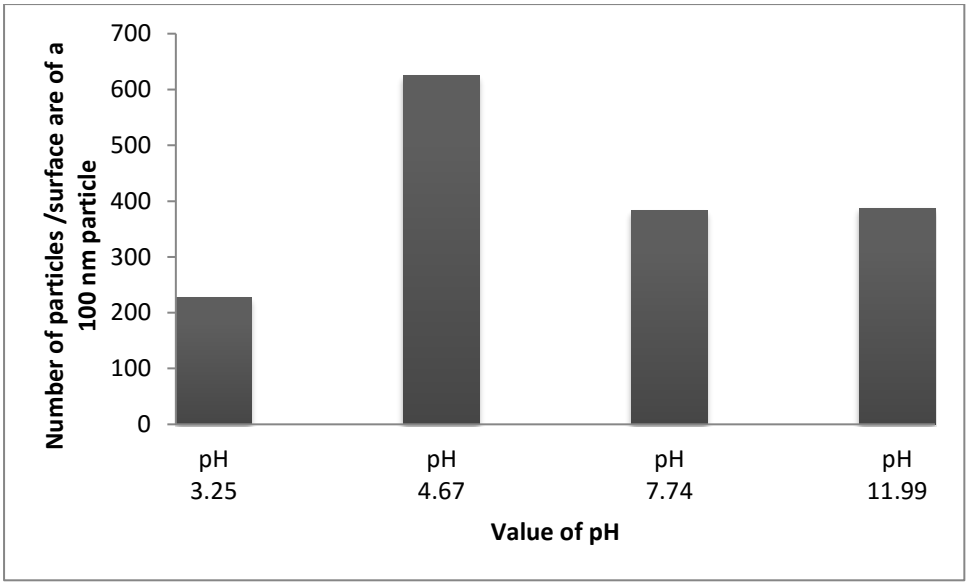

Figure 27 The variation the number of gold particles or clusters on the surface of the silica with pH

The chart in Figure 27 depicts the number of gold colloids on the surface of the silica cores for the four different values of pH. The summary of the size and number of particles at each value of pH is indicated in Table 3 below.

pH	*Number of particles*	*Size of particles (clusters)*
3.25	227	2-3, 2 nm particles/particle
4.63	624	2 nm
7.74	383	Combinations of 2 and 5 nm particles
11.99	387	5-8 nm particles

Table 3 Number of particles attached at different values of pH

The results obtained at high pH values, 11.99, were consistent with the results obtained by Park et al (2006) who studied the effect of the pH on the attachment of THPC-gold colloids to 80 nm silica nanoparticles. Park et al also reported the formation of gold clusters on the surface of the silica at high values of pH, 12. These results may be interpreted as being due to the presence of a high concentration of OH^- ions in the solution, as a result of the addition of NaOH. The presence of these ions has two different effects. The first is that they mask the surface charge on the gold colloids and thus causes them to be attracted to one another. The second is that the amine groups on the surface of the silica are de-protonated, reducing the number of sites to which the 2 nm gold colloids may attach.

Hence for a given amount of gold colloids in solution the gold forms clusters and attaches to the sparingly available functional groups on the surface of the silica.

In the case of the low values of pH, 3.25, the addition of H^+ ions to the solution causes the reduction of the zeta potential (compression of the electric double layer) of the gold colloids and thus allows them to come into close contact with one another forming the distribution depicted in Figure 28 (a). The difference in this case, compared to the case of the pH of 11.99, is that the amine groups are protonated, also due to the presence of the H^+ ions in solution, thus the gold is not forced to attach in a cluster form.

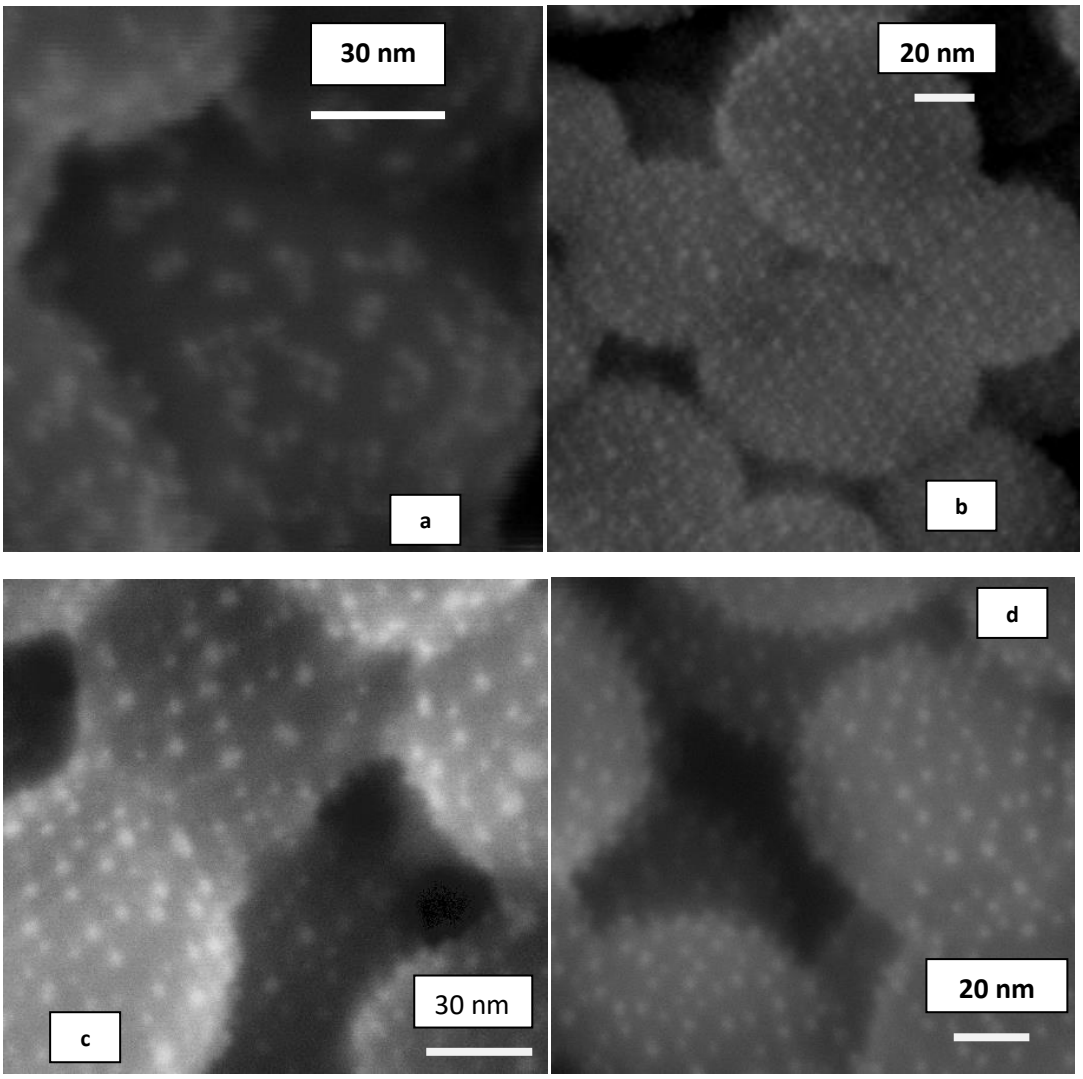

Figure 28 SEM images illustrating effect of pH on coverage of silica particles with gold (a) pH of 3.25 (b) pH of 4.63 (standard condition) (c) pH of 7.74 (d) pH of 11.99 (backscattered imaging mode)

Although the analysis of the effect of pH on the seed particles yielded significant information regarding the attachment of the gold particles to the silica, it was not possible

to determine the optimum pH at which the best seed particles were formed. The following section presents this in terms of investigating the effect of these seeds on the nanoshell formation.

- **Nanoshell growth**

The images in Figure 29 illustrate the nanoshells obtained from the seed particles presented in the previous section. All the nanoshells presented here have an average shell thickness of 14- 17nm. Figure 29 (a) presents the nanoshells formed from pH 3.25- seed particles. The image indicates that the nanoshells have a rough surface with several protrusion, thus they are not perfectly spherical; they appear to be hexagonal in shape. As the value of the roughness was less than 10 nm it was not possible to measure the surface roughness using atomic force microscopy (AFM). Nanoshells made from pH-4.63 seed particles were more spherical than those made from pH 3.25 seed particles . Although it was not possible to measure the surface roughness, it was clear from the images, Figure 28 (b),that the shells had smoother surfaces and less protrusions than those of the pH-3.25 nanoshells. Nanoshells made from seed particles where the attachment pH was 7.74 appeared to have a smoother surface, compared to particles formed at pH values of 3.25 and 4.63, as depicted in Figure 29 (c). Nanoshells resulting from the use of 11.99-pH seed particles, on the other hand, had an rougher morphology compared to pH-3.25 nanoshells. These particles were determined to have an average roughness of 26-32 nm using the method for determining roughness explained in Appendix A. It should be noted that nanoshells obtained from seed particles made at pH values of 7.74 and 11.99 contained more nanoshell 'dimers' than those obtained from seed particles made at lower values of pH. Nanoshell dimers (Halas, 2001) are particles where two nanoshells have fused to one another and will be discussed in a later section of this chapter.

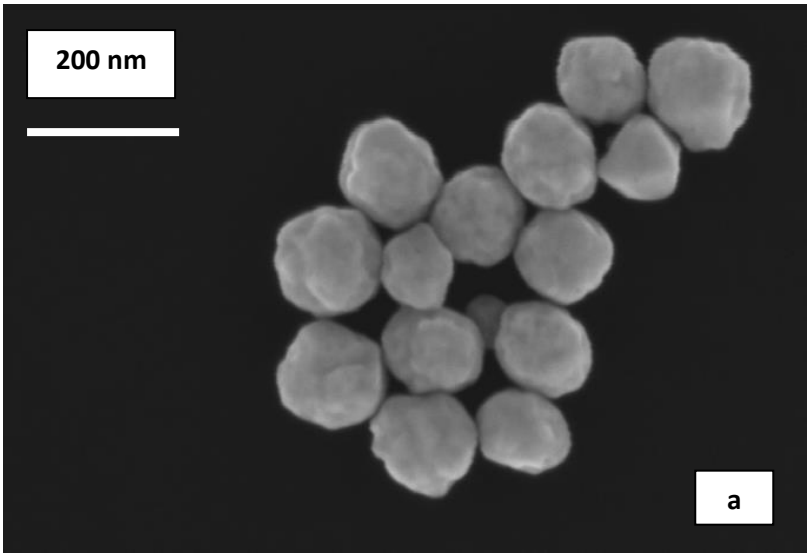
200 nm
a

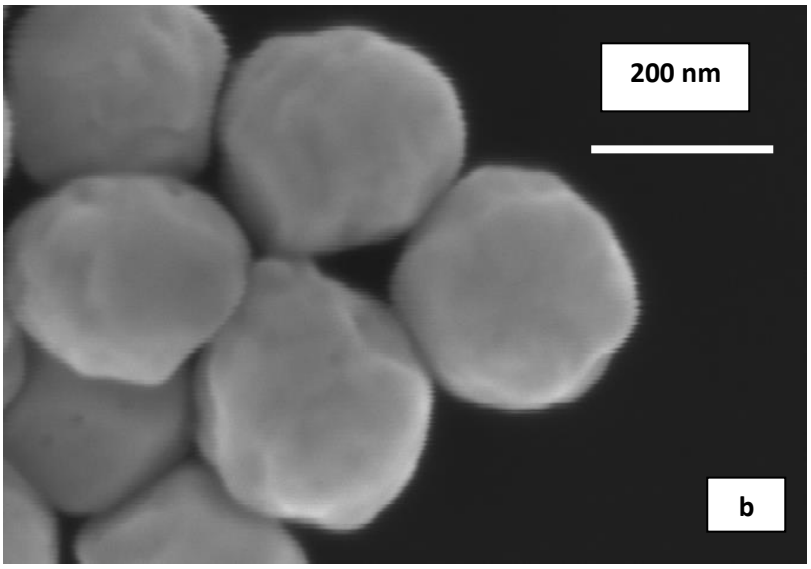
200 nm
b

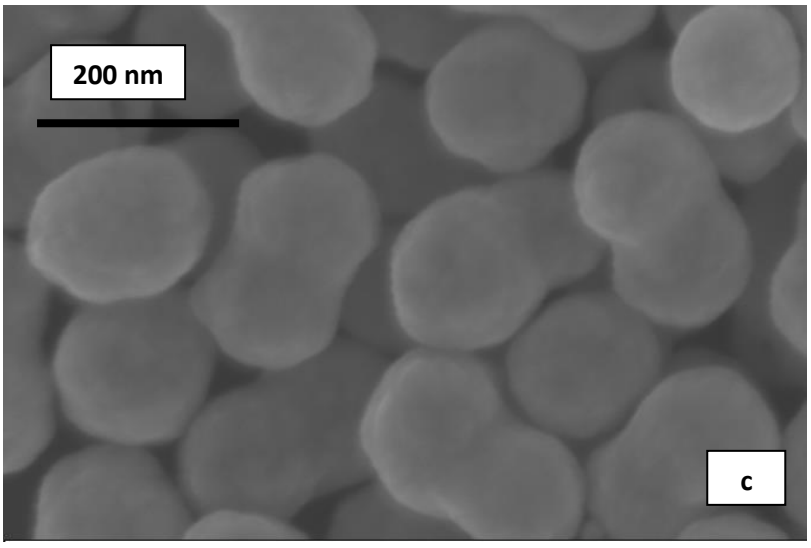
200 nm
c

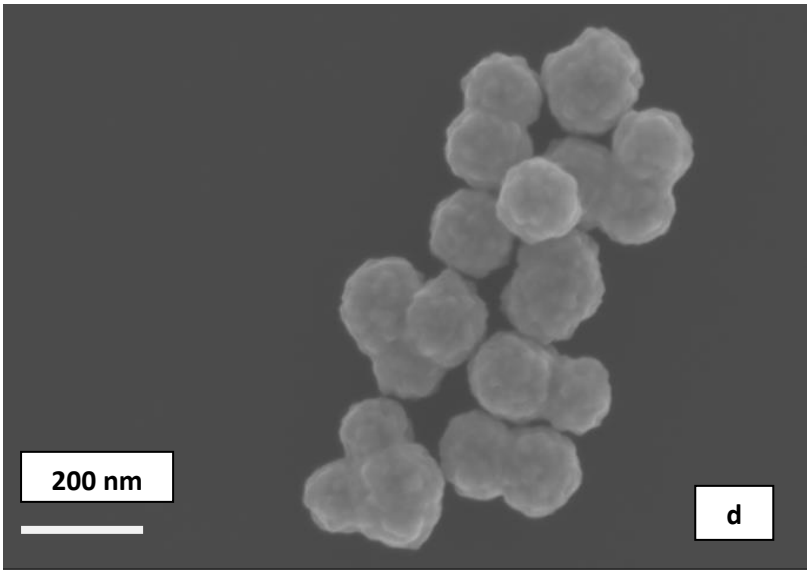

Figure 29 SEM images illustrating effect of pH variation on nanoshell formation (a) pH of 3.25, (b) pH of 4.63 (standard condition), (c) pH of 7.74 and (d) pH of 11.99 (backscattered imaging mode)

Summary of results: The results obtained from this research into the effect of the pH at which the seed particles were formed indicate that there is no 'optimum pH' at which the attachment should be done. Rather, the pH chosen for the formation of the seed particles should be determined in accordance with the required morphology of the nanoshells. Seed particles for rough or 'textured' (Wang et al, 2005 and 2006) nanoshells should be made at pH values close to 11 and seed particles for smoother nanoshells should be made at pH values ranging between 4.63 and 7.74. The final assessment of nanoshell quality is made by evaluating of the optical properties of each group of nanoshells.

2. Effect of ratio of gold to silica on seed particle quality

The second parameter investigated here, was the effect of the ratio of gold to silica used in making the seed particles. Initially, the amount of gold colloids required to cover each silica particle was determined by calculating the number of 2 nm gold colloids required to cover the surface area of the 100 nm silica particles. This amount was determined to be five thousand of the 2 nm gold particles per 100 nm silica particle. This number was estimated on assumption that the gold particles were to cover an area equivalent to the projection of a circle with a 2 nm diameter on the surface of the silica. This value was determined to be equivalent to approximately 5.71×10^{-8} ml of gold per ml of silica. Preliminary experimental work indicated that this ratio was too low. The effect of various ratios of gold to silica on the attachment of the colloidal particles was investigated in order to determine the optimum ratio yielding the best surface coverage without resorting to the use of highly excessive amounts of gold, as previously discussed. In this study, ratios were varied from 1 up to 2.05×10^{8} times in excess of the calculated amount required for coverage.

In the following sections, the effect of the different ratios of gold to silica on the surface coverage of the silica is examined. Additionally, the effect of the resulting seed particles on the quality of nanoshells formed using these seed particles is presented.

- **Seed particles**

The images in Figure 30 summarize the results of experiments that were conducted to determine the effect of the ratio of gold colloids to silica colloids (during seed particle formation) on the coverage on the surface of the silica. Only results in which the seed particles were used in making nanoshells are depicted. As a result of preliminary studies, the ratio of 12.49 g of gold per 1.625 mg of silica was determined to be a reasonable point of comparison since using this ratio led to the formation of nanoshells having a complete shell of the required size and optical absorbance. This amount was considered the *standard ratio* to which other variations in the ratio of gold to silica were compared. The ratios presented here are of seed particles that are: 59.9 % of the standard ratio (Figure 30 (a)), 150% of the standard ratio (Figure 30 (b)), and 176% of the standard ratio (Figure 30 (c)). The standard seed particles (made at the standard ratio) were found to have a coverage of approximately 20 % gold on the surface of the silica particles; coverage was determined as explained in Appendix A. Figure 30 (d) depicts the coverage obtained by using the standard ratios.

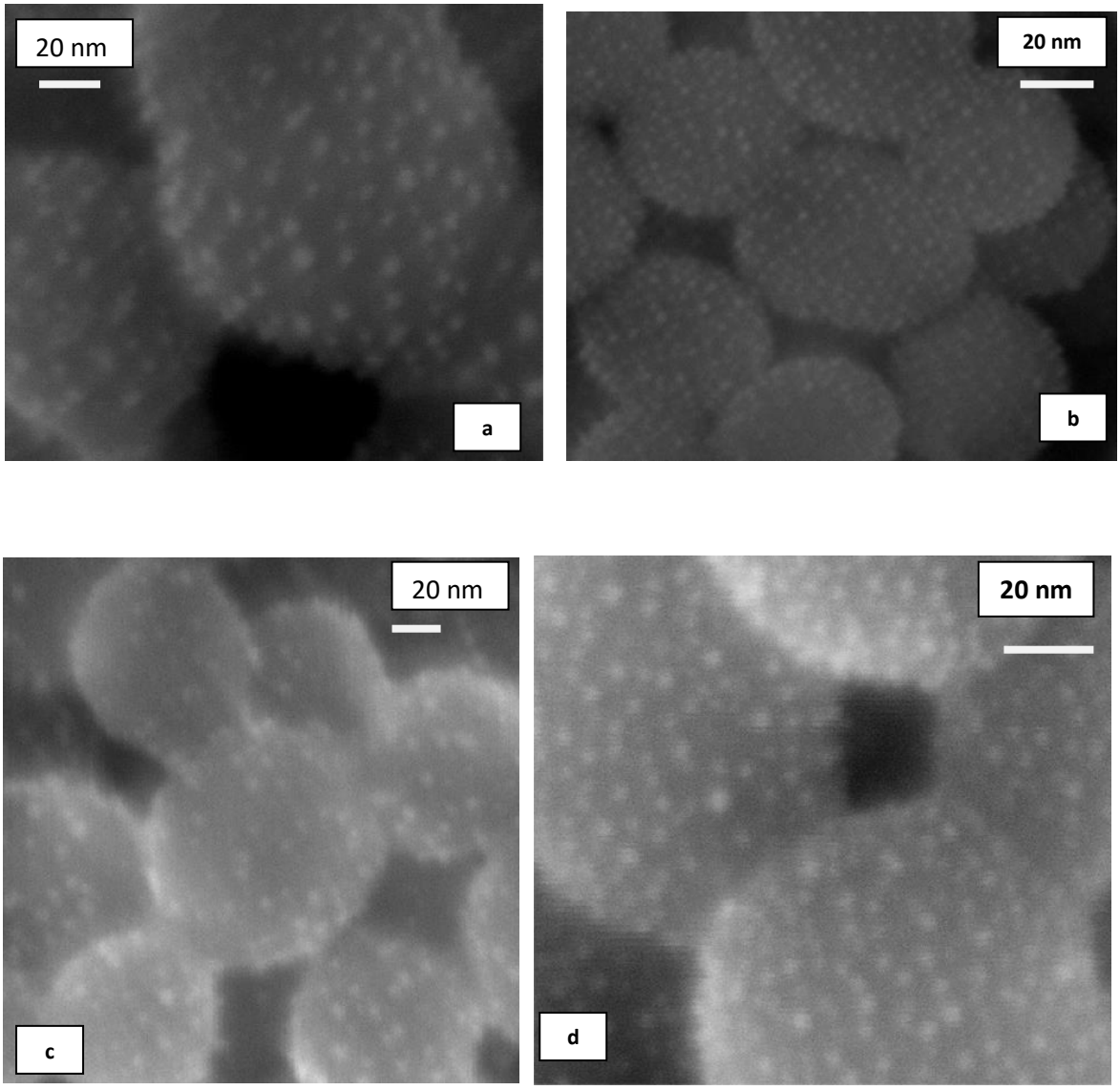

Figure 30 SEM images illustrating effect of the ratio of gold to silica on the surface coverage of the silica with gold (a) 76% in excess of the standard ratio, (b) 50 % in excess of the standard ratio, (c) 59.9 % of the standard ratio and (d) the standard ratio (backscattered imaging mode)

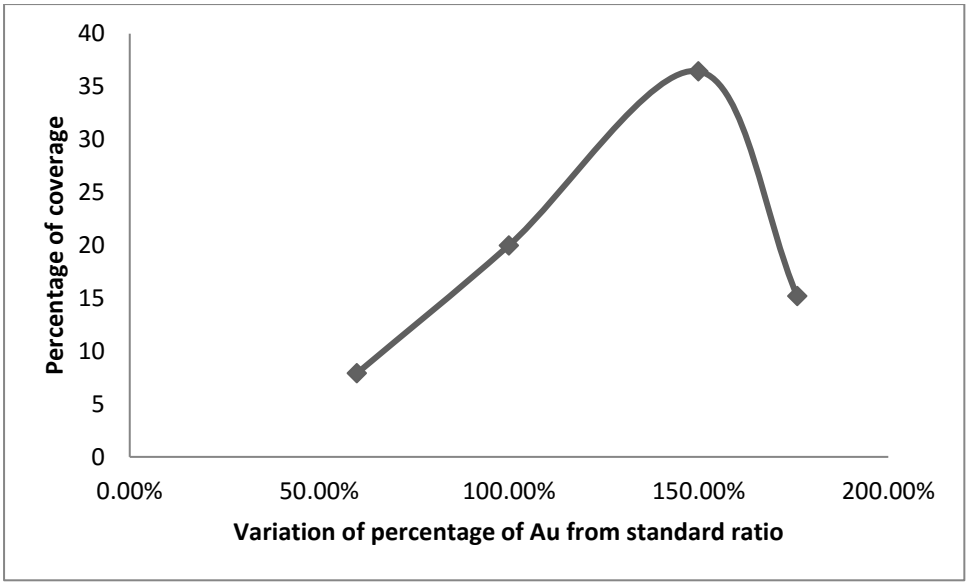

Figure 31 Graph illustrating the percentage of surface coverage versus the ratio of gold colloids relative to silica

The results of these images are summarized in Figure 31. The graph presents the percentage of surface coverage of the silica in relation to the ratio of gold to silica in the colloidal solution used to make the seed particles. As depicted, it was found that as the ratio of gold to silica increases, the percentage of coverage increases proportionally, until a threshold is reached where adding more gold to the colloidal solution causes the aggregation of the colloids, resulting in very little coverage compared to the case of the standard ratio. This is thought to be due to a depletion interaction resulting from the presence of excess gold in the dispersion. Additionally, the results indicate that ratios in excess of 150 % of the standard ratio result in the formation of small clusters of the 2nm gold colloids, ranging between 6.8-9.6 nm in size, compared to the apparent single attachment of the gold onto the surface of the silica found at lower ratios of gold to silica. The highest percentage of surface coverage, 36 %, was found at 150 % of the standard ratio. The percentage of coverage obtained at standard ratios is comparable to the ratio reported by Pham et al who reported 25 % gold coverage. Although the percentage of coverage obtained at 150% of the standard ratio is 11 % greater than the coverage reported by Pham et al, the difficulties encountered in removing the excess gold, at 150 % of the standard ratio, outweigh the benefit obtained by the extra coverage.

- **Nanoshell growth**

A more representative assessment of the quality of the seed particles was determined based on the quality of the nanoshells that were obtained by using each group of seed

particles. This is because although from an SEM image of a seed particle it may seem as though there is enough coverage on the surface of the silica, the coverage may not be sufficient to provide a complete gold shell. Figure 32 (a) depicts attempts to form nanoshells when using a ratio of 40 % less than the standard ratio. The image illustrates that as a result of the poor surface coverage of gold on the surface of the silica, the growth and fusion of the gold colloids into a continuous shell has been hindered. Figure 32 (b) and (c) illustrate the shells obtained from approximately 75 % and 83.4% of the standard coverage, respectively. The images show that for a given shell thickness (15 nm in this case) the shells will not grow to completion unless there is a minimum amount of gold coverage on the surface of the silica. Conversely, as illustrated through Figure 33, the presence of excess 2nm gold colloids in the seed colloidal solution, 150% and 176% conditions, results in the formation of individual solid gold colloids in the solution during the formation of the nanoshells. The presence of excess gold also results in the need for excessive wash cycles to remove the gold particles which have not attached. These excessive wash cycles promote the fusion of the seed particles.

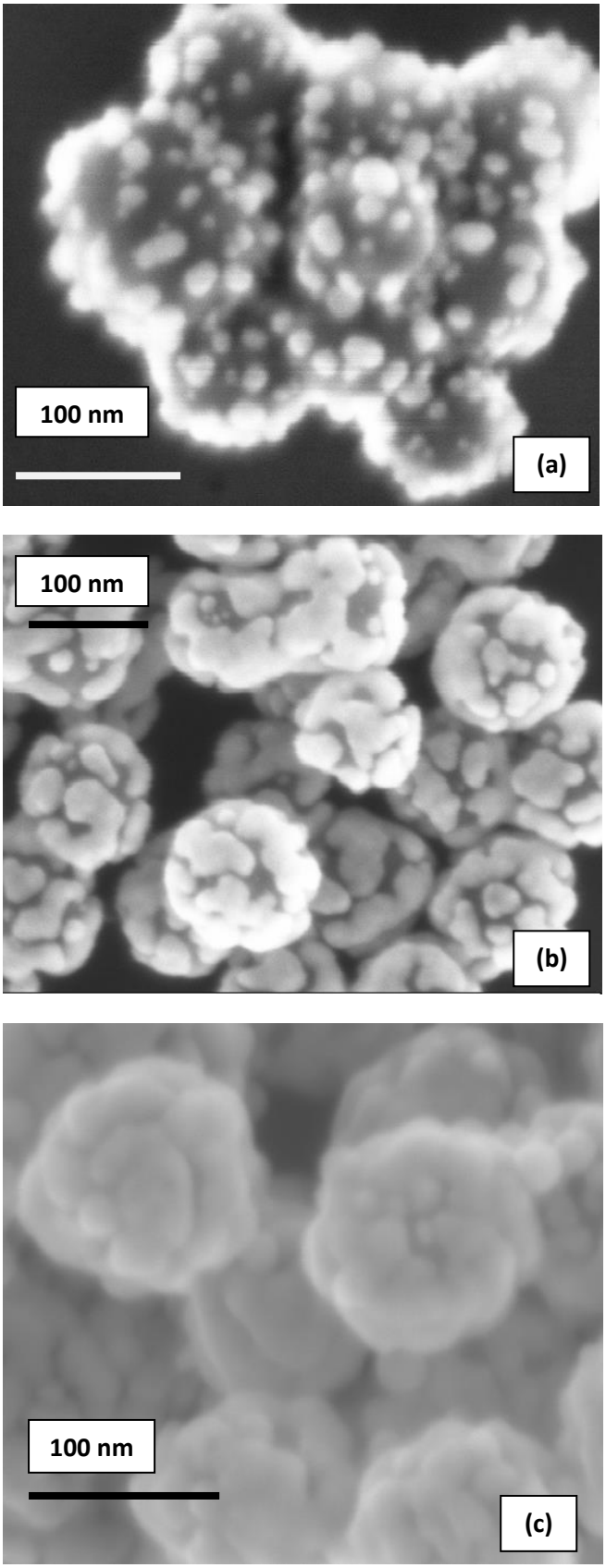

Figure 32 SEM images illustrating effect of low ratios of gold to silica in seed particles on the formation of complete nanoshells (a) 60 % of the standard ratio, (b) 75 % of the standard ratio and (c) 83.4% of the standard ratio (backscattered imaging mode)

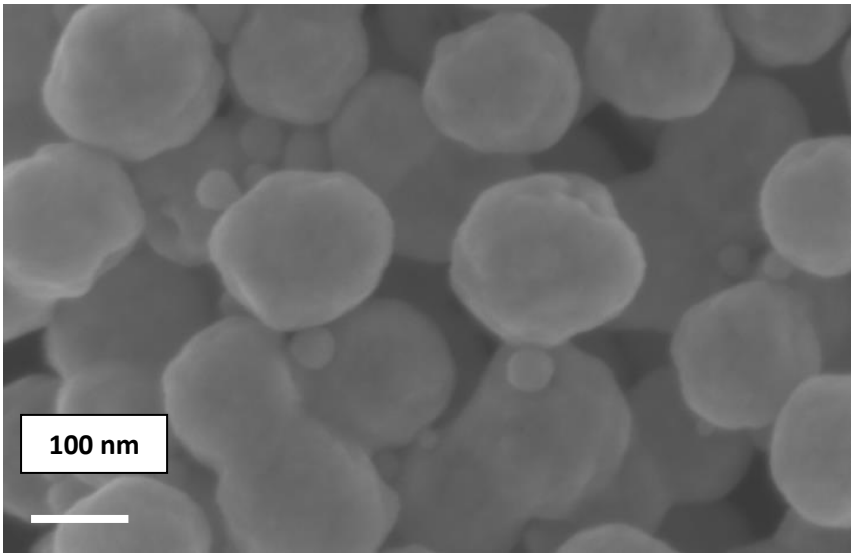

Figure 33 SEM image (backscattered imaging mode) illustrating the presence of individual solid gold colloids as a result of the presence of excess 2 nm colloids in seed solution (176% of the standard ratio of gold to silica)

It was also noted that nanoshells that were formed from seed particles using 83.4% of the amount of gold used for making the standard particles were acceptable in terms of shell completeness and optical absorbance thus also negating the necessity of the excessive amounts of gold used in seed particle formation.

Summary of results: Results obtained from this study indicate that it is not necessary to exceed a ratio of gold to silica of 12.49 g of gold per 1.625 mg of silica. This is in contrast to the initial assumption that the higher the percentage of gold to silica, in the seed particle formation dispersion, the better the quality of the resulting nanoshells. Working with seed particles formed at ratios below this 'standard ratio' yields nanoshells with a degree of incompleteness, depending on the percentage of coverage on the surface of the seed particles. Exceeding this optimum ratio, results in the presence of excess gold colloids in the colloidal dispersion. The removal of these gold colloids subjects the seed particles to unnecessary extra washing cycles. In reducing the number of wash cycles, the gold colloids that remain in solution, during nanoshell formation, hinder the growth of the nanoshells to completion.

III. b. The K-Au plating solution

The second step in the investigation of the conditions leading to the formation of high quality nanoshells was to analyze of the effect of the plating solution. It had been anticipated that the plating solution would only have an effect in terms of the concentration of gold ions in the plating solution; that is, as the number of ions, in the plating solution,

available for reduction on the surface of the silica increased, the thickness of the shells would increase accordingly. Preliminary investigations indicated that the age of the plating solution also had a significant effect on the formation of the gold nanoshells. Therefore, when studying the effect of the plating solution the effects of both the concentration of the gold and the age of the plating solution were investigated. The results are presented in the two subsections below.

1. Availability of Gold ions for reduction

The effect of the concentration of gold ions in solution on the growth of the gold shells was assessed by varying the amount of gold ions available for reduction in the plating solution.

$$HAuCl_4\,(\text{aq.}) + 2K_2CO_3\,(\text{aq.}) + H_2O \rightarrow Au(OH)_3 + 4KCl + 2CO_2\,(\text{g}) \quad \text{Equation 13}$$

As the concentration of the gold in solution increased, the thickness of the shells increased proportionally. The thickness of the shells was found to vary linearly with the amount of gold in the solution. This was in accordance with the predicted Equation 13, presented in Appendix A.

As the thickness of the gold shells increased, it was no longer possible to control the roughness of the shells by controlling the pH and the nanoshells became smoother. Additionally, it was found that as the thickness of the nanoshell increased beyond a certain limit, 73 nm (for the 100 nm core), it was no longer possible to obtain a shift in resonance peak towards longer wavelengths. In this case, the absorption peak resembled that of a solid gold nanocluster, as depicted in Figure 34.

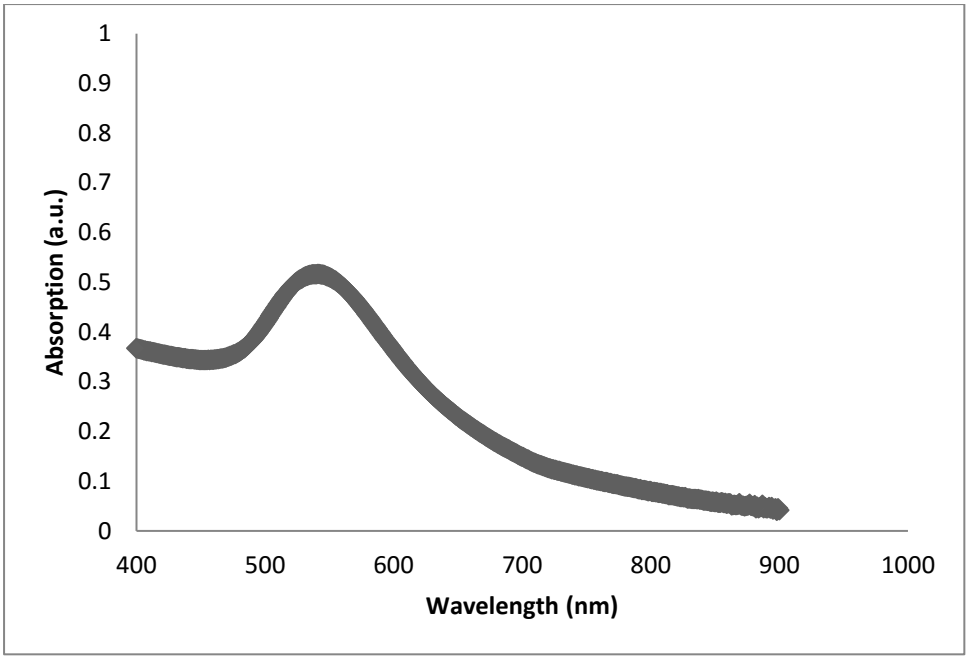

Figure 34 Absorption curve of a nanoshell with a 73 nm thick shell. The absorption resembles that of a solid gold nanocluster and the resonance is at 545 nm.

2. Age of the plating solution and its effect on nanoshell formation

Investigations on the effect of the age of the plating solution on nanoshell growth were carried out over a 30-day time period. Plating solutions of 1 to 30 days old were used to make nanoshells using the same seed particles. Experiments were performed using seed particles of standard gold coverage on the surface of the silica. No experiments were attempted with poorly decorated silica nanoparticles. The results of these investigations are presented in Figure 35, where image (a) depicts nanoshells made from a 1-day old plating solution and images (b) and (c) present nanoshells made from 15- and 30-day old plating solutions, respectively. The results led to the conclusion that it is not possible to make nanoshells with a plating solution that is excessively aged. Further studies have indicated that the best results are obtained using plating solutions that are 1-2 days old.

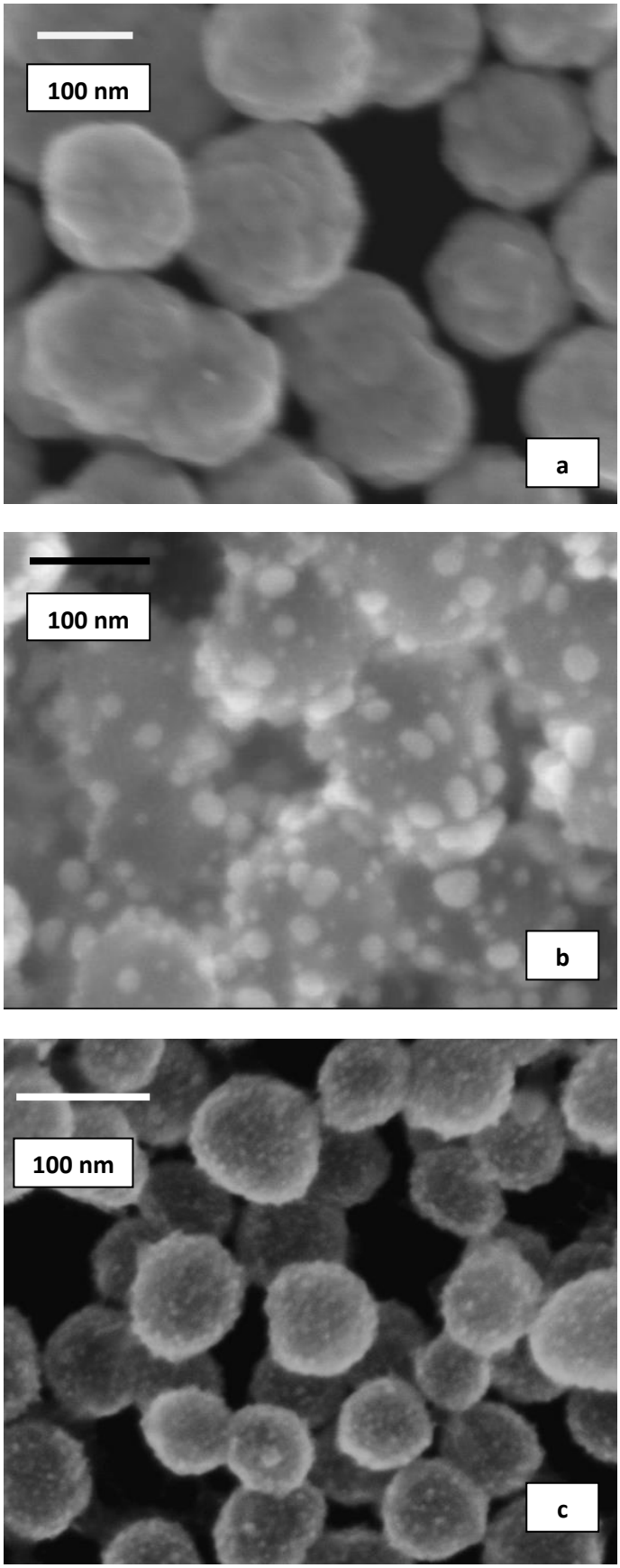

Figure 35 SEM images illustrating effect of old plating solutions on shell formation in a: (a) 1- day old plating solution, (b) 15-day old plating solution and (c) 30-day old plating solution. No growth of gold particles (backscattered imaging mode)

Summary of results: The influence of the plating solution on the formation of the nanoshell was straightforward in comparison to the influence of the seed particles. There was a linear relation between the amount of gold in the plating solution and the growth of the gold shell, given that there were no excess 2 nm colloids present in the solution, as illustrated in Figure 36. Experimental results also indicate that the use of freshly made plating solutions is optimum for the generation of good quality nanoshells.

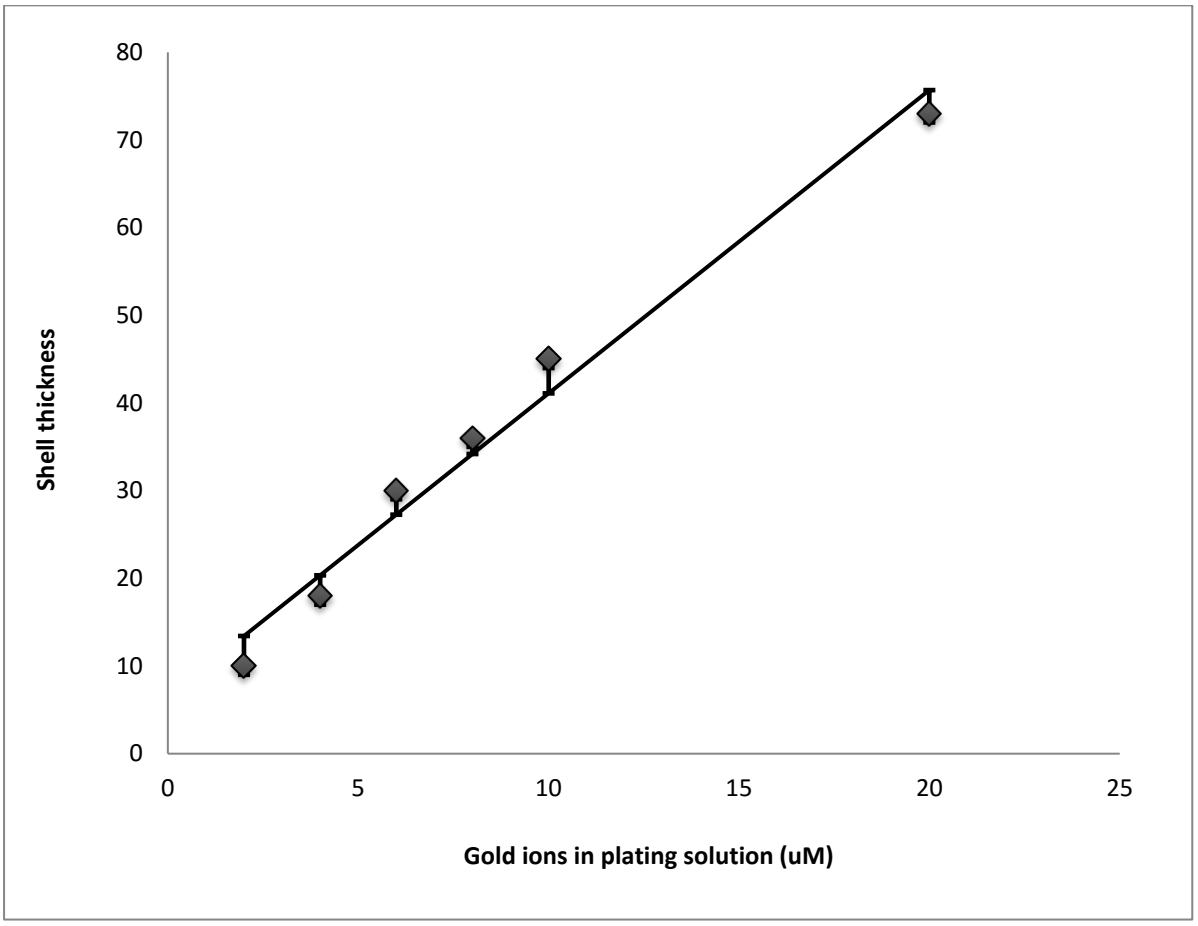

Figure 36 Effect of the amount of gold in the plating solution on the average shell thickness

III. c. Other factors affecting nanoshell growth

The above sections have provided detailed accounts of the effect of the seed particles, as well as the plating solution, on the formation of complete nanoshells. This section discusses the secondary factors that also influence on the formation of nanoshells. In the following sections, I discuss the effect of the size of the decorating gold particles, the effect of the elimination of stirring during the formation of the seed particles, the effect of the washing and centrifuging cycles in addition to the effect of temperature on nanoshell morphology.

1. Effect of temperature on the formation of nanoshells

In this section, the effect of temperature on the formation of nanoshells is discussed. The effect of temperature was investigated through the formation of the nanoshells in a plating solution at an elevated temperature, as opposed to the formation of the shells at room temperature, as was carried out in the standard procedure described in Appendix A.

This effect was evaluated at two temperatures, 45^{O}C and 90^{O}C. The temperature of the plating solution was raised to 45^{O}C or to 90^{O}C, while stirring at a speed of 1200 rpm, by use of a hot plate/magnetic stirring plate. After reaching the required temperature, the heat was removed and the seed particles were added. Stirring was continued at 1200 rpm for 10 minutes after which the dispersion was allowed to cool down before the nanoshells were removed.

Heating the plating solution to a temperature of 90^{O}C was found to result in the formation of nanoshells with a relatively smooth morphology, as presented in Figure 37, without having to resort to thicker shells. Meanwhile heating to 45^{O}C resulted in nanoshells with a less smooth shell, see Figure 38. This process of shell formation, at an elevated temperature while stirring, was found to be one of the factors that promoted the fusion of the particles, as depicted in Figure 38. This fusion was though, attributed mainly to the rapid stirring which accompanied the process. This rapid stirring, in addition to the element of heat, aided the particles in overcoming the energy barrier in Figure 14 and promoted the fusion of the nanoshells into larger particles.

Heating of the plating solution was found to have a positive effect on the absorption spectra of the nanoshells, as depicted in Figure 39 and Figure 40. Figure 39 provides a comparison between the optical spectra obtained for the nanoshells in Figure 37 (heated to 90^{O}C) and Figure 38 (heated to 45^{O}C) respectively.

Heating the plating solutions was found to result in a spectral shift to longer wavelengths. The point of reference in this case being the estimated position of the theoretical peaks calculated from Mie theory. The shift was by 29 nm in the case of the plating solutions that were heated up to 90^{O} C and by 5 nm in the case of the plating solution that was heated up to 45^{O}C. The spectral results also indicated that although the shell of NS 24 is thicker than that of NS 33 by approximately 5 nm, the absorption spectrum of NS 24 (heated to 90^{O} C) exhibits a resonance peak at 729 nm compared to the peak at 681 nm exhibited by NS 33 (heated to 45^{O}C).

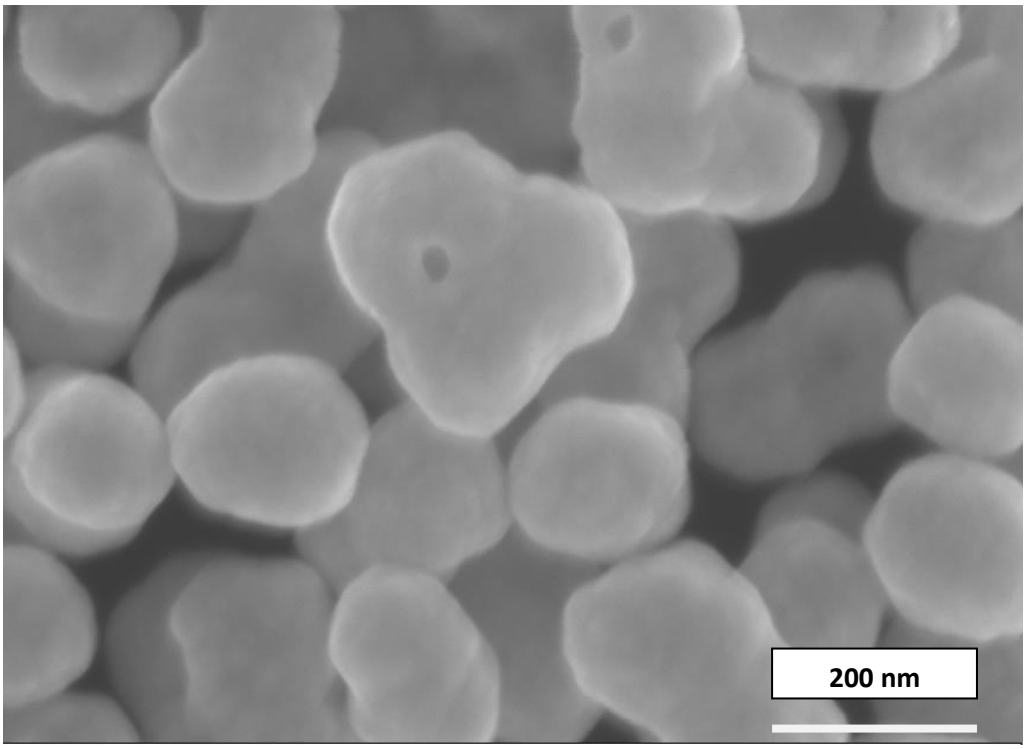

Figure 37 SEM image (backscattered imaging mode) illustrating smooth surface of the nanoshells made from heated plating solutions (Seed particles added at 90^{O}C)

Thus it can be concluded that the introduction of heat to the nanoshell formation process, via the elevation of the temperature of the plating solution prior to the addition of the seed particles, has the following effects:

1. It promoted the formation of larger particles through particle fusion in the event that the stirring speed was high,
2. It resulted in the generation of smoother nanoshells and
3. Most importantly, the use of heat during the growth of the nanoshells resulted in a shift to longer wavelengths. This shift was approximated to being 29 nm in the case of a temperature rise of 70^{O} C and 5 nm in the case of a temperature rise of 25^{O} C.

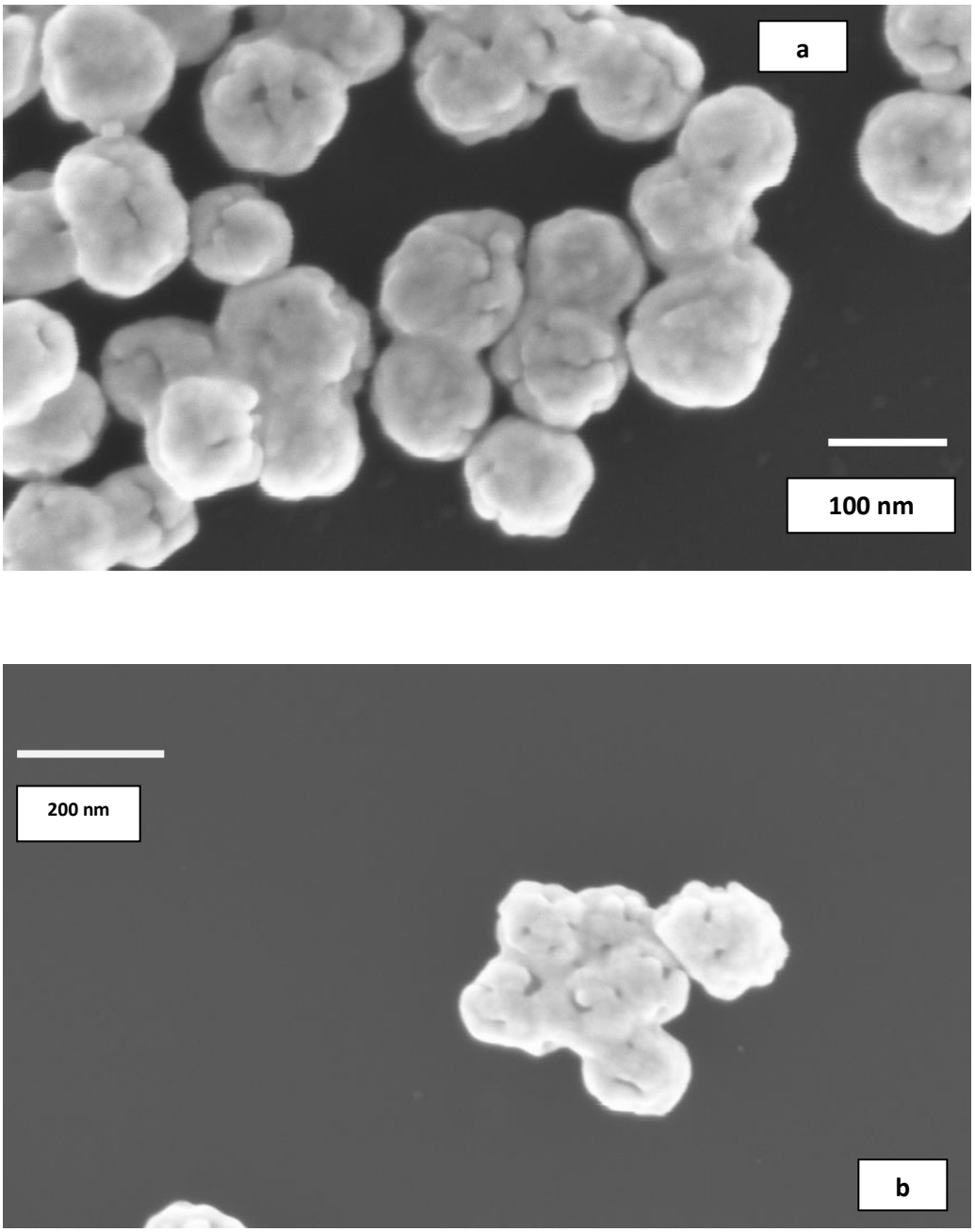

Figure 38 SEM images (backscattered imaging mode) illustrating (a) effect of heating plating solution on nanoshell formation (b) the same nanoshells as (a) illustrating the effect of the heating and rapid stirring of the plating solution on the monodispersity of nanoshells. The particles fuse together forming much larger particles (Seed particles added to plating solution at 45^{O}C).

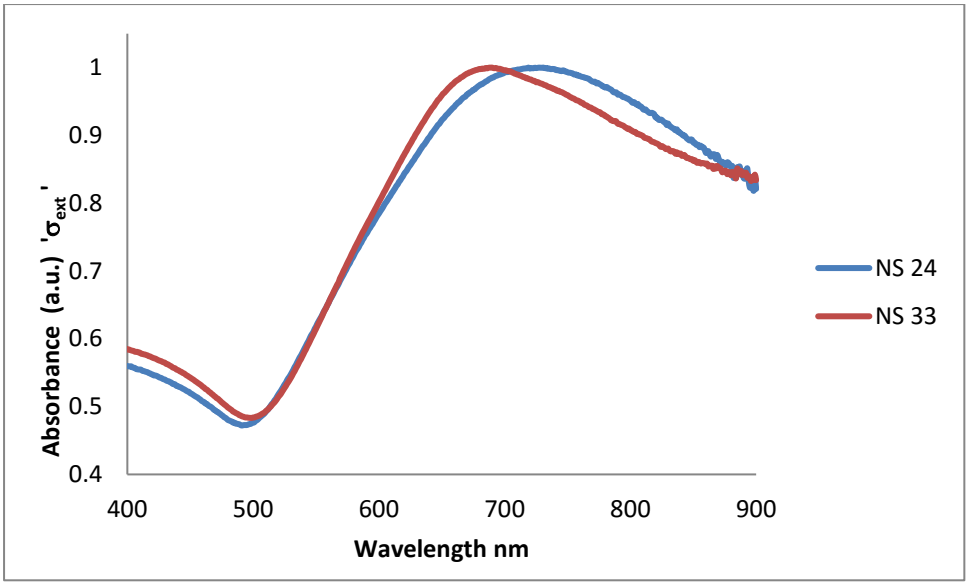

Figure 39 Absorption curve of particles made from heated plating solutions-NS 33 (heated to 45^{O}C) has a 15 nm shell and NS 24 (heated to 90^{O}C) has a 20 nm shell

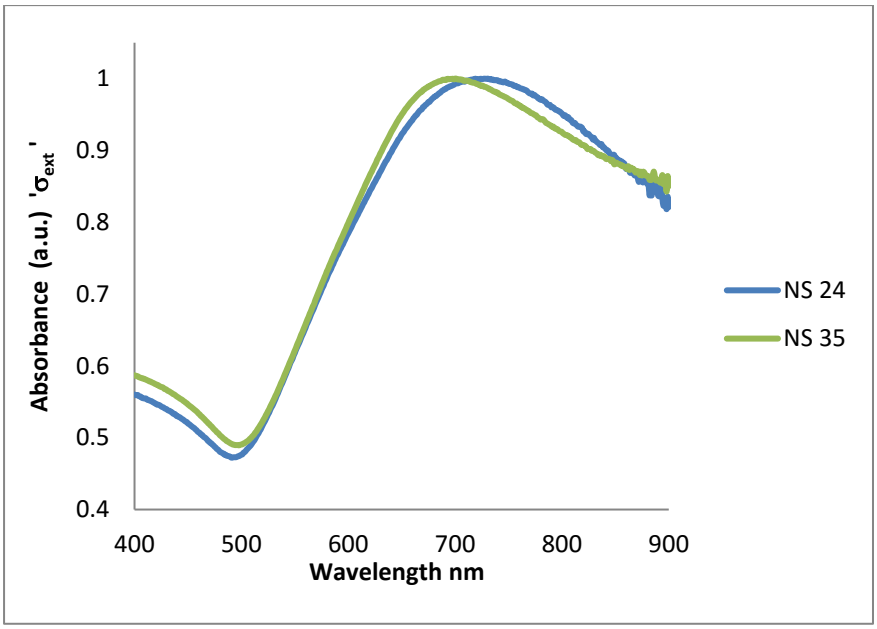

Figure 40 A 32 nm shift in the resonance peak caused by raising the temperature of the plating solution by 70^{O}C. Nanoshells NS 24 formed when the plating solution was heated to 90^{O}C and nanoshells NS 35 formed at standard conditions, without heat.

The addition of heat to the nanoshell formation process would thereby enable the design of the plasmon resonance peak to be placed further into the near infrared region of the spectrum without having to increase the size of the silica core.

2. *Effect of Stirring*

Another important factor affecting the attachment of the gold particles to the silica, is stirring during the addition of the silica to the gold. This is not discussed in the literature and Pham et al (Pham, 2002) and Ashayer et al (Ashayer, 2003) report the gentle shaking of the container during the addition of the silica. The results of the experiments carried out in the scope of this thesis have indicated that it is not possible to, uniformly, attach the gold particles to the surface of the silica without stirring. For the work presented in the thesis, a stirring speed of 950-1000 rpm had been employed during the formation of the seed particles. Results of attempts to instigate the attachment of gold to silica at the standard ratio, and without stirring, are illustrated in Figure 41. In comparison with the results obtained while stirring, presented in Figure 28 (b), the gently shaken samples tended to form large clusters on the surface of the silica, as opposed to the homogenous distribution presented in Figure 28 (b). Through further experimentation, it was found that, during seed particle formation, a stirring speed of approximately 480 to 620 rpm was enough to generate a uniform distribution of gold on the surface of the silica and also reduce the number of agglomerations caused by seed particle fusion.

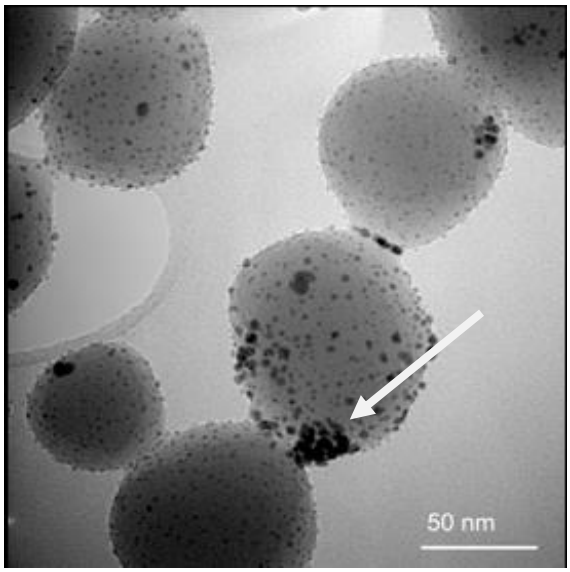

Figure 41 TEM image (bright-field) of seed particles made without stirring at standard concentrations. The arrow indicates clusters formed due to absence of stirring

It can be thus concluded that continuous stirring during the formation of the seed particles is a factor that should not be eliminated in order to obtain silica cores with gold seeds that are uniformly distributed on the surface. Also, although no nanoshells were

grown from the seed particles in Figure 41, it was anticipated that nanoshells grown would not have a homogenous shell due to the uneven distribution of the gold on the surface of the silica.

3. Effect of Centrifuging speed

One of the unavoidable challenges, one faces in the process of making nanoshells is the formation of agglomerations within the final nanoshell population. These agglomerations are the result of the fusing of a percentage of the nanoshells into larger particles made of pairs, threes and in some cases larger particles composed of four or five particles fused together, as depicted in Figure 42 (a) and (b).

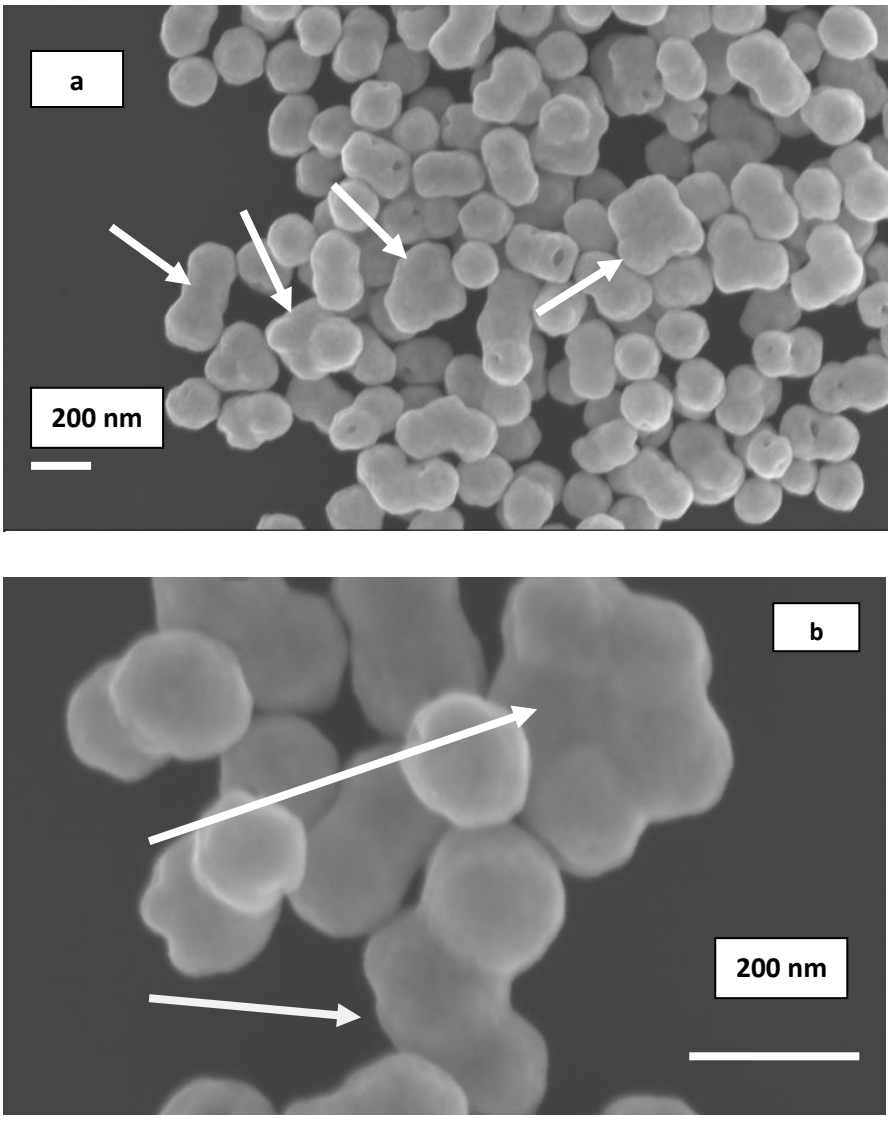

Figure 42 SEM images illustrating the formation of larger core-shell particles through fusion of two or more particles together (backscattered imaging mode)

The speed at which the seed particles were centrifuged was found to affect the number of agglomerations within the nanoshell population. It is thought that this fusion is caused by the 2 nm gold colloids as is evident from the image in Figure 43 below. The image indicates that the decorated silica particles have fused together prior to the formation of the gold shell. It is thought that the fusion is the result of the speed of the centrifuging, causing the particles to overcome the energy barrier shown in Figure 14 and fuse together. It can be deduced that excessive washing of the gold decorated silica particles particularly at high centrifuging speeds, should be avoided so as to reduce the number of particles that fused together. This experimental work suggests that centrifuging at 400 rpm will result in a much lower percentage of particle fusion.

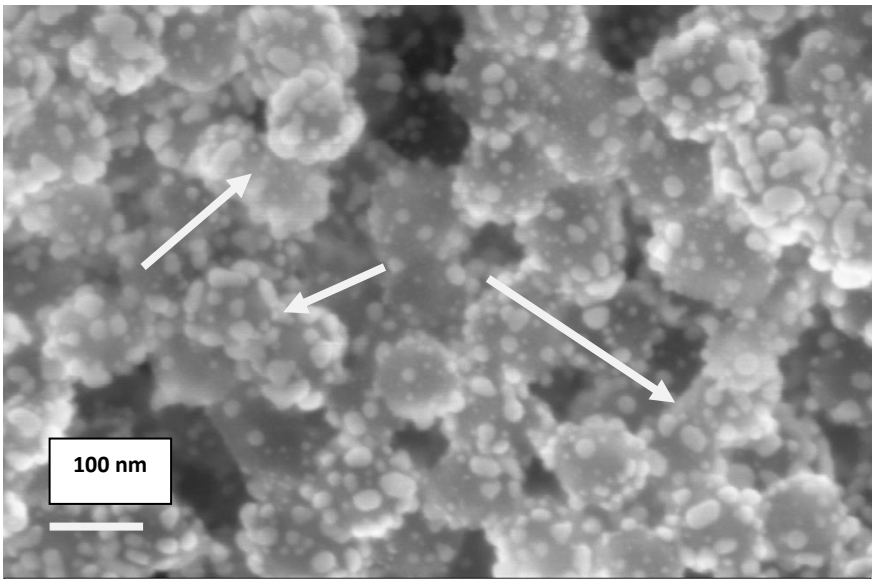

Figure 43 SEM image illustrating the growth of the 2 nm gold nanoparticle on surface of silica. Arrows indicate silica particles fused together by decorating gold colloids (backscattered imaging mode)

4. Roughening of the nanoshell surface

Textured (rough) gold surfaces are required for several applications such as Surface Enhanced Raman Spectroscopy as well as chemical and biological sensing and wave-guiding (Wang et al, 2005 and 2006). The use of 'textured' nanoshells for such applications ensues larger local field enhancement in comparison other colloidal surfaces. Wang et al (Wang et al, 2005 and 2006) have reported two methods for the formation of textured nanoshells. The first is using chemical etching of nanoshells and the second is the growing of nanoshells using ascorbic acid reduction of gold salt in solution, in the presence of cetyltrimethyl ammonium bromide (CTAB- Aguirre et al, 2003). In this study, the formation of textured gold

nanoshells was accomplished by using two different techniques: the successive deposition of gold onto the surface of the silica and the growth of gold nanoshells from the attachment of the gold colloids to the surface of the silica, under basic pH attachment conditions. The results of these experiments are presented in Figure 44- Figure 47.

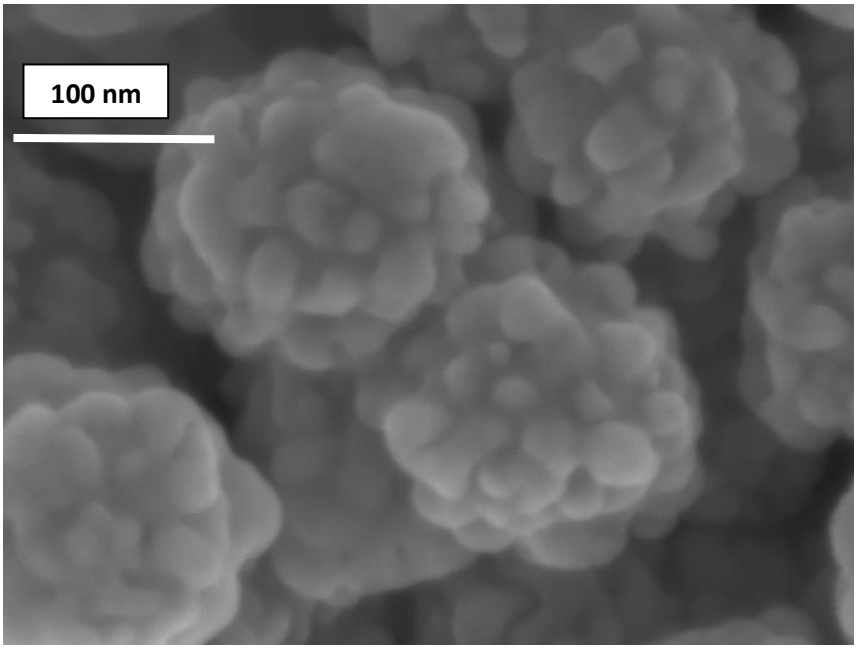

Figure 44 SEM image illustrating textured nanoshells formed by minimizing gold ions in solution and using a two step growth method (backscattered imaging mode)

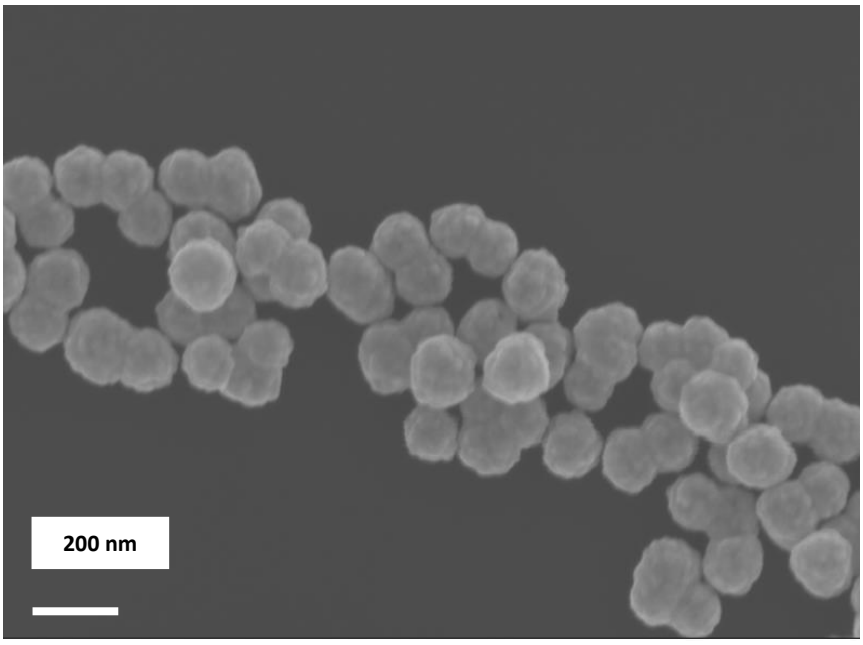

Figure 45 SEM images (backscattered imaging mode) illustrating textured nanoshells made using a two step growth method (1.5 times the gold available for reduction in Figure 44)

It was found that the surface roughness or texturing may be tailored by modifying the conditions under which the shells are formed. The shells of highest surface roughness, depicted in Figure 44, were obtained by using the two step growth technique. Within this method the nanoshells were grown using two reduction steps rather than one. The first step was to grow nanoshells using the standard method, described in Appendix A, while terminating the reaction 1.5 minutes after the addition of the reducing agent. This time duration results in the growth of the gold seeds on the surface of the silica, but does not constitute enough time for the gold particles to fuse and form continuous shells. These particles, with partially complete shells, were in turn used as seed particles. The same reduction process was repeated once more, but to completion. Using this method, the surface roughness was controlled by altering the amount of gold ions available for reduction in the solution during the second reduction step. In the first reduction step, the amounts of gold stated in Appendix A were used. In the second step, 2.5ml of a 15 mM solution of aurochloric acid, in the plating solution, were enough to form a continuous gold shell around the silica and form shells of the morphology presented in Figure 44. This technique was found to yield nanoshells having a surface roughness of approximately 58 nm, as determined by the method described in Appendix A.

In attempting the formation of the nanoshells with a lower value of surface roughness, the particles depicted in Figure 45, the same process described above was used. In this case, 1.5 times the gold ions, available for reduction in the second step described for the nanoshells in Figure 44, were used. This rendered nanoshells having a surface roughness of approximately 22 nm.

Figure 46 illustrates textured nanoshells that have a surface roughness of approximately 28 nm and were obtained using seed particles formed at high pH conditions.

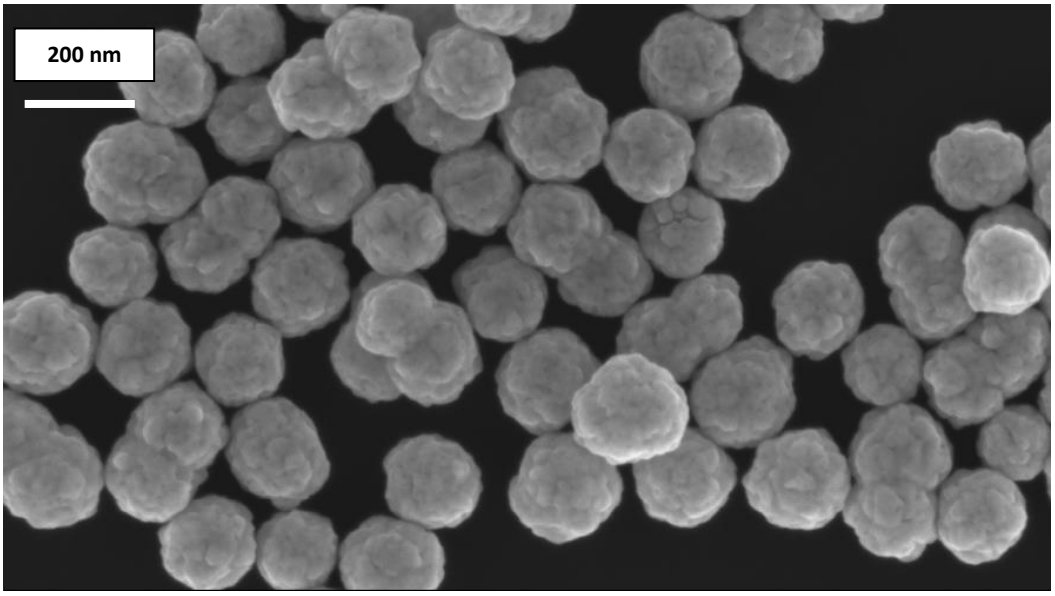

Figure 46 SEM images (backscattered imaging mode) illustrating nanoshells having a surface roughness of 28 nm. Shells formed by use of seed particles formed at high pH conditions (pH 11.99)

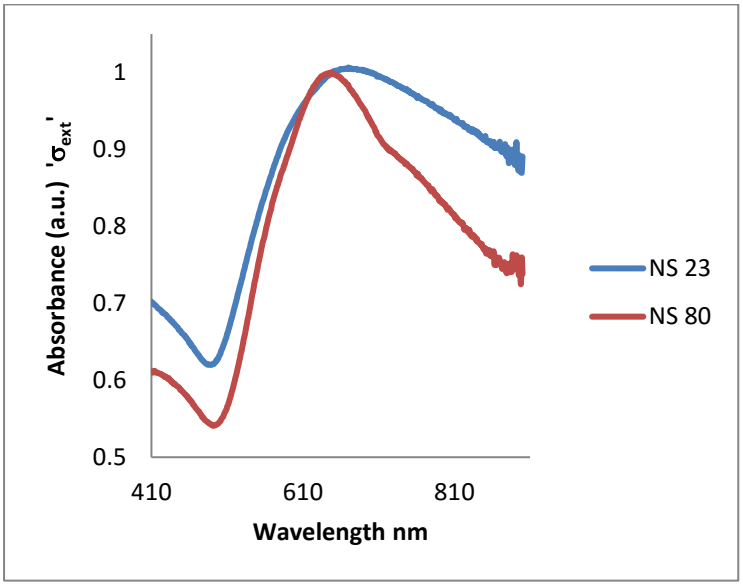

Figure 47 Comparison between optical spectra of textured nanoshells NS 23, made by the two-step growth, and NS 80 made using pH 11.99 seed particles.

Figure 47 illustrates the difference between optical absorption spectra of the textured nanoshells made within this research. NS 80 is the spectrum of the nanoshells made using seed particles made at a pH of 11.99 and NS 23 is the spectrum of nanoshells made via the two-step growth method. The absorption spectra obtained indicate that the particles made

via the two-step growth method have an absorption peak at 741 nm compared to the 696 nm peak of the particles made at a pH of 11.99. The spectrum of the former though is broader in comparison to the latter which was found to have a sharper peak. Reasons for spectral broadening are discussed latter in the chapter.

Thereby it has been found that the texturing of nanoshells may be achieved through the use of minimal amounts of gold reduced onto partially complete particles. The nanoshells generated by this method are quite textured. The roughness may be reduced by thickening the shell. Alternatively, textured nanoshells may be formed by one step-growth of a continuous shell from pH-11.99 seed particles. The two-step growth method was found to provide a 45 nm shift, towards longer wavelengths, more than that achieved by the high pH nanoshells. The pH-11.99 particles did though exhibit less spectral broadening in comparison to the two-step growth nanoshells. These methods of nanoshell texturing are deemed better in comparison to the methods described by Wang as these methods do not make use of aggressive chemicals in the etching away of the nanoshell surface. Additionally, the techniques described in this study result in the formation of pure gold shells not contaminated with other chemicals that were added during the formation.

III. c. Ultraviolet-Visible Spectroscopy

This section of the thesis presents an analysis of the spectra obtained of nanoshells grown under the various conditions detailed within this chapter. Thus we are able to determine the optimum conditions for nanoshell formation. The absorption spectra of the nanoshells provide information regarding the wavelength at which resonance occurs as well as the magnitude of the optical absorption displayed by the nanoshells. The results presented here are of the extinction spectra, total absorbance.

1. Effect of pH on the optical absorption of nanoshells

This section presents details of the effect of the pH of formation, of seed particles, on the optical absorption spectra of the nanoshells created in this study.

The results presented below for NS 70, NS 22, NS 75 and NS 80 are for groups of nanoshells that correspond to seed particles made at pH values of 3.25, 4.63, 7.74 and 11.99, respectively. Figure 48 illustrates a comparison of the normalized spectra of NS 70, NS 22, NS 75 and NS 80. For more clarity regarding the shape of each spectrum, the individual spectra are presented in Figure 49. Moreover, Figure 50 illustrates the un-normalized spectra, also for the purpose of further comparison. The data in Table 4 provide a comparison between the spectra of the nanoshells, in Figure 48, in terms of the spectral width and the magnitude of the absorption peak. As explained in Appendix A, these are two parameters by which one may measure quality of nanoshells thus facilitating the comparison of the different conditions under which the nanoshell were formed.

Shell number	Seed particle description	Spectral width	Magnitude of absorption peak	Absorption peak
NS 70	pH 3.25	221 nm	1.99	651 nm
NS 22	pH 4.63	273 nm	2.1	700 nm
NS 75	pH 7.74	235 nm	1.7	639 nm
NS 80	pH 11.99	171 nm	1.8	653 nm

Table 4 Summary of quality of nanoshells made using seed particles made different values of pH

Results indicate that nanoshells made from pH 11.99 seed particles were found to present the least spectral width, 171 nm. Also, the least magnitude of absorption, 1.7, was demonstrated by the nanoshells made from pH 7.74 seed particles.

Additionally, particles formed at a pH of 4.63 (standard conditions) were found to have the largest spectral width, 273 nm. The particles formed at a pH of 4.63 were also found to have a resonance peak at 700 nm. This was a further shift of 47 nm into the near infrared compared to the other particles, as illustrated in Figure 48. Moreover, the magnitude of the absorption peak of the 4.63 pH particles was found to be 6% more than the particles made at a pH of 3.25, 20% more than the particles formed at a pH of 7.74 and 14% more than particles made at a pH of 11.99. The results depicted in Figure 50 indicate that the absorption peak is suppressed when the nanoshells originate from seed particles formed at high pH values in comparison to particles made from seed particles made at lower pH values. This finding is in agreement with results presented by Park et al (Park et al, 2006). The results indicated no trend for the variation of the optical absorption relative to the pH at which the seed particles were formed; this too is in agreement with the results obtained by Park et al.

As a consequence, it can be concluded that nanoshells from particles formed at lower values of pH were found to have a higher absorption peak magnitude compared to those formed at higher pH values. In comparison to results obtained by Kim et al and Park et al (summarized in Table 2), the spectra obtained within this study were found to have a magnitude of absorption 20.9% greater than the particles produced by Kim et al and 22.38% greater than those produced by Parker et al, at a pH of 3. Also, results of the magnitude of absorption of particles obtained in this study, at a pH of 7.74, were 17.6% greater than particles produced by Parker et al at a pH of 9. The amount of gold used in this study was 33.3% less than amounts used by Kim et al. No amounts were stated by Parker et al. Also, the amount of gold used in this study was a twentieth of the amount of gold indicated by Brinson et al for comparable nanoshells.

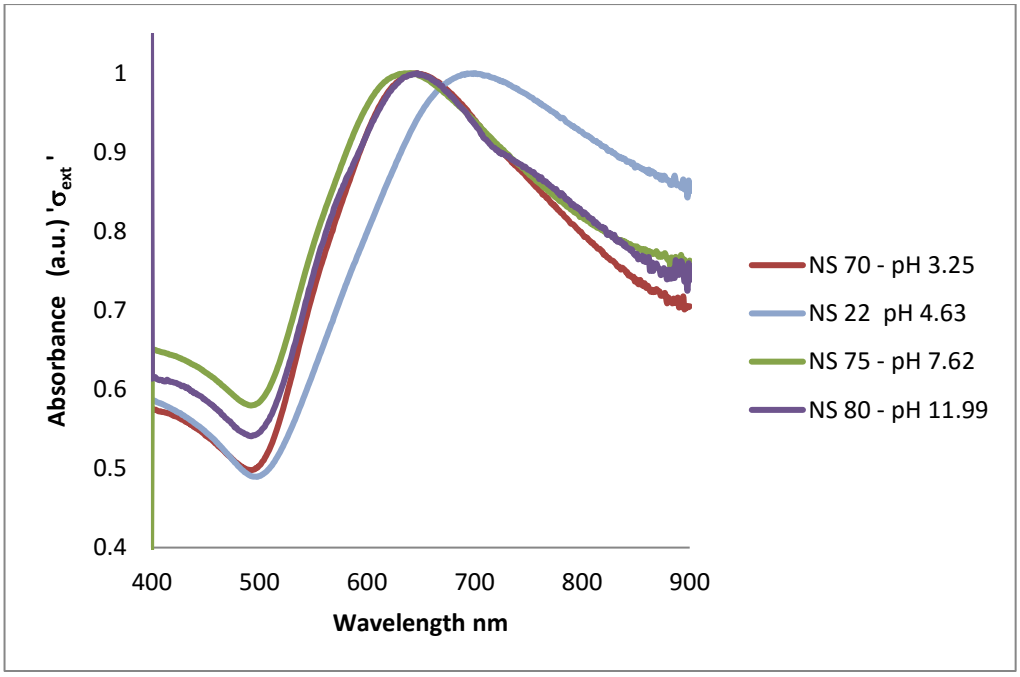

Figure 48 Effect of seed particle formation pH on the optical spectra of nanoshells

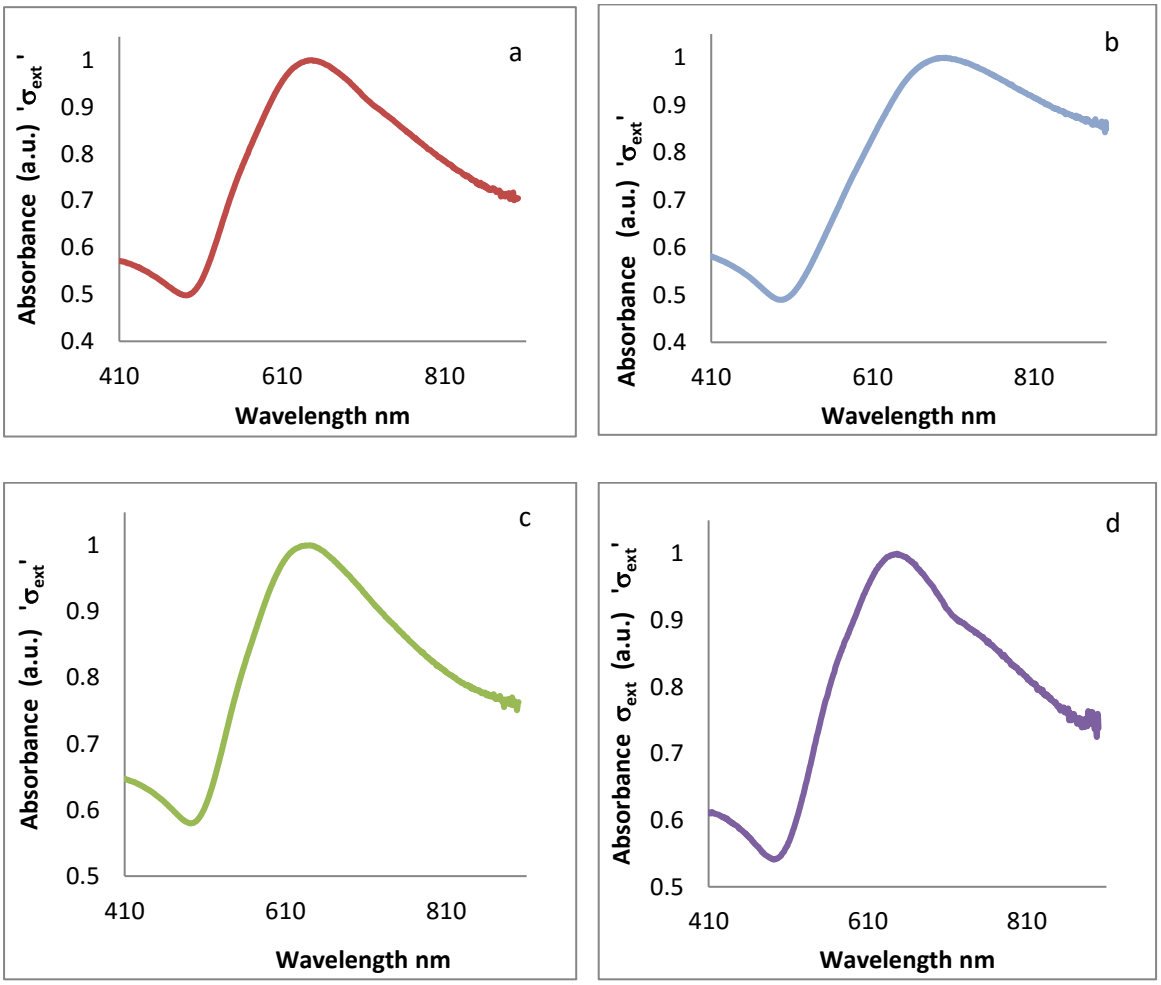

Figure 49 Spectra of nanoshells made from (a) pH 3.25 seed particles, (b) pH 4.63 seed particles, (c) pH 7.74 seed particles and (d) pH 11.99 seed particles

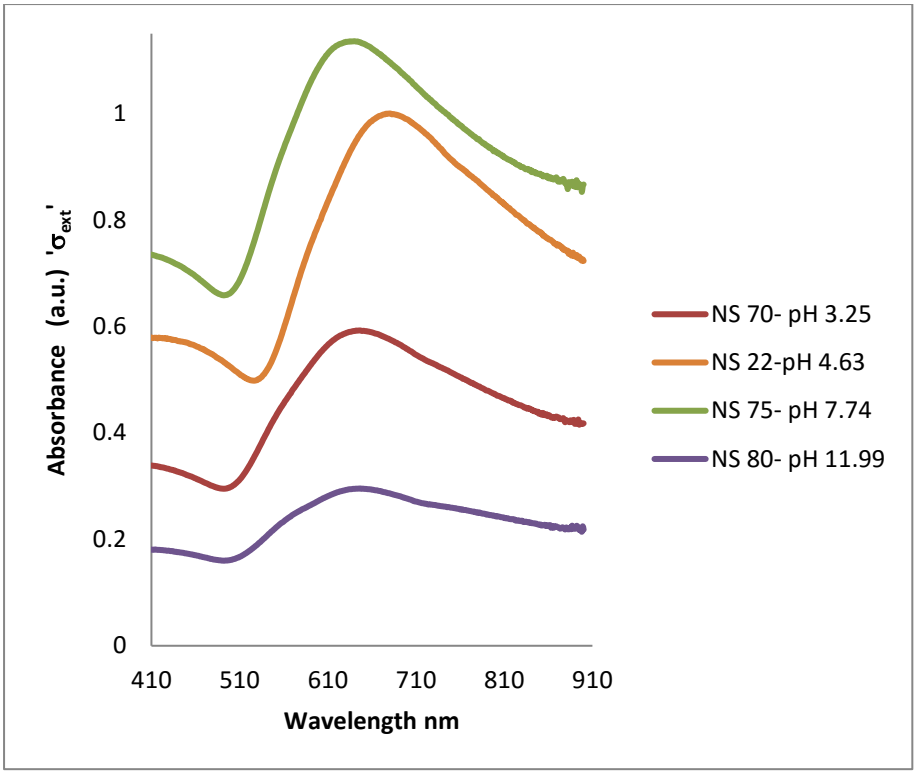

Figure 50 Effect of attachment pH on final nanoshell absorption spectrum

2. *Effect of seed particles on the optical absorption of nanoshells*

The results presented in Figure 51 provide a comparison between the spectra obtained for the nanoshells formed using seed of various ratios of 2 nm gold colloids to silica colloids. The concentrations attempted were: the standard ratio, 59.9% of the standard, 150% of the standard and 176% of the standard, as previously stated.

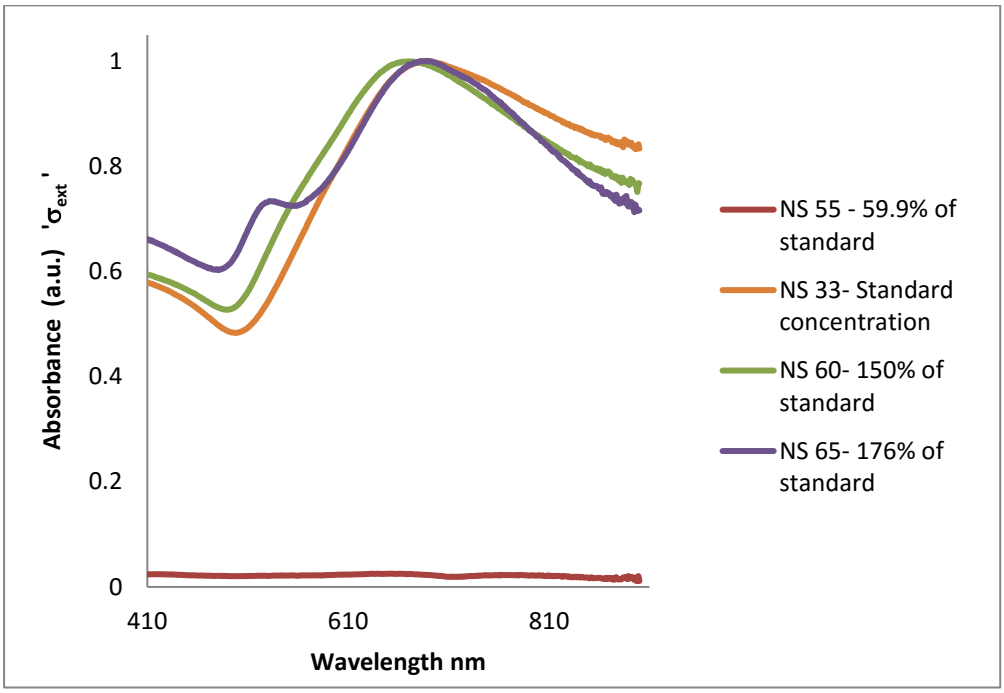

Figure 51 Effect of ratio of gold to silica (seed particles) on optical absorption spectra

Shell number	Seed particle description	Spectral width	Magnitude of absorption peak	Absorption peak
NS 55	59.9% of Std	Not evaluated		
NS 33	Standard conc.	277 nm	2.08	711 nm
NS 60	150 % of Std	259 nm	1.89	683 nm
NS 62	176 % of Std	228 nm	1.66	702 nm

Table 5 Summary of results from spectra of Figure 51

The data presented in Table 5 provides a comparison between the optical spectra of Figure 51 in terms of the spectral width and the average absorption. The results indicate that nanoshells NS 33, formed at standard attachment conditions, have the largest spectral width, 277 nm, and the highest magnitude of absorption, 2.08. NS 60, formed using 1.5 times more gold, have a spectral width that is narrower by 18 nm and a magnitude of

absorption equal to 1.89. The results also indicate that as the ratio of gold relative to silica increases beyond 1.5 times the standard ratio, the spectral width and absorption magnitude continue to decease by 30 nm and 10%, respectively. Therefore, although Preston et al (Preston, 2006) argue that as the amount of gold on the surface of the silica is increased the shells are more complete and have a higher absorbance, the results obtained in this study indicate that there is a limit to the amount of gold relative to silica that can be used in creating seed particles. Beyond that point, as illustrated through the optical spectra in Figure 51, the plasmon resonance no longer shows a pronounced peak and starts to become suppressed with the addition of more gold. This may be explained as follows: As the particles come closer to one another, the interaction between their plasmons causes a pronounced peak. Eventually, they merge and form larger clusters, resulting in a rougher shell (when using a constant amount of K-Au plating solution) thus resulting in a lower and less-pronounced peak. This finding is in agreement with results obtained by Brinson et al (Brinson, 2008). The absorption peaks of all three groups of nanoshells are comparable occurring at wavelengths ranging from 687 to 711 nm. The resonance peak occurs at 711 nm under standard formation conditions and at 687 nm for particles formed with 1.5 times more gold. The nanoshells made from seed particles with 1.76 times the standard coverage were found to have a resonance peak at 702 nm.

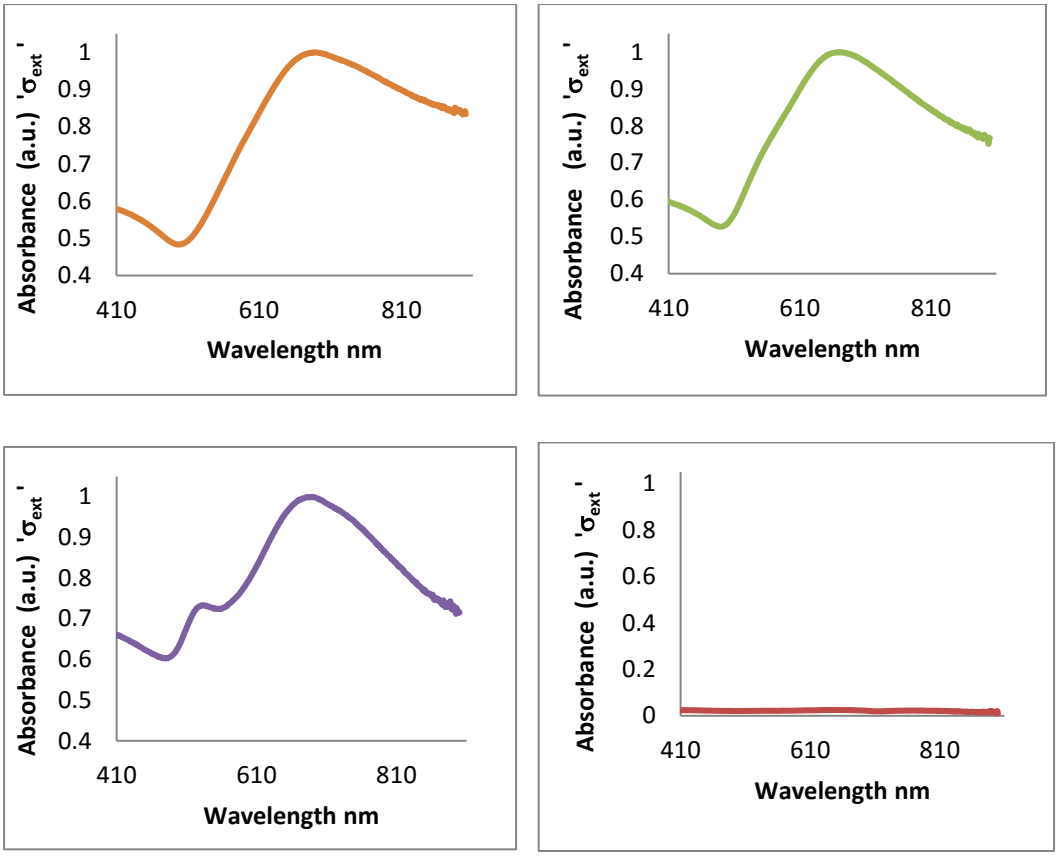

Figure 52 Spectra of nanoshells formed at *(a)* standard ratio of gold to silica, with peak at 724 nm (NS 33) *(b)* 1.5 times the standard ratio, with peak at 673 nm (NS 60) *(c)* 1.76 times the standard ratio, with peak at 691 nm (NS 65) and *(d)* 0.6 times standard ratio –peak undefined

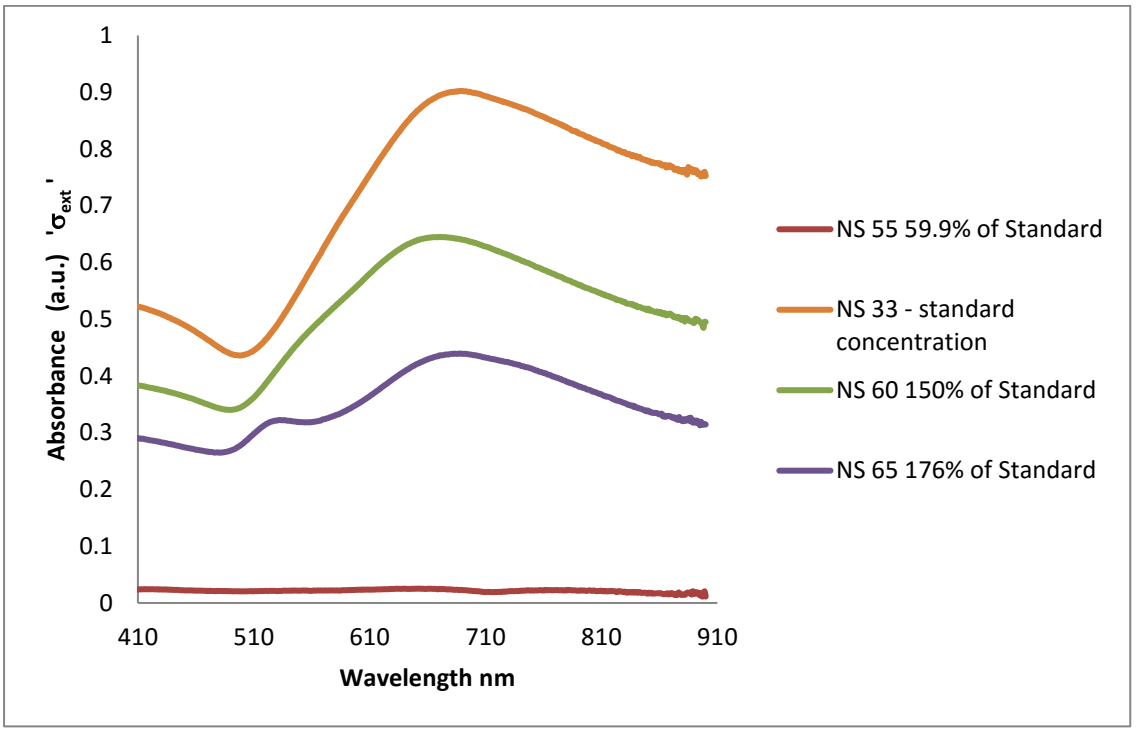

Figure 53 Un-normalized spectra of nanoshells formed at various ratios of gold to silica, the highest value of absorption being that of the nanoshells resulting from seed particles formed under standard conditions

3. *Theoretical and Experimental Spectral Differences and the Reasons for Spectral Broadening*

The results illustrated in the above sections have shown certain deviations from the theoretical spectra, calculated through the Quasistatic Approximation of Mie theory, presented in Chapter II. The deviations are represented as the broadening of the experimentally obtained optical spectra from the theoretical one. These deviations are summarized in Figure 54 below and possible reasons for this broadening are discussed below.

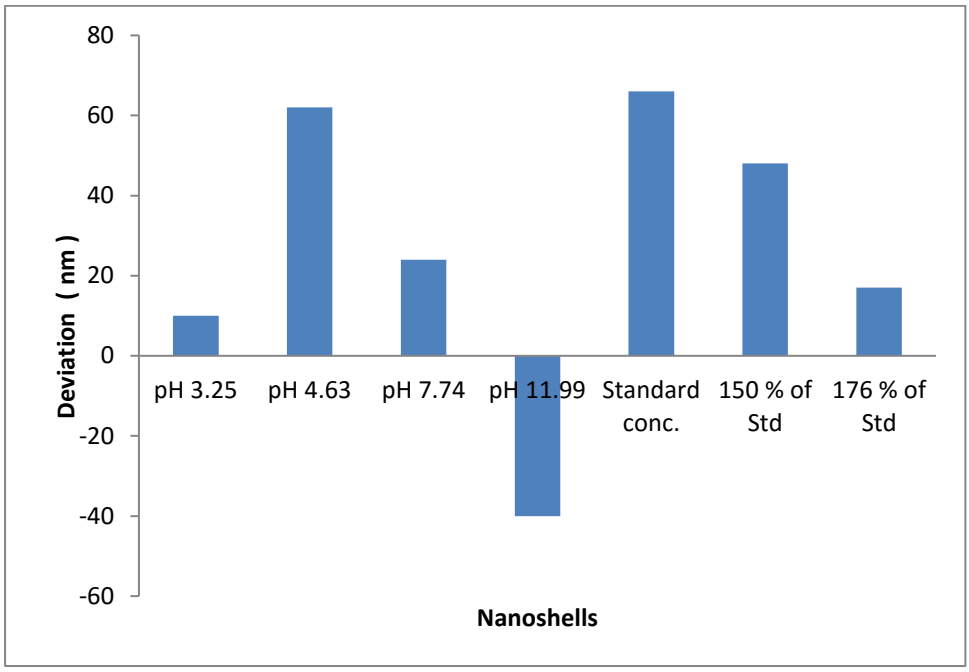

Figure 54 Amount of deviation (nm) of experimental spectral width from the corresponding theoretically determined spectra.

- ***Double nanoshells and larger particles resulting from fusion***

As illustrated throughout this chapter, the process leading to the formation of nanoshells is a multistep processes that results, at various steps of the process, in double nanoshells fused together and in the fusion of two or more particles together. The Mie theory solutions to Maxwell's equation, for the boundary conditions of nanoshells, predict the spectra of nanoshells based on the assumption that the particles have spherical symmetry (Kreibig et al, 1995). 'Dimers'(Halas), which are two fused nanoshells, and larger particles fused together forming shapes like those depicted in Figure 55 and Figure 56 below, as would be expected, have optical properties that are different from monodisperse nanoshells. Their presence in nanoshell dispersions alters the shape of the absorption

spectrum, in comparison to solutions containing only monodisperse nanoshells, consequently causing the broadening of the optical spectrum (Oldenburg et al, 1999, Westcott et al 1998).

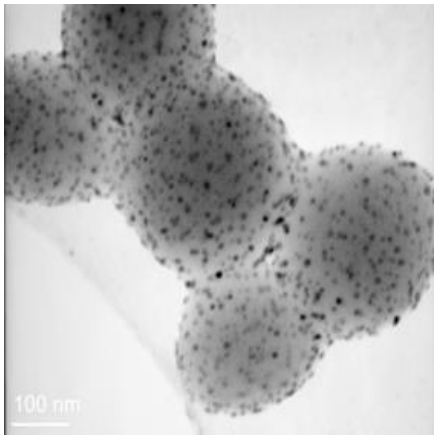

Figure 55 TEM image (200 kV, bright-field) of several seed particles fused together prior to nanoshell formation

- ***Size distribution of core particles***

Another size-related factor affecting the shape of the spectrum of nanoshells is the size distribution of the core particles. Once again referring to the Mie theory assumption that the particles are monodisperse and have a narrow size distribution, the fact that the 100 nm silica particles have a wide size distribution, ranging from 70-110 nm, also causes a broadening of the spectrum. Additionally, TEM and SEM imaging indicate that a small percentage of the silica colloids are not all spherical, as depicted in Figure 57. The non-uniformity of the shape of the silica cores is an additional factor responsible for the broadening of the optical spectra (Oldenburg et al, 1999).

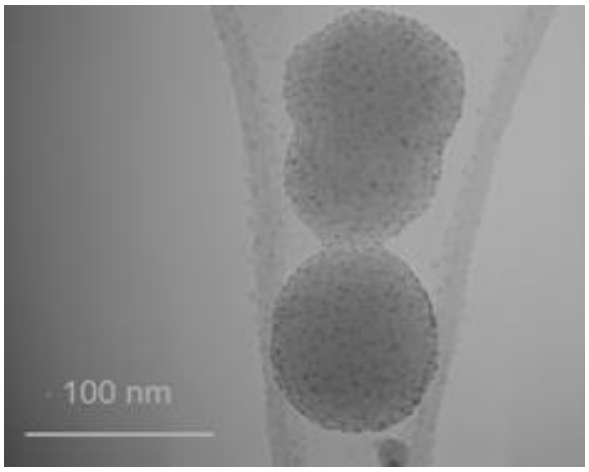

Figure 56 TEM image of (200 kV, bright-field) fused and non spherical silica particles with 2 nm gold colloids attached

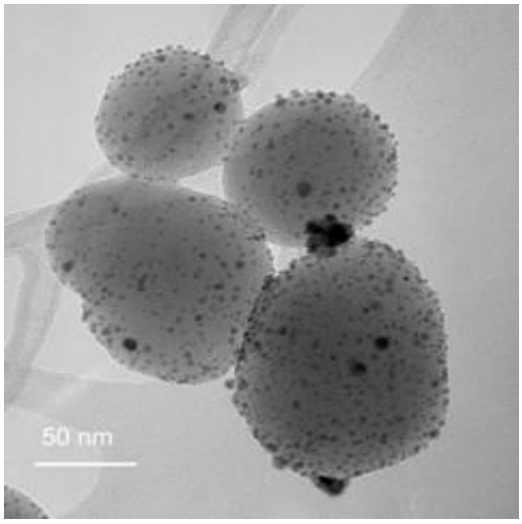

Figure 57 TEM image (200 kV, bright-field) of non spherical silica particles of larger sizes

It can also be predicted that this variation in core size is accompanied by a variation in shell thickness. This variation in shell thickness is a parameter as equally influential, on the optical absorption of the nanoshells, as the fused particles. These findings regarding the size and shape influenced-spectral variation are in agreement with findings by Oldenburg et al, 1999, Averitt et al, 1998 and Cortie et al, 2001. The results of this study indicate that the variation in the size of the silica cores is accompanied by the anticipated variation in shell thickness, as illustrated through the graph in Figure 58. For a required shell thickness of 15 nm, the actual thickness of the shells was found to vary between 16 and 28.7 nm for a core variation of between 110 and 70 nm.

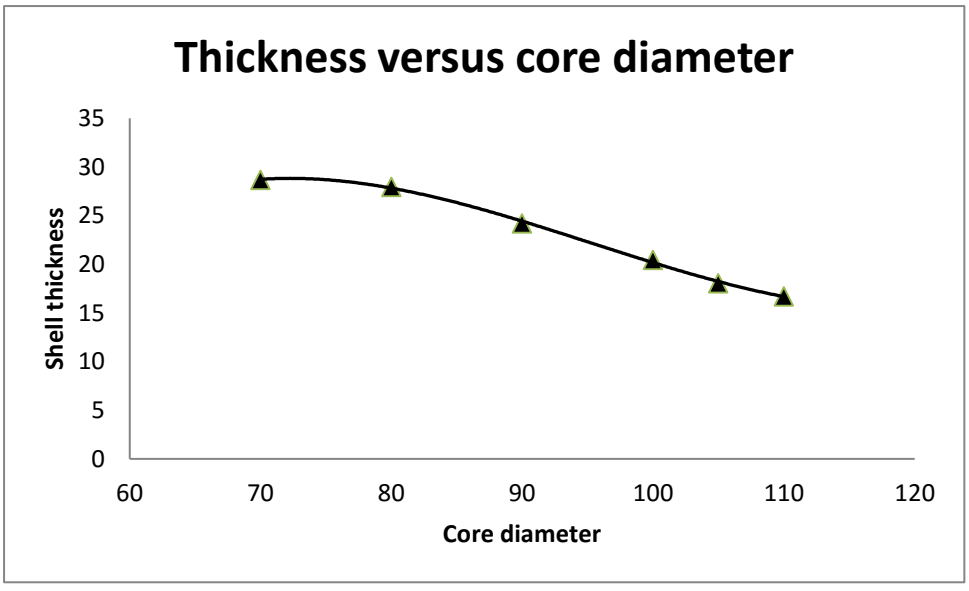

Figure 58 Variation of nanoshell thickness in relation to core diameter

- ***Dielectric constant of gold***

Lastly, the dielectric constant of gold also has an effect on the deviation of the spectra, obtained experimentally, from that obtained theoretically. The two main reasons for this deviation are thought to be the interband transition of the electrons of gold in the visible region of the spectrum and the reduced mean free path of electrons within the shell (Oldenburg et al, 1998). As for the latter, in all the experiments, carried out in this study, whose results are given in detail above, the thickness of the shells was below the mean free path of electrons in bulk gold, which is approximately 42 nm at room temperature. This reduction in the mean free path of the electrons, caused by the shell thickness, affects the value of the dielectric constant of the gold that was used in the prediction of the theoretical spectrum through Equation 4 and Equation 5 of Chapter II. A correction for the reduction of the mean free path of the electrons may be made by incorporating a term for 'modified collision frequency' into the dielectric constant of the gold (Oldenburg et al, 1999, Kreibig et al, 1995 and Preston et al, 2006) thereby accommodating for additional collisions caused by the boundaries of the gold shell.

The second reason for the broadening is thought to be the interband transition of the electrons between the d and s shells (Hermann, 1993) in the gold. This is, though, subject to controversy since interband transition occurs at wavelengths below 600 nm (Halte et al, 2006). In the case of the nanoshells obtained in this study, I adapt the view that the broadening is not a result of the interband transitions and is rather a result of the other factors discussed earlier in this section.

Finally, Figure 59 (a) illustrates the thinnest nanoshell obtained within this study the thickness of which was approximately 4.5 nm. The shells were found to be of a rough texture and a peak resonance at approximately 940 nm. The absorption peak is illustrated in Figure 59 (b). This group of nanoshells indicates that using the protocol and methods developed in this study, it is possible to obtain a 420 nm shift of the plasmon resonance peak towards longer wavelengths. This result is of value because it enables the use of these nanoparticles in applications that require absorption in the near infrared region of the spectrum.

Although, my protocol uses approximately 1/20th of the amount of gold used by other researchers in the field, I have been able to produce particles that have a resonance peak in the mid-near infrared region of the spectrum where absorption by water and tissues is minimal.

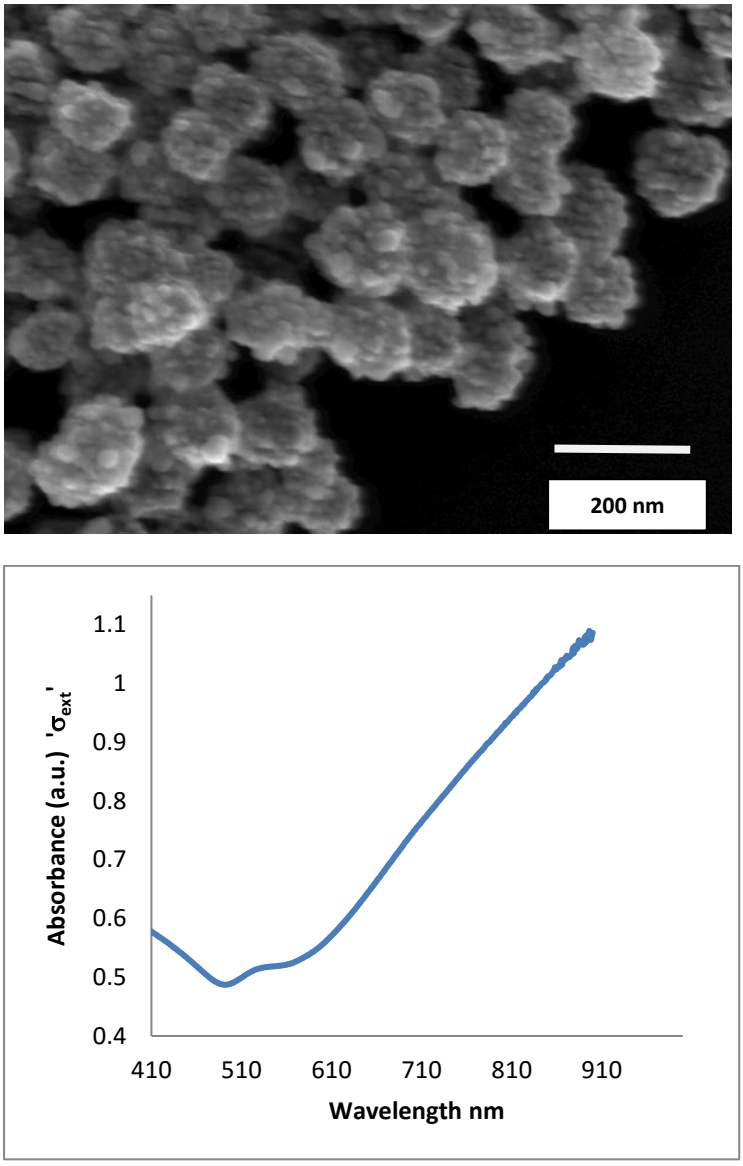

Figure 59 a) SEM image (backscattered imaging mode) and b) Optical spectra of thinnest shell formed from seed particle formed at standard conditions

Summary of results and experimental findings

To summarize the results obtained in this research, it has been found that

- Gold colloids used as seed particles for the growth of gold shells must not be of a size exceeding 2-3 nm. The use of larger colloids results in the formation of nanoshells with a very rough surface morphology. The use of smaller colloids has also been proven to fail, in research conducted by others (Westcott et al, 1998)
- The variation of the pH of the colloidal dispersion, during the process of the seed particles formation, does not have a significant effect on the number of 2 nm gold colloids that attach to the surface of the silica. Rather, varying the pH during seed particles formation affects the organization of the gold particles on the surface of the silica. A pH of 3.25 was found to cause the gold colloids to form groups of 5-7 colloids, on the surface of the silica. At pH values of 11-12, the gold colloids formed clusters made up of approximately 5-7 gold colloids, on the surface of the silica.
- Varying the pH during seed particle formation was found to affect the final morphology of the nanoshells. Nanoshells made from seed particles coined at high values of pH had a more visible surface roughness compared to nanoshells made from low-pH seed particles; the roughness varied between 28 and 36 nm, as estimated by means of the method described in Appendix A.
- Varying the ratio of gold to silica colloids, during the formation of the seed particles, had the foremost effect on the formation of the seed particles and in turn on the nanoshells. By varying the ratio of gold to silica, the coverage on the surface of the silica was modified. The threshold was found to be 12.45 g of gold per 1.625 mg of silica. Ratios of gold to silica below this value resulted in incomplete nanoshells due to the insufficient gold coverage on the surface of the silica. Ratios of gold to silica exceeding this value resulted in the formation of complete nanoshells. However, it was found that the addition of excess gold caused the presence of new gold nuclei which grew during the shell formation process. The formation of these new nuclei hindered the process of nanoshell formation. Additionally, the removal of these newly formed gold colloids, from the nanoshell colloidal solution, was not a straightforward process. Although the use of excessive washing resulted in the

removal of the excess gold colloids from the seed particle dispersion, the wash cycles resulted in the fusion of a percentage of the seed particles. This fusion resulted in the production of large particles made of agglomerated nanoshells.

- This research provides two new methods for forming textured nanoshells. The first is one using two-step, successive growth of gold shells on the silica cores and the second is using seed particles made under high pH attachment conditions.
- This Chapter has also provided a comparison between the optical responses of different nanoshells by comparing the experimentally obtained spectra of nanoshells produced in this study. The shapes of the different spectra, and their deviation from those of the theoretically determined spectra, were discussed. Comparisons between optical spectra indicate that it is possible to obtain nanoshells of good quality from seed particles of 12.45 g of gold per 1.625 mg of silica and that there is no significant benefit from the use of gold ratios in excess of this amount.
- The effect of heat was assessed in terms of raising the temperature of the plating solution prior to the addition of the seed particles. This resulted in the shift, of the spectra of nanoshells made using this method, towards longer wavelengths. This discovery is of additional value because the further the shift of the peak into the near infrared region of the spectrum the more suited the particles are for biological applications.
- The study illustrates that it is possible to generate an even larger 'red shift' of the peak by reducing the thickness of the shell to approximately 5 nm. However, it was not possible to evaluate the spectrum obtained for these nanoshells due to the wavelength limit of the spectrophotometer.

Chapter IV: Summary and Conclusion

The main achievement of this research has been the development of a modified procedure for the formation of gold nanoshells. Modifications made in this study, to procedures described in literature have involved of optimizing of the amount of gold necessary for the formation of the seed particles. The study has also established the effect of the seed particle formation procedure, with emphasis on the pH level and ratio of gold to silica, on the final morphology of the gold nanoshells.

Through this study it has been determined that, ratios of gold to silica below 12.45 g of gold per 1.625 mg of silica do not sustain the formation of complete gold shells. Moreover, ratios of gold to silica in excess of 12.45 g of gold per 1.625 mg of silica hinder the formation of the nanoshells due to the presence of excess gold seeds in the seed particle dispersion which cause the formation of gold clusters during nanoshell formation. Attempts to remove the excess gold require several wash cycles, which lead to the formation of particles that are fused to one another.

The protocol followed to create nanoshells in this study has led to the formation of nanoshells with a thickness of approximately 4.5 nm and a resonance peak at 940 nm. This nanoshell was found to be the thinnest achievable nanoshell using the 100 nm silica cores and the method of nanoshell formation described in this thesis.

Chapter V: Proposed Future Work

This Chapter proposes future biological work that will be done on the basis of the present study. Although gold nanoshells may have numerous applications requiring the enhancement of the electromagnetic field in the proximity of the particles, this chapter provides a description of biological work that may be conducted with particular emphasis on nano-oncology. Preliminary experimental work has been conducted, in the course of this research, in this field.

V. 1 Introduction

The design and development of a drug that enables physicians to target cancer cells only, while having no effect on healthy cells, has been the aspiration of many cancer researchers. Traditional procedures, including chemical and radio therapy, affect all proliferating cells of the body equally resulting in undesirable side effects. The realization of the aim of targeting cancerous cells may become possible with the use of nanoparticles (Melancon et al, 2008, Yih et al, 2005, Xiaohua Huang et al, 2007, West et al, 2003, Veronese et al, 2005, Aslan et al 2005). Nanoparticles enable cell-specific targeting through the attachment of targeting moieties to their surface. The cell targeting is usually through antibody – antigen binding. Additionally, the similarity in size between nanoparticles and many bio-molecules, as depicted in Figure 60, enables the use of nanoparticles in diagnostic and therapeutic medical applications (Wang et al., 2006, West et al, 2003). However, it is more important to note that the significance of the use of nanostructures arises from the new and unique properties that they bring to therapeutic applications. As shown in the thesis, by controlling the dimensions of nanostructures, it becomes possible to control and tailor their optical properties with utmost precision. This enables the utilization of gold nanoshells, for example, in applications that are not possible using their macroscopic counterpart. Additionally, it is possible to enhance the biocompatibility and aqueous solubility of nanostructures simply by chemical modification of their surface through the attachment of molecules such as polyethylene glycol to the surface of the nanoparticles thus making them more suited for integration with biological systems (West et al, 2003, Veronese et al, 2005, Hirsch et al, 2005, Choi et al, 2006, Jaian et al, 2006 and El-Sayed et al 2001).

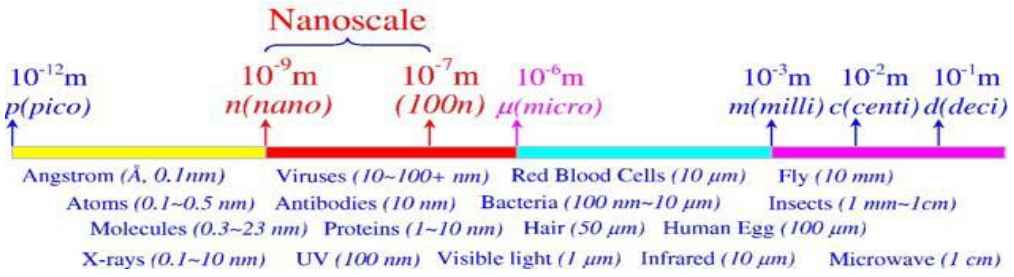

Figure 60 The Nanoscale Yih et al, 2005

V. 2 The need for future research:

Current research (Al-Mayhani et al, 2009, Johansson et al, 1999, Zhang, et al 2000) in the field of oncology, specifically, brain cancer, has indicated an inclination towards adopting of the hypothesis that a group of cells exist within every tumour population that may be considered responsible for the initial growth of a tumour and its re-growth post-treatment, or when removed using traditional surgical techniques. In the case of GBM brain tumours, it is assumed (Zhang et al, 2000) that a certain percentage of the oligodendrocyte precursor cells (OPCs) present in the brain are responsible for the growth of GBM brain cancer.

The reasons behind this hypothesis are that OPCs represent 70% of the total population of neural progenitor cells (NPCs) in the brain. These NPCs have a wide anatomical distribution within the brain, they are highly proliferative and they are capable of giving rise to all different types of neural cells. It has also been found that 70% of the OPCs express a surface proteoglycan, termed Chondroitin Sulfate Proteoglycan 4 (CSPG4) more commonly known as an NG2 proteoglycan, or just NG2. The NPCs that express NG2 are all OPCs. The remaining 30%, of the NPCs, do not express NG2 and are non-OPCs (Zhang et al, 2000). Moreover, studies conducted over the past five year have indicated that the OPCs are capable of giving rise to oligodenrocytes, astrocytes and neurons (Berry et al, 2002 and Sanai et al, 2005), thus supporting the idea that OPCs are multi-potent.

It has thus been concluded that OPCs are cells with stem-like capabilities since they are capable of self-renewal, are multi-potent and show a wide anatomical distribution in the brain. The multi-potency of these cells combined with the anatomical evidence regarding GBM tumours and the distribution of the OPC cells within the tumour has led to the hypothosis that OPCs are responsible for the origination and growth of GBM cancer (Chekenya et al, 2008 and Nishiyama et al , 2009).

Recent studies (West et al, 2002, Bernardi et al, 2008), using nanoparticles in targeting GBM brain tumours, have not been directed towards eliminating the cells of origin therefore allowing for the re-growth of the tumour. Research by Jordan et al (Jordan et al, 2006) has been via non-specific binding of magnetic nanoparticles to the entire population of cells within the brain. This means of indirect targeting relays only on the accumulation of nanoparticles within tumours through Enhanced Permeability and Retention (EPR).
The future research, proposed here, will be directed towards the thermal ablation of giloblastoma multifome cancer cells of origin through the use of gold nanoshells and NG2 antibodies as targeting moieties attached to the surface of the nanoshells.
Experiments will be designed to study the effect of the heat generated by gold nanoshells at resonance conditions on the capability of thermally ablating the $NG2^{+}$ OPC cells present in a tumour population. Another set of experiments will aim to study localized drug delivery using nanoshells encapsulated in a hydrogel.

V. 3 Preliminary biological work

Experiments carried out to determine the biocompatibility of the gold colloids by subjecting GBM cell lines to gold colloids of 100 nm and 150 nm have indicated that gold colloids of these sizes do not have an effect on the growth or proliferation of the oligodendrocytes under consideration. The detailed experimental work is shown in Appendix B.

Bibliography

Aden, Arthur L., and Milton Kerker. “Scattering of Electromagnetic Waves from Two Concentric Spheres.” Journal of Applied Physics 22, no. 10 (October 0, 1951): 1242-1246.

Aguirre, Carla M., Tara R. Kaspar, Corey Radloff, and Naomi J. Halas. “CTAB Mediated Reshaping of Metallodielectric Nanoparticles.” Nano Letters 3, no. 12 (December 1, 2003): 1707-1711.

Al-Mayhani, Talal M. Fael, Siolian L.R. Ball, Jing-Wei Zhao, James Fawcett, Koichi Ichimura, Peter V. Collins, and Colin Watts. “An efficient method for derivation and propagation of glioblastoma cell lines that conserves the molecular profile of their original tumours.” Journal of Neuroscience Methods 176, no. 2 (January 2009): 192-199.

Ashayer, Roya, Samjid H. Mannan, and Shahriar Sajjadi. “Synthesis and characterization of gold nanoshells using poly(diallyldimethyl ammonium chloride).” Colloids and Surfaces A: Physicochemical and Engineering Aspects 329, no. 3 (November 5, 2008): 134-141.

Aslan, Kadir, Joseph R Lakowicz, and Chris D Geddes. “Plasmon light scattering in biology and medicine: new sensing approaches, visions and perspectives.” Current Opinion in Chemical Biology 9, no. 5 (October 2005): 538-544.

Averitt, R. D., D. Sarkar, and N. J. Halas. “Plasmon Resonance Shifts of Au-Coated Au2S Nanoshells: Insight into Multicomponent Nanoparticle Growth.” Physical Review Letters 78, no. 22 (June 2, 1997): 4217.

Averitt, Richard D., Sarah L. Westcott, and Naomi J. Halas. “Linear optical properties of gold nanoshells.” Journal of the Optical Society of America B 16, no. 10 (October 1, 1999): 1824-1832.

Badley, Rickey D., Warren T. Ford, Frank J. McEnroe, and Roger A. Assink. “Surface modification of colloidal silica.” Langmuir 6, no. 4 (April 1, 1990): 792-801.

Baker, A., and F. L. Usher. “Nuclear gold sols. II. Mechanism of formation.” Transactions of the Faraday Society 35 (1940): 385-392.

Bernardi, Ronald J, Amanda R Lowery, Patrick A Thompson, Susan M Blaney, and Jennifer L West. “Immunonanoshells for targeted photothermal ablation in medulloblastoma and glioma: an in vitro evaluation using human cell lines.” Journal of Neuro-Oncology 86, no. 2 (January 2008): 165-72.

Berners-Price, Susan, and Peter Sadler. “Phosphines and metal phosphine complexes: Relationship of chemistry to anticancer and other biological activity.” In Bioinorganic Chemistry, 27-102, 1988. http://dx.doi.org/10.1007/3-540-50130-4_2.

Berry, M., Hubbard, P., and Butt, A. M. (2002). Cytology and lineage of NG2-positive glia. J Neurocytol 31, 457-467.

Bohren, Craig F., and Donald R. Huffman. Absorption and Scattering of Light by Small Particles. New edition. Wiley VCH, 1998.

Brinson, Bruce E., J. Britt Lassiter, Carly S. Levin, Rizia Bardhan, Nikolay Mirin, and Naomi J. Halas. “Nanoshells Made Easy: Improving Au Layer Growth on Nanoparticle Surfaces.” Langmuir 24, no. 24 (December 16, 2008): 14166-14171.

Chekenya, M, H K Rooprai, D Davies, J M Levine, A M Butt, and G J Pilkington. “The NG2 chondroitin sulfate proteoglycan: role in malignant progression of human brain tumours.” International Journal of Developmental Neuroscience: The Official Journal of the International Society for Developmental Neuroscience 17, no. 5-6: 421-35.

Choi, Mi-Ran, Katie J Stanton-Maxey, Jennifer K Stanley, Carly S Levin, Rizia Bardhan, Demir Akin, Sunil Badve, et al. “A cellular Trojan Horse for delivery of therapeutic nanoparticles into tumors.” Nano Letters 7, no. 12 (December 2007): 3759-65.

Crochet,J.J.,S.C.Gnyawli. “Temperature distribution in selective laser-tissue interaction.” Journal of Biomedical Optics 11(3):34031. (2006)

Demirovic, R. A., C. Marty, S. Console, S M Zeisberger, C. Ruch, R. Jaussi, R. Schwendener, and K. Ballmer-Hofer. “Targeting human cancer cells with VEGF receptor-2-directed liposomes.” Journal Article, 2005.

Dewhirst MW, Connor WG, Sim DA. “Preliminary results of a phase III trial of spontaneous animal tumors to heat and/or radiation: early normal tissue response and tumor volume influence on initial response”. (1982) International Journal of Radiation Oncology, Biology, Physics.8:1951-1962.

Doremus, Robert , Shou-Chen Kao, and Roberto Garcia. “Optical absorption of small copper particles and the optical properties of copper.” Applied Optics 31, no. 27 (1992): 5773-5778.

Duff, Daniel G., Alfons Baiker, and Peter P. Edwards. “A new hydrosol of gold clusters. 1. Formation and particle size variation.” Langmuir 9, no. 9 (1993): 2301-2309.

Dupree, R., and M. A. Smithard. “The electronic properties of small metal particles: the electric polarizability.” Journal of Physics C: Solid State Physics 5, no. 4 (1972): 408-414.

El-Sayed, Ivan H., Xiaohua Huang, and Mostafa A. El-Sayed. “Selective laser photo-thermal therapy of epithelial carcinoma using anti-EGFR antibody conjugated gold nanoparticles.” Cancer Letters 239, no. 1 (July 2006): 129-135.

Everett, Douglas. Basic Principles of Colloid Science, 1988.

Fluck, Ekkehard. “The chemistry of phosphine.” In Inorganic Chemistry, 1-64, 1973. http://dx.doi.org/10.1007/BFb0051358.

Frens, G. “Particle size and sol stability in metal colloids.” Colloid & Polymer Science 250, no. 7 (July 21, 1972): 736-741.

Fricker, Simon P. “Medicinal chemistry and pharmacology of gold compounds.” Transition Metal Chemistry 21, no. 4 (1996): 377-383.

Furusawa, K., K. Nagashima, and C. Anzai. “Synthetic process to control the total size and component distribution of multilayer magnetic composite particles.” Colloid & Polymer Science 272, no. 9 (1994): 1104-1110.

Gazelle, G.S., S.N. Goldberg, et al (2000). “Tumor Ablation with Radio-frequency Energy.” Radiology 217:633-646.

Graf, Christina, and Alfons van Blaaderen. “Metallodielectric Colloidal Core−Shell Particles for Photonic Applications.” Langmuir 18, no. 2 (January 1, 2002): 524-534.

Griffiths, G., Burke, B., and Lucocq, J. 1993. Fine structure immunocytochemistry. Springer-Verlag, Heidelberg, Germany.

Halas, Naomi . “The Optical Properties of Nanoshells.” Optics and Photonics News 13, no. 8 (2002): 26-30.

Halas, Naomi J. Plasmonics: Metallic Nanostructures and Their Optical Properties: Proceedings of Spie. SPIE-International Society for Optical Engine, 2003.

Halté, A. Benabbas, and J.-Y. Bigot, "Optical response of periodically modulated nanostructures near the interband transition threshold of noble metal," Opt. Express 14,2909-2920 (2006).

Hao, Encai, Shuyou Li, Ryan C. Bailey, Shengli Zou, George C. Schatz, and Joseph T. Hupp. “Optical Properties of Metal Nanoshells.” The Journal of Physical Chemistry B 108, no. 4 (January 1, 2004): 1224-1229.

Hayat, M. A. Colloidal Gold: Principles, Methods, and Applications. Academic Press, 1989.

Hazle, John D., Chris J. Diederich, Marko Kangasniemi, Roger E. Price, Lars E. Olsson, and R. Jason Stafford. “MRI-guided thermal therapy of transplanted tumors in the canine prostate using a

directional transurethral ultrasound applicator." Journal of Magnetic Resonance Imaging 15, no. 4 (2002): 409-417.
Hermann, M., U. Kreibig, and G. Schmid. "The optical extinction of ligand-stabilized Au13- and Au55-clusters: The vanishing of the Mie-resonance." Zeitschrift für Physik D Atoms, Molecules and Clusters 26, no. 0 (March 1, 1993): 1-3.
Hilger, Ingrid, Robert Hiergeist, Rudolf Hergt, Klaus Winnefeld, Harald Schubert, and WERNER A. KAISER. "Thermal Ablation of Tumors Using Magnetic Nanoparticles: An In Vivo Feasibility Study." Investigative Radiology October 2002 37, no. 10 (2002): 580-586.
Hirsch, L R, J B Jackson, A Lee, N J Halas, and J L West. "A whole blood immunoassay using gold nanoshells." Analytical Chemistry 75, no. 10 (May 15, 2003): 2377-81.
Hirsch, L. R., R. J. Stafford, J. A. Bankson, S. R. Sershen, B. Rivera, R. E. Price, J. D. Hazle, N. J. Halas, and J. L. West. "Nanoshell-mediated near-infrared thermal therapy of tumors under magnetic resonance guidance." Proceedings of the National Academy of Sciences of the United States of America 100, no. 23 (November 11, 2003): 13549-13554.
Hirsch, Lee R, Naomi J Halas, and Jennifer L West. "Whole-blood immunoassay facilitated by gold nanoshell-conjugate antibodies." Methods in Molecular Biology (Clifton, N.J.) 303 (2005): 101-11.
Hirsch, Leon, Andre Gobin, Amanda Lowery, Felicia Tam, Rebekah Drezek, Naomi Halas, and Jennifer West. "Metal Nanoshells." Annals of Biomedical Engineering 34, no. 1 (January 1, 2006): 15-22.
Hulst, H. C. van de. Light Scattering by Small Particles. Dover Publications, 1981.
Hunter, Robert J. Introduction to Modern Colloid Science. OUP Oxford, 1993.
Ito, Akira, Kouji Tanaka, Kazuyoshi Kondo, Masashige Shinkai, Hiroyuki Honda, Kazuhiko Matsumoto, Toshiaki Saida, and Takeshi Kobayashi. "Tumor regression by combined immunotherapy and hyperthermia using magnetic nanoparticles in an experimental subcutaneous murine melanoma." Cancer Science 94, no. 3 (2003): 308-313.
Jain, Prashant K., Ivan H. El-Sayed, and Mostafa A. El-Sayed. "Au nanoparticles target cancer." Nano Today 2, no. 1 (February 2007): 18-29.
Johansson, C B, S Momma, D L Clarke, M Risling, U Lendahl, and J Frisén. "Identification of a neural stem cell in the adult mammalian central nervous system." Cell 96, no. 1 (January 8, 1999): 25-34.
Johnson, PB, and RW Christy. "Optical Constants of the Noble Metals." Phys. Rev. B 6 (1972): 4379, 4370.
Jordan, Andreas, Regina Scholz, Klaus Maier-Hauff, Frank Landeghem, Norbert Waldoefner, Ulf Teichgraeber, Jens Pinkernelle, et al. "The effect of thermotherapy using magnetic nanoparticles on rat malignant glioma."
Kandpal, Deepika, Suchita Kalele, and S. Kulkarni. "Synthesis and characterization of silica-gold core-shell (SiO2@Au) nanoparticles." Pramana 69, no. 2 (2007): 277-283.
Kim, H and TR Lee - Journal of Biomedical & Pharmaceutical Engineering, 2008
Kong, Garheng, Rod D. Braun, and Mark W. Dewhirst. "Hyperthermia Enables Tumor-specific Nanoparticle Delivery: Effect of Particle Size." Cancer Res 60, no. 16 (August 1, 2000): 4440-4445.
Kreibig, Uwe, and Michael Vollmer. Optical Properties of Metal Clusters. Springer, 1995.
Kumar, Challa S. S. R. Nanomaterials for Cancer Therapy, 2006.
Lal, Surbhi, Stephan Link, and Naomi J. Halas. "Nano-optics from sensing to waveguiding." Nat Photon 1, no. 11 (November 2007): 641-648.

Li, Hong, Jeannie Han, Alexei Panioukhine, and Eugenia Kumacheva. “From Heterocoagulated Colloids to Core-Shell Particles.” Journal of Colloid and Interface Science 255, no. 1 (November 1, 2002): 119-128.

Li, Yu, and Brian C. Benicewicz. “Functionalization of Silica Nanoparticles via the Combination of Surface-Initiated RAFT Polymerization and Click Reactions.” Macromolecules 41, no. 21 (November 11, 2008): 7986-7992.

Li, Yu, and Brian C. Benicewicz. “Functionalization of Silica Nanoparticles via the Combination of Surface-Initiated RAFT Polymerization and Click Reactions.” Research-article, October 10, 2008. zotero://attachment/7949/.

Loo, Christopher, Leon R. Hirsch, Min-Ho Lee, Emmanuel Chang, Jennifer West, Naomi Halas, Rebekah Drezek, "Gold Nanoshell Bioconjugates for Molecular Imaging in Living Cells," Optics Letters 30, 1012-1014 (2005).

Loo, Christopher, Amanda Lowery, Naomi Halas, Jennifer West, and Rebekah Drezek, "Immunotargeted Nanoshells for Integrated Cancer Imaging and Therapy," Nano Letters 5, 709-711 (2005).

Lowery, Amanda, A.M. Gobin et al. (2006).”Immunonanoshells for targeted photothermal ablation of tumor cells.” International Journal of Medicine 1: 149-154.

Lukyanov, Anatoly N., Tamer A. Elbayoumi, Ananthsrinivas R. Chakilam, and Vladimir P. Torchilin. “Tumor-targeted liposomes: doxorubicin-loaded long-circulating liposomes modified with anti-cancer antibody.” Journal of Controlled Release 100, no. 1 (November 5, 2004): 135-144.

Maier, Stefan A. Plasmonics: Fundamentals and Applications. 1st ed. Springer, 2007.

Maier, Stefan A., and Harry A. Atwater. “Plasmonics: Localization and guiding of electromagnetic energy in metal/dielectric structures.” Journal of Applied Physics 98, no. 1 (July 1, 2005): 011101-10.

Melancon, Marites P., Wei Lu, Zhi Yang, Rui Zhang, Zhi Cheng, Andrew M. Elliot, Jason Stafford, Tammy Olson, Jin Z. Zhang, and Chun Li. “In vitro and in vivo targeting of hollow gold nanoshells directed at epidermal growth factor receptor for photothermal ablation therapy.” Mol Cancer Ther 7, no. 6 (June 1, 2008): 1730-1739.

Michaelis K, Hoffmann MM, Dreis S, Herbert E, Alyautdin RN, Michaelis M, Kreuter J, Langer K.
“Covalent linkage of apolipoprotein e to albumin nanoparticles strongly enhances drug transport into the brain.”The Journal of Pharmacology and Experimental Therapeutics. 317 (3) (2006), pp. 1246–1253

Moores, Audrey, and Frederic Goettmann. “The plasmon band in noble metal nanoparticles: an introduction to theory and applications.” New Journal of Chemistry 30, no. 8 (2006): 1121-1132.

Mulvaney, Paul. “Surface Plasmon Spectroscopy of Nanosized Metal Particles.” Langmuir 12, no. 3 (January 1, 1996): 788-800.

“Neural Stem Cells and the Origin of Gliomas,” August 25, 2005. http://content.nejm.org/cgi/content/extract/353/8/811.

Nishiyama, A., Komitova, M., Suzuki, R., and Zhu, X. (2009). Polydendrocytes (NG2 cells): multifunctional cells with lineage plasticity. Nat Rev Neurosci 10, 9-22.

Nordlander, P., C. Oubre, E. Prodan, K. Li, and M. I. Stockman. “Plasmon Hybridization in Nanoparticle Dimers.” Nano Letters 4, no. 5 (May 1, 2004): 899-903.

Oldenburg, S. J., G. D. Hale, J. B. Jackson, and N. J. Halas. “Light scattering from dipole and quadrupole nanoshell antennas.” Applied Physics Letters 75, no. 8 (1999): 1063-1065.

Oldenburg, S. J., J. B. Jackson, S. L. Westcott, and N. J. Halas. “Infrared extinction properties of gold nanoshells.” Applied Physics Letters 75, no. 19 (November 8, 1999): 2897-2899.

Park, J.W., D.B. Kirpotin, et al (2001). “Tumor targeting using atio-her2 immunoliposomes.” Journal of Controlled Release 74(1-3):95-113

Park Sang-Eun. “The effect of pH-adjusted gold colloids on the formation of gold clusters over APTMS-coated silica cores.” http://cat.inist.fr/?aModele=afficheN&cpsidt=18220220.

Perenboom, J. A. A. J, P. Wyder, and F. Meier. “Electronic properties of small metallic particles,” November 1981.

Pham, Tan, Joseph B. Jackson, Naomi J. Halas, and T. Randall Lee. “Preparation and Characterization of Gold Nanoshells Coated with Self-Assembled Monolayers.” Langmuir 18, no. 12 (June 1, 2002): 4915-4920.

Preston, Thomas C., and Ruth Signorell. “Growth and Optical Properties of Gold Nanoshells Prior to the Formation of a Continuous Metallic Layer.” ACS Nano 3, no. 11 (November 24, 2009): 3696-3706.

Prodan, E., P. Nordlander, and N. J. Halas. “Effects of dielectric screening on the optical properties of metallic nanoshells.” Chemical Physics Letters 368, no. 1-2 (January 2003): 94-101.

Prodan, E., and P. Nordlander. “Plasmon hybridization in spherical nanoparticles.” The Journal of Chemical Physics 120, no. 11 (March 15, 2004): 5444-5454.

Prodan, E., P. Nordlander, and N. J. Halas. “Effects of dielectric screening on the optical properties of metallic nanoshells.” Chemical Physics Letters 368, no. 1-2 (January 14, 2003): 94-101.

Prodan, E., C. Radloff, N. J. Halas, and P. Nordlander. “A Hybridization Model for the Plasmon Response of Complex Nanostructures.” Science 302, no. 5644 (October 17, 2003): 419-422.

Reynolds, Andrew R., S. Moein Moghimi, and Kairbaan Hodivala-Dilke. “Nanoparticle-mediated gene delivery to tumour neovasculature.” Trends in Molecular Medicine 9, no. 1 (January 2003): 2-4.

Richard, Zsigmondy, John Foote Norton, and Ellwood Barker Spear. The Chemistry of Colloids. BiblioBazaar, LLC, 2009.

Sanai, Nader, Arturo Alvarez-Buylla, and Mitchel S Berger. “Neural stem cells and the origin of gliomas.” The New England Journal of Medicine 353, no. 8 (August 25, 2005): 811-22.

Sanvicens, Nuria, and M Pilar Marco. “Multifunctional nanoparticles--properties and prospects for their use in human medicine.” Trends in Biotechnology 26, no. 8 (August 2008): 425-33.

Sassaroli, E., K. C. P. Li, and B. E. O'Neill. “Numerical investigation of heating of a gold nanoparticle and the surrounding microenvironment by nanosecond laser pulses for nanomedicine applications.” Physics in Medicine and Biology 54, no. 18 (2009): 5541-5560.

Sarkar, Dipankar , and N. J. Halas. “General vector basis function solution of Maxwell's equations.” Physical Review E 56, no. 1 (July 1, 1997): 1102.

Schiffelers, Raymond M., Gerben A. Koning, Timo L. M. ten Hagen, Marcel H. A. M. Fens, Astrid J. Schraa, Adriënne P. C. A. Janssen, Robbert J. Kok, Grietje Molema, and Gert Storm. “Anti-tumor efficacy of tumor vasculature-targeted liposomal doxorubicin.” Journal of Controlled Release 91, no. 1-2 (August 28, 2003): 115-122

Skepper, Jeremy N., and Janet M. Powell. “Immunogold Staining of Ultrathin Thawed Cryosections for Transmission Electron Microscopy (TEM).” Cold Spring Harbor Protocols 2008, no. 7 (June 1, 2008): pdb.prot5018.

Solbiati, L and T. Ierace (1997). “Percutaneous US-guided Radio-frequency Tissue Ablation of Liver Metastases: Treatment and Follow-up in 16 Patients.”Radiology 202:195-203

Steele, J.M., N.K. Grady, P. Nordlander, and N.J. Halas. “Plasmon hybridization in complex nanostructures.” In Surface Plasmon Nanophotonics, 183-196, 2007. http://dx.doi.org/10.1007/978-1-4020-4333-8_13.

Stiles, Charles D, and David H Rowitch. “Glioma stem cells: a midterm exam.” Neuron 58, no. 6 (June 26, 2008): 832-46.

Stöber, Werner, Arthur Fink, and Ernst Bohn. “Controlled growth of monodisperse silica spheres in the micron size range.” Journal of Colloid and Interface Science 26, no. 1 (January 1968): 62-69.

Stuart, D.A., A.J. Haes, C.R. Yonzon, E.M. Hicks, and R.P. Van Duyne. “Biological applications of localised surface plasmonic phenomenae.” Nanobiotechnology, IEE Proceedings - 152, no. 1 (2005): 13-32.

Veronese, Francesco M., and Gianfranco Pasut. “PEGylation, successful approach to drug delivery.” Drug Discovery Today 10, no. 21 (November 2005): 1451-1458.

Waddell, Thomas G., Donald E. Leyden, and Mary T. DeBello. “The nature of organosilane to silica-surface bonding.” Journal of the American Chemical Society 103, no. 18 (1981): 5303-5307.

Wang, H., K. Fu, R.A. Drezek, and N.J. Halas. “Light scattering from spherical plasmonic nanoantennas: effects of nanoscale roughness.” Applied Physics B: Lasers and Optics 84, no. 1 (July 1, 2006): 191-195.

Wang, Hui, Daniel W. Brandl, Fei Le, Peter Nordlander, and Naomi J. Halas. “Nanorice: A Hybrid Plasmonic Nanostructure.” Nano Letters 6, no. 4 (April 1, 2006): 827-832.

Wang, Hui, Daniel W. Brandl, Peter Nordlander, and Naomi J. Halas. “Plasmonic Nanostructures: Artificial Molecules.” Accounts of Chemical Research 40, no. 1 (January 1, 2007): 53-62.

Wang, Hui, Glenn P. Goodrich, Felicia Tam, Chris Oubre, Peter Nordlander, and Naomi J. Halas. “Controlled Texturing Modifies the Surface Topography and Plasmonic Properties of Au Nanoshells.” The Journal of Physical Chemistry B 109, no. 22 (June 1, 2005): 11083-11087.

Wang, Hui, Felicia Tam, Nathaniel K. Grady, and Naomi J. Halas. “Cu Nanoshells: Effects of Interband Transitions on the Nanoparticle Plasmon Resonance.” The Journal of Physical Chemistry B 109, no. 39 (October 1, 2005): 18218-18222.

Weissleder, Ralph. “A clearer vision for in vivo imaging.” Nat Biotech 19, no. 4 (April 2001): 316-317.

West, Jennifer L, and Naomi J Halas. “Engineered nanomaterials for biophotonics applications: improving sensing, imaging, and therapeutics.” Annual Review of Biomedical Engineering 5 (2003): 285-92.

Westcott, Sarah L., Steven J. Oldenburg, T. Randall Lee, and Naomi J. Halas. “Formation and Adsorption of Clusters of Gold Nanoparticles onto Functionalized Silica Nanoparticle Surfaces.” Langmuir 14, no. 19 (1998): 5396-5401.

Xiaohua Huang, Prashant K Jain, Ivan H El-Sayed, and Mostafa A El-Sayed. “Gold nanoparticles: interesting optical properties and recent applications in cancer diagnostics and therapy,” November 2, 2007. http://www.futuremedicine.com/doi/abs/10.2217/17435889.2.5.681.

Yih, Tachung C. , PE, Chiming Wei MD, and PhD. “Nanotechnology, Biology and Medicine : Nanomedicine in cancer treatment.” Nanomedicine 1, no. 2 (June 2005): 191-192.

Zhang, Quan Bin, Xiao Yan Ji, Qiang Huang, Jun Dong, Yu De Zhu, and Qing Lan. “Differentiation profile of brain tumor stem cells: a comparative study with neural stem cells.” Cell Res 16, no. 12 (0): 909-915.

Zsigmondy, Richard. The Chemistry of Colloids. BiblioBazaar, LLC, 2008.

Appendix A: Materials and Methodology

a. Introduction

Making gold nanoshells is a multistep process. Success in forming nanoshells is a function of the quantities of the reagents used, in addition to their purity. This chapter presents the reagents that were used in the making of nanoshells, and also provides a detailed description of the procedure followed for nanoshell formation, in this study.

b. Materials

This section describes the materials used in the formation of the gold nanoshells. The concentrations of these chemical, where applicable, and names of the suppliers is also presented.

Silica nanoparticles were obtained from G. Kisker GbR Produkte für die Biotechnologie, Germany. Tetrakis hydroxymethyl phosphonium chloride (80%) was purchased from Sigma Aldrich, U.K. The 98.9% aurochloric acid was obtained from Alfa Aesar, U.K. Sodium hydroxide pellets (98%, anhydrous) were also obtained from Sigma Aldrich,U.K. The 3-Aminopropyl trimethoxysilane (APTMS) was also obtained from Sigma, U.K. Scientific-grade deionized water and millipore water (18.9mΩ) were used for all experiments. Fisher brand,U.K., borosilicate glass bottles and vials were used for the experiments. Centrifuge tubes were also purchased from Fisher Scientific, U.K. The lacey carbon TEM grids and silicon wafers used for TEM and SEM imaging were purchased from Agar, U.K.

c. Experimental Procedures

This section details the 6 -step process by which gold nanoshells were made in this research.

1. Making THPC-capped gold colloids

The 2 nm colloids were made using the Duff method (Duff et al, 1993) for making nanoparticles of this size. Precisely, 90 ml of Millipore water, 2ml of NaOH (2mM) and 3ml of THPC were added consecutively to a 200ml, flat bottom, borosilicate glass bottle, while stirring. After 20 minutes, 1.1 ml of 30 mM aged aurochloric acid were added. The solution was stored away from light at 4^{O}C until further use.

2. Silica nanoparticles

Silica nanoparticles made in accordance with the Stöber method (Stöber et al, 1968) were purchased from G. Kisker. Particles were purchased bare, free from any surface functional groups and were stored at room temperature. Prior to the functionalization of the silica particles, they were subjected to a series of washing cycles. Within this thesis, 'washing cycle' is used to refer to the washing of particles with deionised water, the removal of the water through ultracentrifugation and then the re-suspension of the particles in water using ultrasonication for 15 minutes.

The final suspension of the particles was in ethanol. The final concentration of the particles was 50 mg/ml.

3. Functionalizing the silica nanoparticles

The silica particles were functionalized using 3-aminopropyl-trimethoxysilane (APTMS). The particles used in this study were functionalized in accordance to the following considerations. It has been reported (Waddell et al, 1981) that the APTMS molecule has a footprint of 0.3 nm^2. An adequate amount of APTMS was added to in order to provide a single monolayer of APTMS on the surface of the silica. The APTMS was added to the silica while stirring rapidly for 45 minutes in a polypropylene bottle, after which the particles were washed five times to remove any excess reagent. Silica particles, both bare and APTMS-functionalized, were stored in a polypropylene container.

4. Formation of nanoshell seed particles

The formation of the seeds was accomplished by the addition of an aliquot of the silica colloids to gold colloids, while stirring. The modification of the zeta potential of the gold particles, by varying the pH of the colloidal dispersion, was attempted in order to determine the conditions that rendered the highest quality seed particles. The quality of the seed particles was determined, based on the amount of gold colloids that decorated the surface of the silica. The investigation of the effect of the pH on particle attachment was done by using 2 M HCl and 3 M NaOH. Due to the small amounts of silica used in the process, it was easier and more adequate to adjust the pH of the gold, only. The effect of the variation in pH on the coverage of the gold colloids on the surface of the silica was assessed at pH values of 3.25, 4.67, 7.74 and 11.99.

Additionally, the effect of the ratio of gold to silica on the coverage of the seed particles was assessed, in order to determine the conditions that would yield the best possible coverage of gold on the surface of the silica. This assessment was performed at gold to silica ratios of 1:1, 2:1, 4:1, 6.67:1, 8:1, 10:1 and 11.75:1.

5. Preparing the plating solution

The 'K-Au plating solution', or just plating solution, is a term that is used to refer to the solution that contains the gold salt used for the formation of the gold shells. The gold salt is reduced from the solution; as a result, the 2nm gold colloids on the surface of the silica grow, coalesce and form the continuous gold shell of the required thickness. The plating solution is made of a mixture of potassium carbonate and aurochloric acid. The mixture of K_2CO_3 and $HAuCl_4$ give rise to gold hydroxide via the reaction shown in Equation 13 below.

$$HAuCl_4\,(\text{aq.}) + 2K_2CO_3\,(\text{aq.}) + H_2O \rightarrow Au(OH)_3 + 4KCl + 2CO_2\,(\text{g})$$

Equation 13

It is this $AuOH_3$ that is reduced by the reducing agent to Au (0). The gold nanoshells illustrated and discussed within this thesis were made using formaldehyde as a reducing agent. The K-Au plating solution was prepared at least a day prior to the formation of the nanoshells and was stored at room temperature without subjection to light prior to its use.

6. Formation of gold nanoshells

In the final step of nanoshell formation, the seed particles were ultrasonicated for at least 10 minutes using an ultrasonic probe. Eight mls of the K-Au plating solution were placed in 28 ml vials. Varying amounts of the ultrasonicated, seed particles were added while stirring rapidly with a Teflon coated magnetic stir bar. After 10 minutes of stirring, 20 ul of formaldehyde were added to the K-Au plating solution containing the seed particles. The nanoshells formed instantaneously. The last step before storing the nanoshells was to introduce, once more, a series of wash cycles that would rid the nanoshells of any excess reagents. At this stage, the particles were washed twice with deionized water and then charged stabilized to insure that the particles would remain suspended in solution.

d. Characterization techniques

The following sections describe the methods used for characterization of the seed particles or the nanoshells created within this study.

1. Transmission Electron Microscopy Imaging

Transmission electron microscopy (TEM) imaging was done using the FEI Tecnai 20 at the Cavendish Laboratories (200 kV, bright-field), the FEI Philips CM100 TEM at the Multi-imaging Center, Department of Anatomy, University of Cambridge (80 kV, bright-field) and the JEOL 2000FX TEM at the Material Science Department, University of Cambridge (200 kV, bright-field). TEM samples of nanoparticles were prepared by placing a drop of the solution containing the nanoparticles, or the nanoshells, on a TEM grid that was placed on filter paper until the solvent evaporated. The TEM grids that were used were lacey-carbon coated, 400 mesh, copper TEM grids, purchased from Agar Scientific. All sample preparation was carried out under a fume hood.

2. Scanning Electron Microscopy Imaging

Scanning electron microscopy (SEM) imaging was done using LEO 1530VP FESEM at the Nanoscience Center, University of Cambridge. SEM images of the gold-decorated silica particles were taken at 6 kV. The images taken of the gold nanoshells were taken at 12 kV. SEM samples were prepared by placing a drop of the colloidal dispersion on an isopropanol-cleaned silicon wafer. The solvent was allowed to evaporate. The SEM images were taken at least 24 hrs after samples were prepared. This was because of the difficulty in imaging samples, especially of the gold decorated silica, except when the samples had stabilized.

3. Ultra Violet-Visible Spectroscopy

Ultra Violet-Visible absorption spectroscopy (UV-Vis) was used to determine the absorption spectra of the silica core nanoparticles, the 2 nm gold particles, the seed particles and the final nanoshells. This was done using a 300 Cary Varian Spectrometer. All measurements were done in quartz cuvettes, obtained from Hellma and having a light path of 1 cm. As a baseline, the measurements were first taken for a cuvette containing DI water, in the case of the gold nanoparticles and nanoshells and in ethanol in the case of the silica. The results shown in this thesis represent the results obtained after the subtraction of the

baseline from the readings obtained for the particles. All spectra of nanoshells presented in this thesis are extinction spectra.

4. Zeta-Potential and Size Distribution

Zeta potential were carried out using the Malvern Nano ZS-Zetasizer at the Nanoscience Center, University of Cambridge. Measurements were performed using disposable polystyrene cuvettes having a 10mm light path.

e. Measurements

1. Particle size

In the cases of both the silica cores and the nanoshells, size was determined by SEM imaging. Out of every sample, the diameter of 100 variously sized particles was measured using the SEM annotation tool. It was necessary to determine the size range of each sample of silica prior to the formation of the nanoshells so as to facilitate the determination of the final shell thickness.

2. Shell thickness

In order to determine the thickness of the nanoshells, the values of diameters of the silica particles were subtracted from the diameters of the nanoshell.

3. Roughness

The roughness of the nanoshells was determined by drawing a line around individual nanoshells, as shown in the Figure 61 below, and determining the length of the peaks and valleys on the surface of each nanoshell. The SEM annotation tool was used for the measurements. For each nanoshell, the value of the root mean square of the peaks and valleys was used to determine the approximate surface roughness. One hundred particles were analyzed per sample.

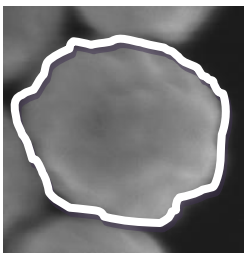

Figure 61 Tracing of particle to determine approximate value of roughness.

4. Evaluating the optical spectra

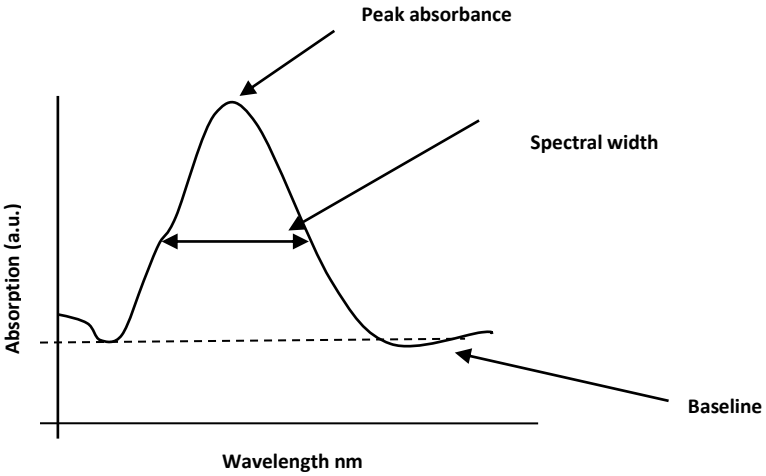

Figure 62 Evaluation of optical spectra (Aguire, 2003,Lal et al, 2007)

In order to facilitate the comparison between the optical spectra of the nanoshells, the approximate values for the spectral line width and the magnitude of the absorption peak were determined. The image in Figure 62 indicates the spectral width; the magnitude of the absorption peak is the ratio of the peak of the absorbance to the value of absorbance at the baseline.

5. Determination of the percentage of gold coverage on the surface of the silica

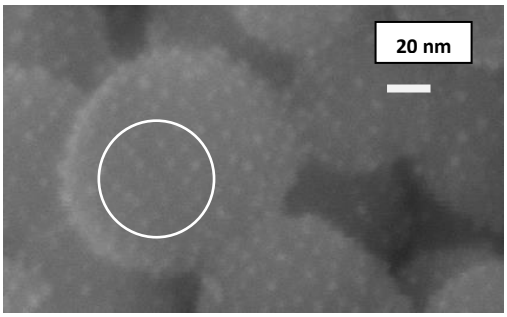

Figure 63 Estimating the percentage of gold particles on the surface of the silica

The number of 2 nm gold colloids decorating the surface of the silica was estimated by counting the number of gold colloids in a circle of known surface area, see Figure 63. This number was then used to estimate the total number of 2 nm gold colloids covering the

entire surface of the silica. The percentage of coverage was estimated by calculating the approximate total surface area of the silica that was covered by gold.

Appendix B- Biological Work

This Appendix describes the experimental work done in order to assess the effect of gold nanoparticles (50 and 150 nm) on the viability and proliferation of the Glioblastoma cancer cells (GBCC).

The experiments were divided into two groups. The first was design in order to determine if the gold colloids are taken up by the cells. In this experiment cells were incubated in culture media that contained the nanoparticles. After 4 days the cells were fixed and prepared for TEM imaging. The TEM imaging enabled the investigation of whether or not the particles were taken up by the cells. The second experiment was designed to determine the effect of the nanoparticles and their uptake on the proliferation and viability of the cells. Details of the experiments are described below.

1. Materials

All the chemicals, antibodies and assay kits used in the cell culturing and the subsequent experiments with the cells were provided by the Addenbroke's Center for Brain Repair, Dr. Watts' Laboratory. The PBS (phosphate buffer saline) was obtained from GIBCO and was used for washing the cells at different stages of the experiments.

The primary (KI67) and secondary antibodies were purchased from Invitrogen. The Trypan blue was obtained from Sigma Aldrich. Triton blue was obtained from Sigma Aldrich. The extra cellular matrix was obtained from GIBCO. The culture media used in the experiments was a serum free medium obtained from GIBCO. Prior to its use, FGF, EGF, N2, B27, glutamate were added to the culture media (neurobasal A) as sources of nutrients; these were obtained from Invitrogen. The Dapi used in the nuclear staining was purchased from GIBCO. Cell-Titer-96 Aqueous One Solution Assay was obtained from Promega and was used for the MTS assay.

2. Methods

The cells used in the assessment of the viability of the cells were cultured in 24 well plates and on cover slips. The cell were exposed to 50 and 150 nm gold nanoparticles concentrations of which are presented below in Table 6. These groups of cells were treated with the gold nanoparticles for 24 hrs, 72 hrs and one week.

Concentration / Size	Low	Standard	High	Control
150	$0.83x10^9$	$1.66x10^9$	$3.32x10^9$	Nil
50	$22.5x10^9$	$45x10^9$	$90x10^9$	Nil

Table 6 Concentration of gold colloid in cell experiments

The cells used for the evaluation of nanoparticle uptake were cultured in six well plates so as to allow for the scraping of the cells off of the bottom of the wells. The six well plates were also use because they provided a larger number of cells; this was required for TEM imaging.

No variation in the concentration of particles was used in the nanoparticle uptake investigation. In the particle-up take analysis, the concentration of the particles was 1.66 x 10^9particles per ml and 45 x 10^9 particles per ml for the 150 nm and 50 nm-sized particles, respectively. Approximately 200 ul, of each size of the gold particles, were added to each well. The cells used in this experiment were cultured for 4 days.

a. Cell fixation

After the cells were cultured, they were fixed so as to prepare them for TEM imaging or for the proliferation assay.

1) Fixation of cells in preparation for TEM imaging

Cells being prepared for TEM imaging were fixed using glutaraldyhyde in accordance with the following procedure.

Hydrogen peroxide, 400 ul, was added to approximately 10 ml of glutaraldyhyde. The mixture was set aside. The cells were washed with a 0.9% sodium chloride solution. The saline solution was aspirated, and then just enough glutaraldyhyde was added to cover the cells. The cells were placed on ice for two hours. The glutaraldyhyde was then removed via aspiration. The cells were then washed four times and then centrifuged to remove the PBS.

The supernatant was discarded and the cells were placed into eppendorf tubes, ready for the next step.

2) Fixation of cells prior to proliferation and nuclear staining assay

The cells fixed for KI-67 staining were fixed using 4% para-formaldehyde. After the MTS assay was performed, PBS was added to wash the cells. The PBS was aspirated. The cells were then covered with para-formaldehyde and stored at $4^{O}C$ for 1 hour. The cells were then washed twice with PBS and were then ready for the proliferation assay.

b. Preparing cells for TEM imaging

The preparation of samples for thin sectioning, which enables them to be viewed using TEM, is a long, multistage process. As explained in detail above, the specimens were fixed and then washed with a buffer. The next step was to add osmium to the fixed cells (Skepper et al, 2008, Hardwick et al, 1996). The purpose of the osmium is to provide contrast to the cells so that they are easily viewed during TEM imaging. Osmium, to which 1.5% potassium ferricyanide had been added, was added to the cells. The cells were then stored in the osmium, at $4^{O}C$, overnight. The cells were then washed using a buffer solution. The next step was to perform bulk staining of the cells, which was carried out as detailed by Hardwick et al (Hardwick et al, 1996). The purpose of the bulk staining was to add contrast to the cells (Skepper et al, 2008, Hardwick et al, 1996). Following the bulk staining, the cells were serially dehydrated using ethanol and acetone, and then embedded in epoxy resin. The embedding renders an epoxy pellet in which the cells are embedded. After the embedding, thin sections (50 nm) were prepared using an ultra microtome. The sections were then mounted on copper grids and were viewed using TEM.

c. MTS assay

Prior to fixation of cells used in the viability analysis, an MTS assay was conducted on the cells whereby, 25 ul of Cell-Titer-96 Aqueous One Solution Assay were placed in each well and the cells were incubated for 1 hour. The cells were then placed in a Universal Microplate Reader in order to determine if the incubation with the gold nanoparticles had a cytotoxic effect on the cells.

d. KI-67 Staining

As previously stated, the purpose of the KI-67 staining was to determine the proliferation of the cells. The protocol for the staining was performed in accordance with the following steps. A 'block' solution was prepared, with the aim of using it to reduce the non-specific binding of the primary antibody. In order to make the block, 3 gm of goat serum were added to 50 ml of 99% albumen bovine serum (ABS). The PBS was removed from the wells and a few drops of triton-X solution were added to each well. The purpose of adding the triton-X was to puncture holes in the membrane therefore causing the cells to become permeable. The cells were treated with the triton-X for only a couple of minutes, after which they were washed two consecutive times with PBS. Then, 30 ul of the primary antibody were added to 1500 ul of the block, described above. Two 15 ul drops of the resulting mixture were then placed some distance apart on a paraffin sheet. The slides, on which the cells had grown, were placed separately on the paraffin drops. The slides were then stored at $4^{O}C$ for 8 hours, after which the secondary antibody was added to the slides, by an identical procedure to that used for the primary antibody. The secondary antibody was purchased conjugated to a florescence marker.

e. Nuclear Staining

In this experimental work, the KI-67 staining was followed by nuclear staining. In this step, 5 drops of Dapi were added to the cover slips containing the cells, while they were in the wells. After 5 minutes, the Dapi was removed and the cells were washed twice with PBS. The samples (cover slips) were then ready for viewing, using light microscopy. The cover slips were mounted onto microscope slides. The optical microscopy was used to image samples of the cells. The aim of this imaging was to determine the percentage of the cells, out of the total cell population, that were proliferating. The results obtained for the three nanoparticles concentrations were compared to the control to which no gold nanoparticles had been added.

3. Results of the cell experiments

This section summarizes the results obtained for the cellular experiments.

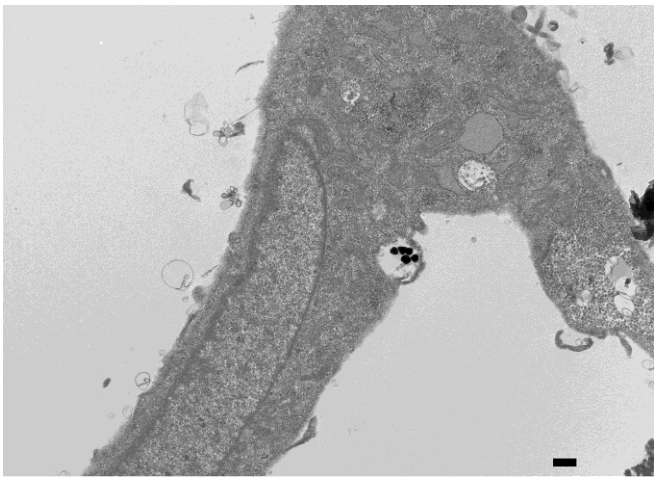

Figure 64 TEM image (80 kV, bright-field) of 150nm gold particles in the process of being taken up by GBCC (scale bar indicating 500um)

Figure 64 portrays a GBCC cell in the process of taking up several 150 nm gold colloids, while Figure 65 depicts a cell that has taken up the nanoparticles. The sections of the cells shown in both Figure 64 and Figure 65 are parts of cell membranes and the densely-coloured dark dots are the gold colloids within the membrane bound compartments.

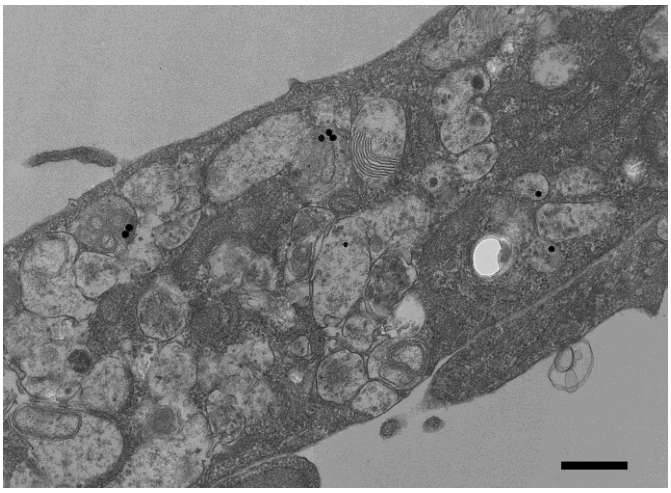

Figure 65 TEM image (80 kV, bright-field) of effect of passage number on cell aging (scale bar indicating 500um)

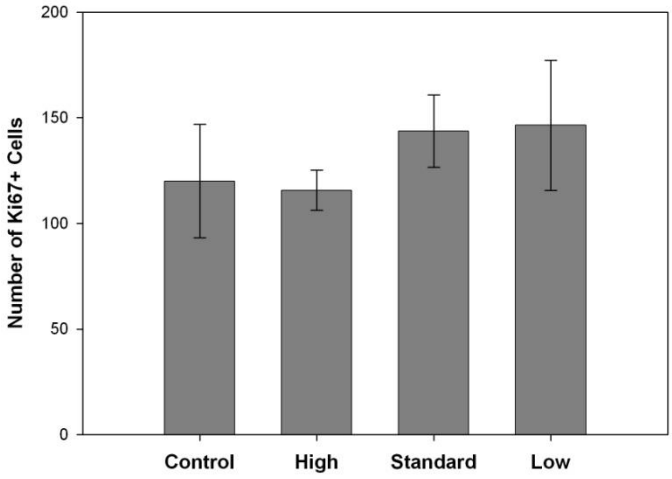

Figure 66 Analysis of proliferation staining results -72 hrs- GBCC and 150 nm gold colloids

Figure 66 and Figure 67 provide a summary of the results of the statistical analysis that was conducted on the data collected from the cell culturing experiments. Figure 66 illustrates the effect of the 150 nm gold nanoparticles on the viability of the cells by analysis of the proliferation marker, Ki-67, while Figure 67 illustrates the effect of the 150 nm gold nanoparticles on the viability of the cells by analyzing the nucleation marker, Dapi.

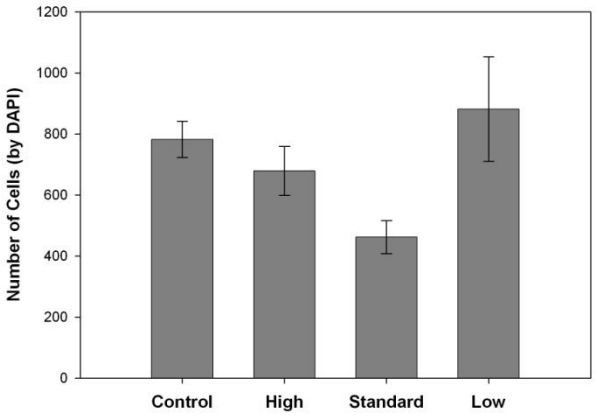

Figure 67 Analysis of nuclear staining results – 72hrs- GBCC and 150 nm gold colloids

The results from Figure 66 and Figure 67 indicate that the number of KI-67+ cells (proliferating cells) was 120 ± 26 out of the total cell population of 782 ± 59. The percentage of K-I67+ cells in the control was 15.3% ± 3.8 compared to 17% ± 3.2, 30% ± 2.4 and 20% ± 5.1 in the high, standard and low concentration samples, respectively.

A statistical analysis was also conducted, using the Analysis of Variance (ANOVA) and T-test, in order to determine the presence of any significant effect resulting from the treatment of the cells with the gold nanoparticles. The P- values obtained from the T-test conducted on the results indicated that there was no significant difference between the three experimental conditions and the control. The results of the T-tests, represented in terms of the P-values, are presented in Table 7. For any significant difference to be found between the experimental conditions the P-values obtained from the T-test should be less than 0.05.

Control	***Low***	***Standard***	***High***
Ki-67	0.531627	0.112502	0.862167
Dapi	0.567089	0.137094	0.367469

Table 7 P values obtained from T-test indicating no significant statistical difference in experimental conditions

The fact that the P-values, of the T-test, are all greater than 0.05 is an indication that there is no difference between the values obtained for the mean of the control and that of each of the individual groups. Hence it may be concluded that the treatment of the cells with the 150 nm gold particles had no significant effect on the viability or proliferation of the cells. Thus any experimental difference between the results is due to the random variability of the samples. Additionally, P-values obtained from the ANOVA, where 0.4122 and 0.206 for the Ki- 67 and the Dapi, respectively. This is also an indication that there is no significant difference, in terms of cell proliferation and viability, between the four different conditions. It may be concluded that the statistical analysis conducted did not provide any indication as to the change of the active proliferation of the viability of the cells, in culture, as a result of their treatment with the gold nanoparticles.

MTS assay

The results depicted in Table 8 and Table 9 below illustrate the results of the MTS assay conducted on the cells treated with 50 and 150 nm particles, respectively. The assay is a colorimetric method for determining the number of cells in active proliferation. The MTS compound that is added to the wells, containing the cells, is metabolized by the cells into a coloured product, 'formazan'. The quantity of the formazan produced is measured by the

amount of absorbance at a wavelength of 490 nm and is directly proportional to the number of living cells in culture. By comparing the absorption values for the different cells one can determine whether or not the conditions of the experiment affected the viability of the cells.

The MTS results, presented in Table 8 and Table 9 indicate that there was no significant effect on the viability of the cells due either to particle size or to the difference in the concentration of the gold particles.

Concentration	***Low***	***Standard***	***High***	***Control***
Well 1	0.489	0.498	0.527	0.548
Well 2	0.535	0.597	0.533	0.503
Well 3	0.518	0.496	0.526	0.521

Table 8 50 nm sample 72hrs- Values of MTS assay absorbance

Concentration	***Low***	***Standard***	***High***	***Control***
Well 1	0.440	0.443	0.492	0.495
Well 2	0.415	0.486	0.454	0.423
Well 3	0.397	0.477	0.449	0.435

Table 9 150 nm sample 72hrs- Values of MTS assay absorbance

4. Conclusion

The results of the two biological experiments conducted in this study indicate that gold nanoparticles, of sizes 50 and 150 nm, have no negative effect on the viability and active proliferation of the GBCC. It must be emphasized, though, that this was a pilot study using gold colloids, not nanoshells. The purpose was to establish the biocompatibility of gold and its effect on this type of cells. In order to assess the effect of nanoshells on the proliferation and viability of the cells, these experiments must be repeated using the nanoshells.

Appendix C- Tables

Table 10 presents the optical constants of gold obtained from Johnson (Johnson et al, 1972). These constants were used in the determination of the dielectric constants of gold and in turn the theoretical extinction spectra presented in this thesis.

TABLE I. Optical constants for copper, silver, and gold as well as the approximate errors in n and k.

	Copper		Silver		Gold		Error	
eV	n	k	n	k	n	k	Δn	Δk
0.64	1.09	13.43	0.24	14.08	0.92	13.78	±0.18	±0.65
0.77	0.76	11.12	0.15	11.85	0.56	11.21	±0.08	±0.30
0.89	0.60	9.439	0.13	10.10	0.43	9.519	±0.06	±0.17
1.02	0.48	8.245	0.09	8.828	0.35	8.145	±0.04	±0.10
1.14	0.36	7.217	0.04	7.795	0.27	7.150	±0.03	±0.07
1.26	0.32	6.421	0.04	6.992	0.22	6.350	±0.02	±0.05
1.39	0.30	5.768	0.04	6.312	0.17	5.663	±0.02	±0.03
1.51	0.26	5.180	0.04	5.727	0.16	5.083	±0.02	±0.025
1.64	0.24	4.665	0.03	5.242	0.14	4.542	±0.02	±0.015
1.76	0.21	4.205	0.04	4.838	0.13	4.103	±0.02	±0.010
1.88	0.22	3.747	0.05	4.483	0.14	3.697	±0.02	±0.007
2.01	0.30	3.205	0.06	4.152	0.21	3.272	±0.02	±0.007
2.13	0.70	2.704	0.05	3.858	0.29	2.863	±0.02	±0.007
2.26	1.02	2.577	0.06	3.586	0.43	2.455	±0.02	±0.007
2.38	1.18	2.608	0.05	3.324	0.62	2.081	±0.02	±0.007
2.50	1.22	2.564	0.05	3.093	1.04	1.833	±0.02	±0.007
2.63	1.25	2.483	0.05	2.869	1.31	1.849	±0.02	±0.007
2.75	1.24	2.397	0.04	2.657	1.38	1.914	±0.02	±0.007
2.88	1.25	2.305	0.04	2.462	1.45	1.948	±0.02	±0.007
3.00	1.28	2.207	0.05	2.275	1.46	1.958	±0.02	±0.007
3.12	1.32	2.116	0.05	2.070	1.47	1.952	±0.02	±0.007
3.25	1.33	2.045	0.05	1.864	1.46	1.933	±0.02	±0.007
3.37	1.36	1.975	0.07	1.657	1.48	1.895	±0.02	±0.007
3.50	1.37	1.916	0.10	1.419	1.50	1.866	±0.02	±0.007
3.62	1.36	1.864	0.14	1.142	1.48	1.871	±0.02	±0.007
3.74	1.34	1.821	0.17	0.829	1.48	1.883	±0.02	±0.007
3.87	1.38	1.783	0.81	0.392	1.54	1.898	±0.02	±0.007
3.99	1.38	1.729	1.13	0.616	1.53	1.893	±0.02	±0.007
4.12	1.40	1.679	1.34	0.964	1.53	1.889	±0.02	±0.007
4.24	1.42	1.633	1.39	1.161	1.49	1.878	±0.02	±0.007
4.36	1.45	1.633	1.41	1.264	1.47	1.869	±0.02	±0.007
4.49	1.46	1.646	1.41	1.331	1.43	1.847	±0.02	±0.007
4.61	1.45	1.668	1.38	1.372	1.38	1.803	±0.02	±0.007
4.74	1.41	1.691	1.35	1.387	1.35	1.749	±0.02	±0.007
4.86	1.41	1.741	1.33	1.393	1.33	1.688	±0.02	±0.007
4.98	1.37	1.783	1.31	1.389	1.33	1.631	±0.02	±0.007
5.11	1.34	1.799	1.30	1.378	1.32	1.577	±0.02	±0.007
5.23	1.28	1.802	1.28	1.367	1.32	1.536	±0.02	±0.007
5.36	1.23	1.792	1.28	1.357	1.30	1.497	±0.02	±0.007
5.48	1.18	1.768	1.26	1.344	1.31	1.460	±0.02	±0.007
5.60	1.13	1.737	1.25	1.342	1.30	1.427	±0.02	±0.007
5.73	1.08	1.699	1.22	1.336	1.30	1.387	±0.02	±0.007
5.85	1.04	1.651	1.20	1.325	1.30	1.350	±0.02	±0.007
5.98	1.01	1.599	1.18	1.312	1.30	1.304	±0.02	±0.007
6.10	0.99	1.550	1.15	1.296	1.33	1.277	±0.02	±0.007
6.22	0.98	1.493	1.14	1.277	1.33	1.251	±0.02	±0.007
6.35	0.97	1.440	1.12	1.255	1.34	1.226	±0.02	±0.007
6.47	0.95	1.388	1.10	1.232	1.32	1.203	±0.02	±0.007
6.60	0.94	1.337	1.07	1.212	1.28	1.188	±0.02	±0.007

Table 10 Values of n and k used to obtain dielectric constants of gold (Johnson et al 1972)